Symbiotic plasmid (pNGR234*a*) copy number in the broad host range bacterium *Sinorhizobium fredii* NGR234 depends on quorum sensing and phenotypic heterogeneity

Dissertation with the aim of achieving a doctoral degree

Doctor rerum naturalium (Dr. rer. nat.)

at

the Faculty of Mathematics, Informatics and Natural Science

of the

Universität Hamburg

Department of Biology

Hilke Johanna Duin

Born in Aurich

July 2021

The following evaluators recommended

the admission of the dissertation:

Prof. Dr. Wolfgang Streit

PD Dr. Eva Spieck

Day of oral defense: 28.10.2021

Declaration on oath

I hereby declare, on oath, that I have written the present dissertation by my own and have not used other than the acknowledged resources and aids.

Hamburg, 06.07.2021

_____

Hilke Duin

Contributions to scientific articles

Bettenworth V, Steinfeld B, Duin H, Petersen K, Streit WR, Bischofs I, Becker A; 2019. Phenotypic Heterogeneity in Bacterial Quorum Sensing Systems. Journal of Molecular Biology, April.

- Literature inquiry
- Writing parts of the articles text
- Generating figures for *Sinorhizobium fredii* NGR234

Petersen K, Duin H, Streit WR; in preparation.

- Literature inquiry
- Writing parts of the articles text
- Copy number variation assays by real-time qPCR
- Nodulation assay with *Sinorhizobium fredii* NGR234 strains and *Vigna unguiculata*
- Constructing and realisation of promoter fusion experiments with *repA0_egfp*

Contents

Abbreviations

3-oxo-C_8 HSL	*N*-3-oxo-octanoyl-homoserine lactone
3-oxo-C_{10} HSL	*N*-3-oxo-decanoyl-homoserine lactone
3-oxo-C_{12} HSL	*N*-3-oxo-dodecanoyl-homoserine lactone
3-oxo-C_{14} HSL	N-3-oxo-tetradecanoyl-homoserine lactone
α	*alpha*
AHL	Acyl homoserine lactone
AI	Autoinducer
Amp	Ampicillin
ANU 265	*Sinorhizobium fredii* ANU265
AU	Arbitrary units
β	*beta*
bp	base pairs
Ca^{2+}	Calcium ion
c-di-GMP	Cyclic diguanylate
csv	Comma-separated valued
Ct	Calculation threshold
dH_2O	Distilled water
DMF	Dimethylformamide
DMSO	Dimethyl sulfoxide
DNA, gDNA	Deoxyribonucleic acid, genomic DNA
EPS	Exopolysaccharide(s)
EtOH	Ethanol
F	Farad
FI	Fluorescence intensity
For	Forward
g	Gravitational force equivalent
Gen	Gentamycin
(p)ppGpp	Guanosine pentaphosphate
H_2O_{bidest}	Bi-distilled water
HSL	Homoserine lactone
IPTG	Isopropyl β-d-1-thiogalactopyranoside
Kan	Kanamycin
M, Mbp	Mega, mega bp
M, 1 M	Molar
MeOH	Methanol
Met-tRNA	Methionine transporter RNA

MIFISC	Mean integrated fluorescence intensity per single cell
NGR234	*Sinorhizobium fredii* NGR234
Δ*traI* c+	NGR234 Δ*traI* copy+
nm	Nano meters
Nod	Nodulation
NOD	Nodulation media
NOPs	Nodulation outer proteins
ns.	Not significant
NTC	No template control
OD_{600}	Optical density at 600 nm
ORF	Open reading frame
Ω	Resistance
PBS	Phosphate-buffered saline
PCR	Polymerase chain reaction
qPCR	Real-time quantitative PCR
QS	Quorum sensing
QQ	Quorum quenching
Rif	Rifampicin
Rev	Reverse
rpm	Rotations per minute
RNA	Ribonucleic acid
RT	Room temperature
RT_XXX	Real-time PCR primer
Spec	Spectinomycin
Ti-plasmid	Tumour inducing plasmid
TLC	Thin layer chromatography
Tet	Tetracycline
USDA257	*Sinorhizobium fredii* USDA257
V	Volt
(v/v)	Volume to volume
WT	Wild type
(w/v)	Weight to volume
X-Gal	5-bromo-4-chloro-3-indolyl-β-D-galactopyranoside

List of Figures

List of Tables

1 Abstract

1.1 English Abstract

Sinorhizobium fredii NGR234 is an Alphaproteobacterium of the *Rhizobiaceae* family. This Gram-negative bacterium is characterised by its remarkably broad host range. It can induce root nodules and fix atmospheric Nitrogen with over 120 legume plant genera and even with one non-legume. *S. fredii* NGR234's genome consists of three replicons, the chromosome and two megaplasmids, pNGR234*b* and pNGR234*a*. The chromosome and the pNGR234*a* plasmid encode each for one quorum sensing (QS) system, consisting of an autoinducer synthase, *ngrI* and *traI* respectively, and their regulators, *ngrR* and *traR*. Recently, studies indicated that deleting both QS system autoinducer synthases, *traI* and *ngrI*, the plasmid copy number of the pNGR234*a* plasmid increased and nearly all genes encoded on the symbiotic plasmid were highly transcribed leading to the identification of new open reading frames (ORFs). Analysis of these data showed a regulatory function of some of these newly discovered small ORFs, like NGR_a01725 or *repX* on plasmid copy number.

This study provides further evidence that the plasmid copy number of the symbiotic plasmid in the rhizobia species *S. fredii* NGR234, besides multiple other factors, like non-coding RNA, small ORFs and some still unknown factors, is influenced by QS. To develop a deeper understanding and provide further information how the plasmid copy number is regulated in *S. fredii* NGR234, effects of copy number changes were investigated by real-time quantitative PCR. Cultivation of NGR234 wild type (WT) and QS autoinducer synthase mutants using spent medium of different Gram-negative bacteria confirmed that the copy number of the symbiotic plasmid of NGR234 is regulated by externally provided autoinducers.

Another main aspect studied here is phenotypic heterogeneity in *S. fredii* NGR234. The promoters of the autoinducer synthases, *traI* and *ngrI,* as well as the quorum quenching (QQ) gene *qsdR1* promoter were linked to individual fluorescent proteins on one broad host range plasmid and after transformation of different NGR234 strains observed by confocal laser scanning microscopy (CLSM). Subsequently, an automated cell counting pipeline and the identification of fluorescence intensity with the CellProfiler 3.1.8 software gave the opportunity to analyse CLSM images comparing NGR234 WT and the NGR234 mutant strains. All promoters showed heterogeneous expression in NGR234 WT and the studied mutant strains, ANU265, NGR234 Δ*repX* and NGR234

ΔNGR_a01725+. Analysing single cells by CLSM and using an automated analysis revealed how population-wide expression patterns are shaped by single cell expression. However, the total range of the heterogeneous expression of each promoter was influenced in each mutant. Interestingly, ANU265 was observed to have three times higher median fluorescence intensities for all measured promoters after 24 h, had similar levels after 48 h and equal or higher levels of median fluorescence intensities after 72 h compared to the WT. The level of the overall phenotypic heterogeneity for the measured promoters was increased after 48 h. Examining the effect of the small ORFs *repX* and NGR_a01725, revealed an effect on phenotypic heterogeneity of the observed promoters as well. Even tough deletion of *repX* leads to a total loss of the symbiotic plasmid comparable to the ANU265 strain, results for the NGR234 *ΔrepX* mutant were different. Here median fluorescent intensities were either on WT level or below for all promoters. The range of expression intensities decreased, resulting in less phenotypic heterogeneity after 48 h. The deletion of the small ORF NGR_a01725 on the other hand increased the promoter activities after 48 h compared to the NGR234 WT. Additionally, the degree of phenotypic heterogeneity for the measured promoter activities was enhanced as well. These results show that QS and QQ are not as homogeneous as expected and that expression of these genes is influenced by the symbiotic plasmid copy number and small ORFs encoded thereon.

1.2 German Abstract

Sinorhizobium fredii NGR234 ist ein Alphaproteobakterium aus der Familie der Rhizobiaceae. Dieses Gram negative Bakterium zeichnet sich durch sein bemerkenswert breites Wirtsspektrum aus. Es kann Wurzelknöllchen induzieren und atmosphärischen Stickstoff mit über 120 Leguminosen-Gattungen und sogar mit einer Nicht-Leguminose fixieren. Das Genom von *S. fredii* NGR234 besteht aus drei Replikons, dem Chromosom und zwei Megaplasmiden, pNGR234*b* und pNGR234*a*. Das Chromosom und das pNGR234*a* Plasmid kodieren jeweils für ein Quorum Sensing (QS)-System, bestehend aus einer Autoinducer-Synthase, *ngrI* bzw. *traI*, und deren Regulatoren, *ngrR* und *traR*. Kürzlich wiesen Studien darauf hin, dass durch die Deletion der beiden Autoinducer-Synthasen der QS-Systeme, *traI* und *ngrI*, die Plasmid-Kopienzahl des pNGR234*a*-Plasmids anstieg und fast alle auf dem symbiotischen Plasmid kodierten Gene hoch transkribiert wurden, was zur Identifizierung neuer offener Leserahmen (ORFs) führte. Die Analyse dieser Daten zeigte eine regulatorische Funktion einiger dieser neu entdeckten kleinen ORFs, wie NGR_a01725 oder *repX* auf die Plasmid-Kopienzahl.

Diese Studie liefert weitere Hinweise darauf, dass die Plasmid-Kopienzahl des symbiotischen Plasmids in dem Rhizobienstamm *S. fredii* NGR234, neben mehreren anderen Faktoren, wie nicht-kodierender RNA, kleinen ORFs und einigen noch unbekannten Faktoren, von QS beeinflusst wird. Um ein tieferes Verständnis zu entwickeln und weitere Informationen darüber zu erhalten, wie die Plasmid-Kopienzahl in *S. fredii* NGR234 reguliert wird, wurden die Auswirkungen von Kopienzahländerungen mittels quantitativer real-time PCR untersucht. Die Kultivierung von NGR234 Wildtyp (WT) und QS-Autoinducer-Synthase-Mutanten unter Verwendung von verbrauchtem Medium verschiedener Gram negativer Bakterien bestätigte, dass die Kopienzahl des symbiotischen Plasmids von NGR234 durch extern hinzugefügte Autoinducer reguliert wird.

Ein weiterer Aspekt, der hier untersucht wurde, ist die phänotypische Heterogenität in *S. fredii* NGR234. Die Promotoren der Autoinducer-Synthasen, *traI* und *ngrI*, sowie der Promotor des Quorum Quenching (QQ)-Gens *qsdR1* wurden mit individuellen fluoreszierenden Proteinen auf einem Plasmid mit breitem Wirtsspektrum verknüpft und nach Transformation verschiedener NGR234 Stämme mittels konfokaler Laser-Scanning-Mikroskopie (CLSM) beobachtet. Eine automatisierte Zellzählung und die Identifizierung der Fluoreszenzintensität mit der Software CellProfiler 3.1.8 ermöglichte anschließend die Analyse von CLSM Bildern, die NGR234 WT und die NGR234-Mutantenstämme verglichen. Alle Promotoren zeigten eine heterogene Expression im NGR234 WT und den untersuchten Mutanten, ANU265, NGR234 Δ*repX* und NGR234 ΔNGR_a01725+. Die Analyse einzelner Zellen mittels CLSM und die Verwendung einer automatisierten Analyse zeigten, wie populationsweite Expressionsmuster durch die Expression einzelner Zellen geprägt werden. Das Ausmaß der heterogenen Expression jedes Promotors wurde jedoch in jeder Mutante beeinflusst. Interessanterweise wurde bei ANU265 beobachtet, dass die medianen Fluoreszenzintensitäten für alle gemessenen Promotoren nach 24 h dreimal höher waren, nach 48 h ähnliche Werte aufwiesen und nach 72 h gleiche oder höhere Werte der medianen Fluoreszenzintensitäten im Vergleich zum WT hatten. Das Niveau der gesamten phänotypischen Heterogenität für die gemessenen Promotoren war nach 48 h erhöht. Die Untersuchung des Effekts der kleinen ORFs *repX* und NGR_a01725, zeigte ebenfalls einen Effekt auf die phänotypische Heterogenität der beobachteten Promotoren. Auch wenn die Deletion von *repX* zu einem Totalverlust des symbiotischen Plasmids führt, vergleichbar mit ANU265, waren die Ergebnisse für die NGR234 Δ*repX* Mutante abweichend dazu. Hier lagen die medianen

Fluoreszenzintensitäten für alle Promotoren entweder auf WT-Niveau oder darunter. Der Umfang der Expressionsintensitäten nahm ab, was zu einer geringeren phänotypischen Heterogenität nach 48 h führte. Die Deletion des kleinen ORF NGR_a01725 hingegen erhöhte die Promotoraktivitäten nach 48 h im Vergleich zum NGR234 WT. Zusätzlich war auch der Grad der phänotypischen Heterogenität für die gemessenen Promotoraktivitäten erhöht. Diese Ergebnisse zeigen, dass QS und QQ nicht so homogen sind wie erwartet und dass die Expression dieser Gene von der Kopienzahl des symbiotischen Plasmids und den darauf kodierten kleinen ORFs beeinflusst wird.

2 Introduction

2.1 Rhizobia

Biological nitrogen fixation in root nodules of legumes was discovered by the German agricultural chemist Hermann Hellriegel and the Dutch microbiologist Martinus W. Beijerinck at the end of the 20th century. Beijerinck discovered that bacteria living inside of root nodules could fix atmospheric nitrogen and convert it into ammonium, making it accessible to the plant host as part of a symbiosis (Beijerinck, 1888, 1901). Shortly after the discovery of bacteria living symbiotically in root nodules, the isolated bacteria were renamed from *Bacillus radicicola* to *Rhizobium leguminosarum* (Frank, 1889) initiating the family *Rhizobiaceae* we know. During the last century further species belonging to the *Rhizobiales* were discovered and cultivated, making Rhizobia one of the best studied phyla. Symbiotic nitrogen fixation is not limited to the family of *Rhizobiaceae* and can also be found in *e.g.* Cyanobacteria or bacteria belonging to the family of *Azoarcus* (Mus et al., 2016; Reinhold-Hurek et al., 1993).

The term 'Rhizobia' refers to a paraphyletic group of bacteria belonging to the Alpha- and Betaproteobacteria (*α*- and *β*-Proteobacteria) or the Actinobacteria, forming a symbiosis with their respective host plant and fixing nitrogen (Mus et al., 2016). Rhizobia are naturally occurring all over the world and competing with other bacteria in the soil and in proximity to plant roots, the rhizosphere. Establishment of symbiosis relies on a finely tuned and harmonised chemical communication between the plant host and the rhizobium.

2.2 Symbiosis

Symbiosis between plants and rhizobia initially starts by host specific flavonoids that are secreted into the rhizosphere. A LysR-type transcriptional activator, *nodD,* performs detection of these flavonoids in the bacteria. NodD is the master regulator of the plant signal induced nodulation response in rhizobia (Bassam et al., 1988; Schlaman et al., 1992). Perception of flavonoids by NodD induces a signalling cascade by binding to a 49 base pair (bp) *nod*-box motif (Feng et al., 2003; Kobayashi et al., 2004), regulating the expression of *nod, noe* and *nol* gene clusters, each composed of several genes encoding for *e.g.* nodulation factors and transporters. These nodulations factors, or nod factors, are lipochitooligosaccharides that are secreted into the cell's environment and detected by the host plant (Schultze and Kondorosi, 1998). This initial exchange of chemical signals, flavonoids on the one hand, and nod factors on the other hand,

represent the crucial first steps in plant-microbe symbiosis between the host plant and the rhizobia. Even though rhizobia share a common nod factor structure, each species has a distinct subset of nod factors with specific modifications (Spaink, 2000). These nod factors are detected by a suitable host plant via a lysine motif receptor (LysM) on the root's surface. The plants gene expression is then altered and nodulation specific genes are being expressed (Goedhart et al., 2000; Poole et al., 2018). Furthermore, the expression of genes required for establishing symbiosis is induced in the respective bacterium.

As a first visible reaction to nod factors, root hair curling is initiated (Esseling et al., 2003; Poole et al., 2018), leading to the formation of a 'Shepherd's crook' (Gehring et al., 1997; Somasegaran and Hoben, 1985). By curling the root hair, rhizobia attached to the respective root hair are entrapped. The formation of an infection thread is induced in curled root hair cells (Denarie et al., 1996; Fournier et al., 2008). Prior to the visible reaction to nod factors, a calcium ion (Ca^{2+}) spiking in the root hair cell can be measured (Ehrhardt et al., 1996; Gehring et al., 1997; Jones et al., 2007; Miwa et al., 2006; Wais et al., 2000, 2002). Following the Ca^{2+} signal, loosening of actin filaments inside the root tips can be observed (Murray, 2011) and a signalling cascade in which *early nodulation genes* (*enod*) are expressed is initiated.

In order to overcome the root hairs cell wall, rhizobia were shown to secrete cellulases, making the initiation of the infection and the subsequently formation of an infection thread possible (Robledo et al., 2008). The infection thread, formed by the plant, enables the rhizobia to further grow and enter the curled root hair. The infection threads extend until they reach the cells of the inner root cortex where rhizobia cells are released into the already proliferating cortical cells, also referred to as the nodule primordium (Oldroyd and Downie, 2008). Before bacteria enter the nodule primordium cells of the root cortex, they are enclosed by a membrane, forming the symbiosome (Calatrava-Morales et al., 2018; Oldroyd and Downie, 2008; Roth and Stacey, 1989). Low oxygen levels and plant originated peptides, initiate the differentiation of bacteria into bacteroids. These bacteroids are no longer capable of proliferation but their gene expression is shifted to fixation of nitrogen. Living inside the symbiosome, metabolite pathways for saprophytic lifestyle are no longer necessary and therefore their gene expression is down regulated. However, it was observed that before terminal differentiation into bacteriods, some rhizobia increased their cell size, and a higher membrane permeability was detectable. Additionally, replication of the bacteria's genome was detected (Alunni and Gourion, 2016; Jones et al., 2007; Mergaert et al.,

2006). It is speculated that this is to further increase transcription and expression of genes required for nitrogen fixation and symbiosis in general. Besides nod factors, rhizobia express small proteins, the nodulation outer proteins (NOPs) as well as exo- and lipopolysaccharides (EPS and LPS) to quench plant immune response. Thereby, some rhizobia can further broaden their host range by lowering the plant immune response, allowing them to enter the root hair cell and pursue the infection (Cooper, 2007; Jones et al., 2007; Nelson and Sadowsky, 2015). To control rhizobial infection, legume plants tightly regulate the infection process. Several gateways detect and control respective rhizobia species, enabling the host plant to screen for specific rhizobia species and forming host-symbiont specificity (Masson-Boivin and Sachs, 2018; Unay and Perret, 2020). Once nodules are formed, subsequent infection and the additional formation of new nodules is suppressed (Jones et al., 2007; Nelson and Sadowsky, 2015).

Overall, symbiosis is a finely balanced interplay between the host plant and the rhizobium. Both participants secrete several chemical signals to identify suitable partners. Furthermore, continuously expression of bacterial nod factors, EPS and LPS during establishment of symbiosis makes it possible for plants to select, even after initial infection, for the most suitable rhizobia symbiosis partner (Unay and Perret, 2020). After differentiation of the rhizobia into nitrogen fixing bacteroids by expression of *e.g.* nitrogenase, bacteria supply nitrogen in form of ammonium to their host plant (Jones et al., 2007). In return, plants supply carbon the in form of malate to bacteria and provide a secure ecological niche (Jones et al., 2007).

Since their discovery, rhizobia have been extensively studied, especially regarding their host range. Many rhizobia species experience a distinct host range, with some species being able to nodulate only one specific host plant (Perret et al., 2000). On the other hand, studies identified rhizobia species inducing nodulation in a broad range of host plants (Pueppke and Broughton, 1999). Therefore, rhizobia can be classified as either narrow or broad host range strains. One species that contains few broad host range strains is the α-Proteobacteria *Sinorhizobium fredii.* Besides the strain *S. fredii* HH103, nodulating up to 15 soybean hosts, and the *S. fredii* USDA257 strain being able to induce nodule formation on at least 79 host plants, the strain *S. fredii* NGR234 stands out with its extraordinary wide host range (Krysciak et al., 2015; Pueppke and Broughton, 1999).

2.3 Sinorhizobium fredii NGR234

The broad host range strain *Sinorhizobium fredii* NGR234 (referred to as NGR234) belongs to the group of α-Proteobacteria, is rod-shaped, Gram-negative, and has a remarkable host range - it is known for its ability to nodulate over 120 plant genera, including the non-legume *Parasponia andersonii* (Pueppke and Broughton, 1999; Trinick, 1980). NGR234 was first isolated from root nodules of the *Lablab purpureus* in Papua New Guinea as one of the fast-growing rhizobia strains (Trinick, 1980). As more and more studies investigated the ability of NGR234 to nodulate a broad host range, interest in its genetic background and its form of communication with its host plants emerged (*e.g.* Stanley and Cervantes, 1991; Flores et al., 1998; He et al., 2003; Perret et al., 2003; Staehelin et al., 2006; Schmeisser et al., 2009; Krysciak et al., 2015).

In 2009, NGR234s' full genome was sequenced (Schmeisser et al., 2009) and enabled extensive studies regarding its genetic tools. NGR234's genome consists of three replicons, the chromosome (cNGR234) with a size of 3.93 mega bp (Mbp), a megaplasmid (pNGR234*b*) with a size of 2.43 Mbp and a smaller plasmid (pNGR234*a*), also referred to as symbiotic plasmid, with a size of 0.54 Mbp (Schmeisser et al., 2009; Schuldes et al., 2012). The symbiotic plasmid and the pNGR234*b* megaplasmid belong to the family of *repABC* plasmids. The small pNGR234*a* plasmid encodes for nearly all genes necessary for establishing symbiosis and nodule formation, like nod factor and nitrogenase-coding genes. No essential genes are encoded on the symbiotic plasmid, since NGR234 can be cured of it, losing its ability to nodulate and fix nitrogen, while not impairing its growth. NGR234 without its symbiotic plasmid is referred to as *S. fredii* ANU265 (Morrison et al., 1983). Besides NGR234's nodulation factors, exopolysaccharides (Staehelin et al., 2006) and a number of secretion systems (Freiberg et al., 1997; Schmeisser et al., 2009), the quorum sensing system of NGR234 became a focus of research. Living as single cells in the soil, intra-species communication via quorum sensing is essential for being competitive against other soil-dwelling bacteria and for the establishment of successful symbiosis with a suitable host plant.

Quorum sensing (QS) is characterised by the expression and secretion of small diffusible compounds into the surroundings of the producing cell and the reception of these chemical signals by neighbouring cells. Upon reaching a certain quorum, gene expression is altered on the population level, initiating processes that are only useful when the population density has reached a high level (Fuqua et al., 1994). QS was first described for *Vibrio fischeri,* now reclassified as *Aliivibrio fischeri,* living in the light

organs of bobtail squids (Nealson and Hastings, 1979). The bacteria living inside the squid reach high populations densities in comparison to bacteria in the open water, leading to the QS-regulated expression of the *lux* operon and therefore to light emission (Nealson and Hastings, 1979). Since the first reports of QS in bacteria, more examples of population-wide gene expression based on population density have been shown. Sporulation, biofilm formation, light emission, antibiotics synthesis and conjugal plasmid transfer are just a few examples (Miller and Bassler, 2001; Williams et al., 2007). In the Gram-negative *A. fischeri,* population density is sensed by the concentration of the autoinducer (AI) produced by the respective AI synthase LuxI. LuxI was shown to produce an acyl homoserine lactone (AHL) AI at low levels even when the population density has not reached a threshold level. The AHL-AI are mostly membrane diffusible compounds, accumulating in the environment with increasing population density. The LuxR regulator, binding AI molecules, mediates AHL-AI detection. When a population density threshold is reached, LuxR binds AHL-AI and thereby enables the binding of LuxR in the promoter region of the *lux* operon, activating its expression and leading to light emission. Thus, LuxI induces its own expression in a positive feedback loop. On the other hand, the LuxR-AI complex leads to a reduced expression of LuxR itself, regulating its own expression negatively (Miller and Bassler, 2001; Whitehead et al., 2001). This LuxI/LuxR type QS system was also identified in a range of other Gram-negative bacteria like *Pseudomonas* spp*., Chromobacterium violaceum, Yersinia* spp*., Burkholderia* spp*.* or *Erwina* spp (Papenfort and Bassler, 2016; Whitehead et al., 2001; Williams et al., 2007). Another extensive studied example of the LuxI/LuxR type system was identified in *Agrobacterium tumefaciens* (Papenfort and Bassler, 2016; White and Winans, 2007; Williams et al., 2007). *A. tumefaciens* is a soil dwelling Gram-negative bacterium causing crown gall disease on plants (Escobar and Dandekar, 2003). In this plant pathogen, AI are synthesised by the LuxI type *traI* AI synthase encoded on the tumour-inducing plasmid (Ti-plasmid). TraI produces a *N*-3-oxo-octanoyl-homoserine lactone (3-oxo-C_8-HSL) (Fuqua et al., 1994), which is detected and bound by TraR, the LuxR homologue. Binding of AHL to TraR, leads to the formation of TraR dimers with enhanced stability and induces conformational changes, increasing its affinity to its cognate promoter binding sites (Zhu and Winans, 2001). The TraR-AHL complex stimulates expression of TraI, forming a positive feedback loop, and stimulating plasmid conjugation genes by binding to the respective promoter regions, *tra*-boxes, on the Ti-plasmid (Fuqua and Winans, 1996; White and Winans, 2007). In contrast to *A. fischeri*, *A. tumefaciens'* QS system is further regulated by the TraR anti-activator TraM, also encoded on the Ti-plasmid

(Fuqua et al., 1995; Miller and Bassler, 2001). TraM provides a tool for *A. tumefaciens* to regulate QS and plasmid conjugation at low cell densities, when QS thresholds are not reached. Therefore, TraM prevents *A. tumefaciens* of premature gene expression and QS response (Fuqua et al., 1995; Lang and Faure, 2014). Another example of how QS shapes infectious traits can be found in the plant pathogen *Burkholderia glumae* PG1. *B. glumae* PG1 encodes for three QS systems, all expressing AHL type AI signals (Gao et al., 2015b). The QS systems have been termed *bgaI1* to *bgaI3.* Using thin layer chromatography (TLC), the respective AI signals were analysed in detail. The AI synthase *bgaI1* probably synthesises a 3-oxo-octanoyl-HSL, *bgaI2* best aligned with a reference of 3-oxo-decanoyl-HSL, whereas *bgaI3* co-migrated with either a 3-oxo-dodecanoyl-HSL or a decanoyl-HSL (Gao et al., 2015b). In *B. glumae* PG1 QS regulates a diverse set of genes necessary for the phytopathogenicity, including motility, secretion of virulence factors or expression of phytotoxins (Kang et al., 2008; Kim et al., 2007; Zhou-qi et al., 2016).

Living in soil makes reception of the direct environment a necessity. QS enables NGR234 to express specific genes in response to environmental signals only when the population has reached a certain threshold. Studies have shown that NGR234's QS system is very similar to that of *A. tumefaciens* and the LuxI/LuxR type system of *A. fischeri* (Freiberg et al., 1997; He et al., 2003). NGR234 was described to encode for two distinct QS systems, one located on the chromosome and designated *ngrI/ngrR* system (see Figure 1) and the other positioned on the symbiotic plasmid and referred to as *traI/traR* system (He et al., 2003; Krysciak et al., 2011). Like the *luxI/luxR* system of *A. fischeri,* the *ngrI/ngrR* system consists only of an AI synthase (NgrI) and its respective regulator protein (NgrR). The AI synthases constantly synthesise low amounts of AI under non-inducing conditions (Cha et al., 1998; Vannini et al., 2002). Most AI molecules freely pass the cell membrane and slowly accumulate in the cells environment when population density rises. Due to the increasing concentration of AI molecules, NgrR can associate with its respective AI, further positively stimulating the expression of *ngrI,* auto-inducing its own expression (see Figure 1). However, the complete functioning mechanism of the *ngrI/ngrR* system still needs further research until fully characterised. The plasmid bound system *traI/traR*, on the other hand, resembles more closely the QS system of *A. tumefaciens* including the TraR anti-activator TraM. It was shown that TraM binds TraR and therefore blocks the detection of the produced TraI AI and diminishes the DNA binding capacities of TraR (see Figure 1) (Chen et al., 2007). Both AI systems of NGR234 produce AHL-type AI. The TraI AI

synthase is likely producing a 3-oxo-C_8-HSL (He et al., 2003; Krysciak et al., 2014), whereas the second QS system NgrI AI synthase synthesises probably a more hydrophobic AHL or an AHL with a longer carbon chain as TLC analysis suggests. Therefore, the second AI is speculated to be either a 3-oxo-dodecanoyl- (C_{12}-), 3-oxo-tetradecanoyl-HSL (C_{14}-) or a HSL in a more reduced state (He et al., 2003; Krysciak et al., 2014).

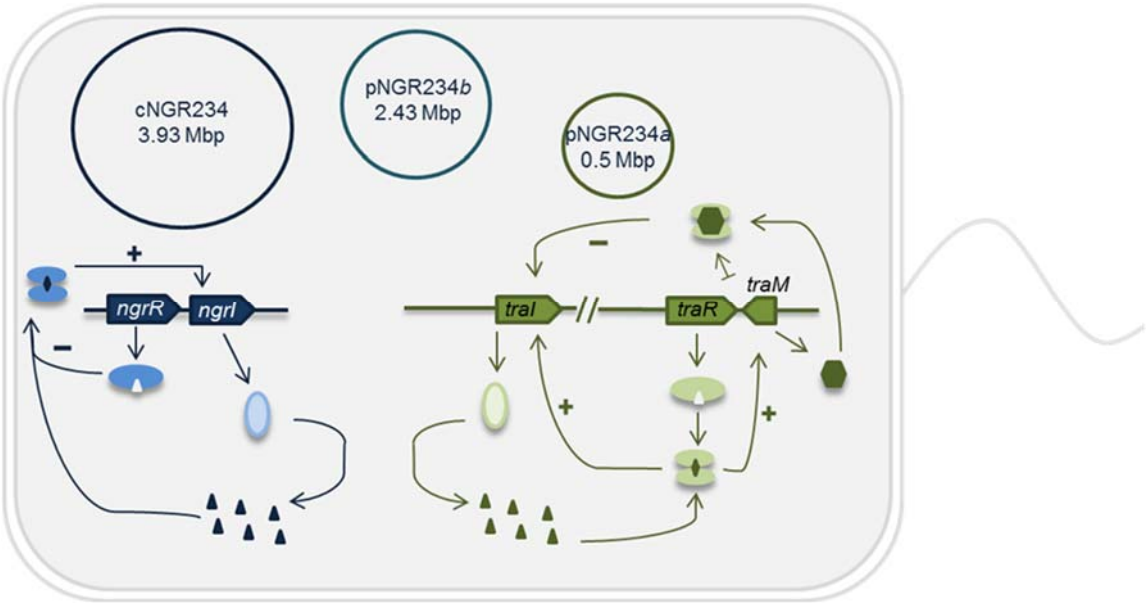

Figure 1: Quorum sensing in *S. fredii* NGR234. *S. fredii* has two QS systems. The *ngrI/R* system (blue) is encoded by the chromosome cNGR234, whereas the *traI/R* QS system (green) is located on NGR234s symbiotic plasmid pNGR234*a*. AI molecules (triangles) are produced by the AI synthases *ngrI* and *traI* (oval, light centre). The *luxR*-type regulators *ngrR*, *traR* respectively (oval, dark centre), form dimers upon the binding of two AI molecules. Thus, conformational alterations enable the regulator protein to bind to the promoter region of its respective AI synthase and increase its expression (autoinduction). The AI-TraR-complex furthermore stimulates the expression of the anti-activator *traM*. TraM (hexagon dark-green) also binds to TraR molecules and negatively regulates the expression of *traI*.

QS regulates a diverse set of genes in NGR234. In an extensive study using single AI synthase deletion mutants of NGR234 a core set of 186 genes, regulated by both AI synthases was identified (Krysciak et al., 2014). By conducting RNA-sequencing of the NGR234 WT and the AI synthase deletion mutants *S. fredii* NGR234 Δ*traI*, Δ*ngrI* respectively, 130 genes were shown to be differentially expressed in the background of a *traI* deletion. In the background of the *ngrI* deletion mutant, 280 genes showed a differential expression pattern compared to the WT. In NGR234, QS was shown to influence motility, expression of secretion systems, co-factor biosynthesis, general energy metabolism and translation amongst others (Krysciak et al., 2014). Furthermore, QS was linked to growth inhibiting effects in NGR234 (He et al., 2003).

Since QS was associated with regulation of this wide range of genes and functions, the impact of a full AI deletion mutant was investigated in another study (Grote et al., 2016). Interestingly, a complete removal of AI signals in NGR234 lead to elevated plasmid copy numbers of the symbiotic plasmid in NGR234 and to an upregulation of nearly all genes thereon (Grote et al., 2016). These results underline how important QS is for gene regulation and expression in NGR234 and raise the question how QS influences host-symbiont interaction in NGR234.

Beside encoding for QS systems, NGR234's genome further incorporates five quorum quenching (QQ) associated genes (Krysciak et al., 2011). QQ refers to the degradation or interference of QS signals. In general, QS signals can be disrupted by either degrading the signal molecule, interfering with the signal reception or by inhibiting the signal synthesis (Fetzner, 2014). Two of five identified QQ enzymes of NGR234 were biochemically characterised and were identified as a metallo-β-lactonase, QsdR1, and a dienelactone hydrolase, DlhR. Both belong to the superfamily of lactonases (Krysciak et al., 2011). Lactonases degrade QS signals by hydrolytic cleavage of the homoserine ring of the AHL AI molecules that many Gram-negative bacteria utilise (Fetzner, 2014). Other soil bacteria like *A. tumefaciens* also synthesise QQ lactonase enzymes that were shown to degrade its own QS signal (Fetzner, 2014; Grandclément et al., 2015). These findings highlight that not only QS signals may shape and interfere with NGR234's surroundings but also that possible signals may be altered by other soil dwelling bacteria.

2.3.1 The *repABC* plasmid family

The plasmid borne QS system of NGR234, the *traI/traR* system, is located on the symbiotic plasmid pNGR234*a.* The symbiotic plasmid, as well as the megaplasmid, belong to the family of *repABC* plasmids. This family of plasmids is abundantly found in α-Proteobacteria like *A. tumefaciens* and NGR234 (Cevallos et al., 2008; Freiberg et al., 1997; Pinto et al., 2012). They are characterised by the *repABC* operon, encoding for three distinct genes in this specified order: *repA-repB-repC.* The operon encodes genes for replication, segregation and partitioning of the respective plasmid (Cevallos et al., 2008; Pinto et al., 2012). RepC is essential for initiating replication (Pappas and Winans, 2003a) and it is the limiting factor. So far, *repC* like genes were only found in α-Proteobacteria (Pinto et al., 2012). Several studies indicate that the *oriV* (the origin of replication) is located inside the coding sequence of *repC*, marked by an A- and T-base rich DNA region (Cervantes-Rivera et al., 2011; Pinto et al., 2012). RepA and RepB are ParA-like and ParB-like proteins and are involved in plasmid partitioning. RepB binds to

RepA, showing a high affinity to a palindromic sequence designated *parS*, a centromere-like structure, in order to direct binding of RepA to the *parS* site. These *parS* sites were found to either lie within the intergenic region of *repA* and *repB* or up- or downstream of the *repABC* operon (see Figure 2) (Pappas and Winans, 2003a; Pinto et al., 2012).

Many rhizobia species harbour more than one *repABC* type plasmid. To ensure that each of these plasmids is stably replicated and maintained in the population, replication is controlled by a tight regulatory network. Plasmids using the same replication mechanism normally cannot co-exist in one cell, since plasmids compete for replication factors, proteins and binding sites (Ebersbach et al., 2005; Novick et al., 1976). Furthermore, cells cannot determine that each plasmid has been replicated according to its plasmid copy number and has been segregated into the daughter cells (Ebersbach and Gerdes, 2005). To overcome this problem, plasmids are grouped into certain incompatibility groups, characterised by incompatibility factors (Novick et al., 1976; del Solar et al., 1998). Each of the *repABC* plasmids in one cell belongs to a different incompatibility group, securing the replication of this plasmid in a characteristic plasmid number and thereby providing an instrument for stable plasmid maintenance. In *repABC* type plasmids, the plasmid copy number is controlled by the expression rate of RepC. Due to the operon structure of this plasmid's replication genes, expression of RepA, RepB and RepC is initiated by the *repA* promoter (Pérez-Oseguera and Cevallos, 2013). In *Rhizobium etli* and *R. leguminosarum,* RepA and RepB negatively affect the activity of the *repA* promoter and thereby negatively regulate RepC expression (Pérez-Oseguera and Cevallos, 2013; Żebracki et al., 2015). In *Agrobacterium* spp. a single point mutation within the coding region of *repB* leads to the increase of the plasmid copy number, further underlining the regulatory function of *repB e.g.* for replication control (Vaghchhipawala et al., 2018). Another factor regulating the plasmid copy number and also the plasmid incompatibility of *repABC* plasmids, is a counter-transcribed non-coding RNA that lies within the intergenic region of *repB* and *repC* (Chai and Winans, 2005; Izquierdo et al., 2005; MacLellan et al., 2005; Venkova-Canova et al., 2004). Finally, replication of *repABC* plasmids is controlled by a *parS* site, downstream of *repC* (Pérez-Oseguera and Cevallos, 2013). Together with RepA, RepB and the non-coding RNA, *parS* strictly regulate the copies of *repABC* plasmids.

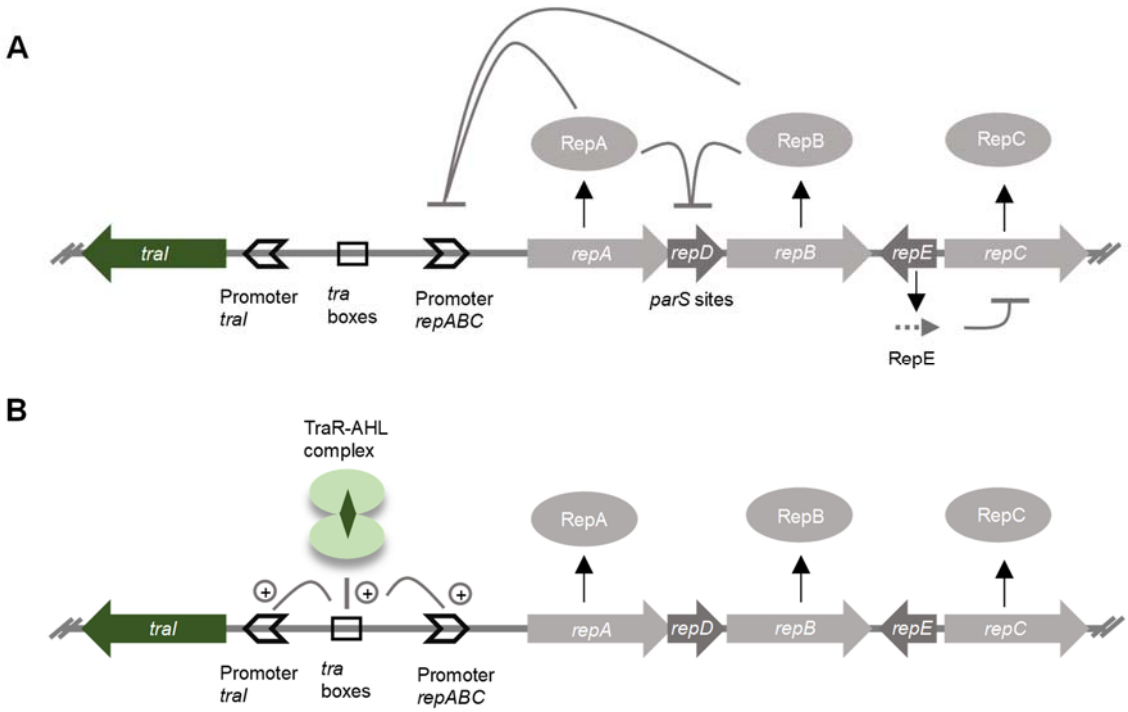

Figure 2: Schematic of RepABC operon regulation of Ti-plasmid in *Agrobacterium tumefaciens*. According to Pinto et al. (2012). **A:** Regulation of *repABC* expression by RepA and RepB themselves, autoregulating the operon expression and inhibiting the binding to *parS* sites. Further, expression of RepC is regulated by a counter-transcribed RNA encoded by *repE*. **B:** Under QS conditions, the QS regulator TraR binds to the AHL-AI and forms a dimer. This TraR-AHL complex stimulates the expression of the respective AI synthase TraI as well as the promoter activity of the *repABC* operon, resulting in an elevated copy number in *A. tumefaciens* induced by QS.

2.3.2 The symbiotic plasmid pNGR234a

Since NGR234 was shown to induce nodules on a wide range of plants, studies were conducted to decipher its genetic background and determine factors that drive its broad host range. Even before the complete genome of NGR234 was sequenced (Schmeisser et al., 2009), the sequence of NGR234's symbiotic plasmid, pNGR234*a*, was published (Freiberg et al., 1996; Viprey et al., 2000). The symbiotic plasmid encodes for nearly all genes that are needed for the establishment of symbiosis and nitrogen fixation (Broughton et al., 1984). The 0.54 Mbp replicon belongs to the group of *repABC* plasmids as described above. In total, the plasmid encodes for 499 genes and, in addition to these, 251 small open reading frames (small ORFs) were just recently identified (Petersen, 2019; Schmeisser et al., 2009). The function of these small ORFs in general is still the focus of ongoing research, but first studies observed regulatory functions for some of these small ORFs regarding *e.g.* plasmid copy number. When deleting the 153 nucleotides sized small ORF *repX*, it was shown that NGR234 lost its symbiotic plasmid, strongly indicating a role in either plasmid stability

or segregation (Petersen, 2019). Furthermore, the symbiotic plasmid harbours a diverse set of genes helping NGR234 to establish a successful symbiosis with 120 plant genera (Pueppke and Broughton, 1999; Trinick, 1980). The symbiotic plasmid enables NGR234 to synthesise at least 80 different NOD factors, which are one element determining NGR234's remarkable host range (Price et al., 1996; Unay and Perret, 2020).

2.4 Phenotypic heterogeneity

When QS was first discovered it was thought to uniformly induce certain genetic expression patterns in a bacterial population. In general, bacteria of an isogeneic population were expected to behave the same when detecting a specific environmental trigger. However, recent studies have shown that the bacteria of one population experience different gene expression or expression intensities in answer to a specific signal or cue. This phenomenon was termed phenotypic heterogeneity, emphasising the isogeneic background of bacteria showing different levels of gene expression in response to a signal and implicating the non-inheritable character of phenotypic heterogeneity (see Figure 3) (Ackermann, 2015; Smits et al., 2006). The reasons why bacteria show phenotypic heterogeneity have been studied in a broad range of bacterial strains so far, and phenotypic heterogeneity was observed for several traits like persistence, competence, biofilm formation, bioluminescence, QS and others (Abda et al., 2015; Anetzberger et al., 2009; García-Betancur et al., 2017; Grote et al., 2014). The mechanisms of phenotypic heterogeneity can either lay in stochastic differences of chemical molecules or proteins within the cell, causing a heterogeneous gene expression in an isogeneic population, or fluctuations in the micro-environment of bacteria of the same population in biofilms *e.g.*, division of labour or bet hedging (Ackermann, 2015; Bettenworth et al., 2019). New studies showed that phenotypic heterogeneity can also be the result of a riboswitch regulation. In *Lactococcus lactis* phenotypic heterogeneity is regulated by a riboswitch, modulating the expression of the *met* transporter operon by sensing the number of uncharged Met-tRNAs (methionine transporter RNA) (Hernandez-Valdes et al., 2020). Phenotypic heterogeneity can enable populations to survive sudden changes in their environment and to cope with changing conditions as well as save resources (Ackermann, 2015; Bettenworth et al., 2019).

Phenotypic heterogeneity was also observed in NGR234. When analysing the QS system expression comparing the exponential and the stationary growth phase, Grote

et al. found that nearly 70 % of the cells did not express *traI* and 60.5 % of the cells did not express *ngrI* during the exponential phase, whereas in the stationary growth phase, 74.1 % and 84.4 % of cells expressed *traI* and *ngrI*, respectively (Grote et al., 2014). Furthermore, it was analysed how deletion of either one of the AI synthases influences the observed phenotypic heterogeneity and how plant root exudates could alter the observed effects. Investigating the expression of *traI* and *ngrI* after deletion of the respective AI synthases lead to the astonishing effect that phenotypic heterogeneity was nearly abolished and almost all cells expressed either *traI* or *ngrI* homogeneously. A very similar observation was made when NGR234 cells were grown in the presence of plant root exudates (Grote et al., 2014). Additionally, phenotypic heterogeneity expression patterns of the QQ genes *dlhR*, a dienelactone hydrolase, and *qsdR1,* a metallo-β-lactamase, were analysed (Krysciak et al., 2011). In general, the observed phenotypic heterogeneity of the QQ genes was more pronounced compared to the AI synthases, but expression could be altered into more homogeneous levels when adding octopine, a flavonoid secreted by plant roots. These results indicate an AI-dependent and - independent, or host-derived, expression control of AI synthases and QQ genes modulating phenotypic heterogeneity in NGR234 (Grote et al., 2014).

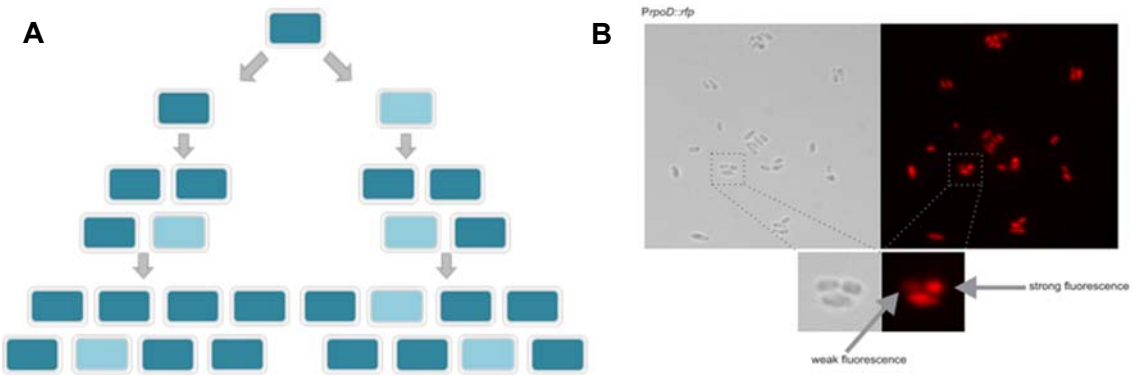

Figure 3: Phenotypic heterogeneity in an isogeneic bacteria culture. **A:** Scheme of phenotypic heterogeneity in an isogeneic bacteria population. Ancestor cell and daughter cells can differ in their gene expression level comparing one gene or operon (light blue versus blue). Even though cells receive the same environmental signals and live under the same conditions, gene expression levels can fluctuate. These fluctuations are not inheritable and therefore only influence the phenotype. **B:** Phenotypic heterogeneity in NGR234. Cells carry promoter fusion of *S. fredii* NGR234 *rpoD* gene fused to dsRed fluorescent protein (adapted from Grote et al., 2014).

2.5 Intention of this work

This work is offering a deeper insight and knowledge of the complex regulatory networks that control not only QS, but how it is linked to phenotypic heterogeneity in *S. fredii* NGR234. Additionally, a better understanding of how QS is connected to plasmid copy number control and nodulation was gained. By using real-time

quantitative PCR (polymerase chain reaction) the plasmid copy number of NGR234s' symbiotic plasmid pNGR234*a* was determined under different conditions, with special attention on how other rhizobia species influence the copy number with their AI. Another aim of this work was to analyse phenotypic heterogeneity of QS AI synthase genes, as well as a QQ gene of NGR234 by CLSM. This was done using fluorescent protein promoter fusions in the background of deletion mutants of the previously identified novel µ-proteins RepX and NGR_a01725 and *S. fredii* ANU265, a NGR234 strain cured of its symbiotic plasmid. Furthermore, nodulation experiments were conducted to evaluate the effect of QS, or QS defective mutants respectively, and the above-mentioned µ-proteins on nodulation of *Vigna unguiculata*.

3 Material and Methods

3.1 Bacterial strains, primers, and vectors

All bacterial strains used in this study are listed in Table 1.

Table 1: Bacterial strains used in this study.

Strain	Characteristics	Reference
Burkholderia glumae PG1	WT strain by CBS 322.89 (CBS, Utrecht, The Netherlands)	(Frenken et al., 1992)
Burkholderia glumae PG2	Deletion of *bgaI 1* AI synthase in *B. glumae* PG1; Gen^R	(Gao et al., 2015b)
Burkholderia glumae PG3	Deletion of *bgaI 2* AI synthase in *B. glumae* PG1; Gen^R	(Gao et al., 2015b)
Burkholderia glumae PG4	Deletion of *bgaI 3* AI synthase in *B. glumae* PG1; Gen^R	(Gao et al., 2015b)
E. coli DH5α	supE44 ΔlacU169 (Φ80 lacZ ΔM15) hsdR17 recA1 endA1 gyrA96 thi-1 relA1	Invitrogen (Karlsruhe, Germany; Hanahan 1983)
S. fredii ANU265	a Muc^+ Sym of strain NGR234; $Spec^R$	(Morrison et al., 1983)
S. fredii ANU265 pBBR1MCS-5::P*traI_gfp*::P*ngrI_dsRed*::P*qsdR1_mCerulean*	ANU265 strain carrying broad host range vector pBBR1MCS-5 with promoter fusions of P$ngrI_{NGR234}$*_dsRed,* P$traI_{NGR234}$*_gfp;* P$qsdR1_{NGR234}$*_mCerulean;* Gen^R	This work
S. fredii NGR234	WT, Rif^R	(Trinick, 1980)
S. fredii NGR234 pBBR1MCS-5::P*traI_gfp*::P*ngrI_dsRed*::P*qsdR1_mCerulean*	NGR234 strain carrying broad host range vector pBBR1MCS-5 with promoter fusions of P$ngrI_{NGR234}$*_dsRed,* P$traI_{NGR234}$*_gfp;* P$qsdR1_{NGR234}$*_mCerulean;* Gen^R	This work
S. fredii NGR234 *ΔngrIΔtraI copy+*	Deletion of AI synthases *ngrI* and *traI.* Together with *traI* gene, 5'UTR of pNGR234*a* new identified ORF *repX* deleted; Gen^R	(Grote et al., 2016; Krysciak et al., 2014)

Strain	Characteristics	Reference
S. fredii NGR234 *ΔngrIΔtraI*	Deletion of AI synthases *ngrI* and *traI.* 5'UTR of pNGR234*a* new identified ORF *repX* intact	(Petersen, 2019)
S. fredii NGR234 *ΔngrI*	Deletion of AI synthases *ngrI.* Gen^R	(Grote et al., 2016; Krysciak et al., 2014)
S. fredii NGR234 *ΔtraI copy+*	Deletion of AI synthases *traI.* Together with *traI* gene, 5'UTR of pNGR234*a* new identified ORF *repX* deleted; Gen^R	(Grote et al., 2016; Krysciak et al., 2014)
S. fredii NGR234 Δ*repX*	Deletion of pNGR234*a* small ORF *repX*	(Petersen, 2019)
S. fredii NGR234 Δ*repX* pBBR1MCS-5::P*traI_gfp::*P*ngrI_dsRed::*P*qsdR1_mCerulean*	NGR234 Δ*repX* strain carrying broad host range vector pBBR1MCS-5 with promoter fusions of P$ngrI_{NGR234}$*_dsRed,* P$traI_{NGR234}$*_gfp;* P$qsdR1_{NGR234}$*_mCerulean;* Gen^R	This work
S. fredii NGR234 Δ*a1725*	Deletion of pNGR234*a* small ORF NGR_a01725, mixed culture with cell harbouring pNGR234*a* and cells without pNGR234*a*	(Petersen, 2019)
S. fredii NGR234 Δ*a1725+*	Deletion of pNGR234*a* small ORF NGR_a01725, all cells harbour the pNGR234*a* plasmid	(Petersen, 2019)
S. fredii NGR234 Δ*a1725+* pBBR1MCS-5::P*traI_gfp::*P*ngrI_dsRed::*P*qsdR1_mCerulean*	ANU265 strain carrying broad host range vector pBBR1MCS-5 with promoter fusions of P$ngrI_{NGR234}$*_dsRed,* P$traI_{NGR234}$*_gfp;* P$qsdR1_{NGR234}$*_mCerulean;* Gen^R	This work
S. fredii USDA257	WT, Rif^R	(Keyser et al., 1982)

Primers used in this study are listed in the following table (Table 2). Vectors and constructs utilised in this study are referenced in Table 3.

Table 2: Primers used in this study. Forward binding primers are named with a 'for'. Reverse binding primers are marked with a 'rev'. A 'RT' indicates primers used for real-time PCR.

Primer	Sequence [5' - 3']	Reference
M13-20 for	TTGTAAAACGACGGCCAGTG	Eurofins MWG Operon (Ebersberg, Germany)
M13 rev	GGAAACAGCTATGACCATGA	Eurofins MWG Operon
RT_c03800_for	GCGAGATGAAGGGCTATCTGG	(Grote et al., 2016)
RT_c03800_rev	GCGCGACGTCCTTGATATG	(Grote et al., 2016)
RT_recA_for	CGGCTCGTAGAGGACAAATCG	(Grote et al., 2016)
RT_recA_rev	CAATGATGCGCCCTTTCGG	(Grote et al., 2016)
RT_repA_for	GCAGCAGTTCCCACCGAATG	(Grote et al., 2016)
RT_repA_rev	GCACGTAGTTCCTGGCTTCC	(Grote et al., 2016)
RT_nifB_for	GCTTGAAAGCCTGACCAACAC	(Grote et al., 2016)
RT_nifB_rev	GGCGCAGTCATATTTGCGATTG	(Grote et al., 2016)

Table 3: Vectors and constructs utilised in this study.

Vector	Characteristics	Reference
pGEM-T	T cloning vector, Amp^R	Promega Corporation (Madison, USA)
pBBR1MCS-2	Broad host range vector, low copy number, Kan^R	(Kovach et al., 1995)
pBBR1MCS-5	Broad host range vector, low copy number, *rep*, *mob*, *lacZ*, Gen^R	(Kovach et al., 1995)
pBBR1MCS-5::P*traI_gfp::*P*ngrI_dsRed::*P*qsdR1_mCerulean*	broad host range vector pBBR1MCS-5 with promoter fusions of P*ngrI*$_{NGR234}$*_dsRed,* P*traI*$_{NGR234}$*_gfp;* P*qsdR1*$_{NGR234}$*_mCerulean;* Gen^R	(J. Grote, unpublished)

3.2 Growth settings and medium supplements

3.2.1 Growth medium and conditions

All media used in this study were autoclaved prior to use. Heat unstable components were sterile filtered with a 0.2 µm sterile, non-pyrogenic, hydrophilic filter (Dominique Dutscher SAS, Brumath, France) and added after autoclaving. Bacteria belonging to the genus *Sinorhizobium* were cultivated using either tryptone-yeast (TY) medium

(Streit and Schmitz, 2004) or yeast extract mannitol (YEM) medium (Allen and Allen, 1950). Cultivation in liquid or on solid media, supplemented with the appropriate antibiotics was conducted at 28 °C for 2-5 days. Lysogeny broth (LB) medium (Bertani, 1951) was used to grow *Escherichia coli* and *Burkholderia glumae* strains. *B. glumae* was grown at 28 °C for 2-5 days as other rhizobia strains, whereas *E. coli* incubation was conducted at 37 °C overnight.

3.2.2 Medium supplements

In order to select specific bacterial strains and to prevent contamination, antibiotics were used during cultivation as supplements (see Table 4). Further, supplements like isopropyl β-d-1-thiogalactopyranoside (IPTG) and 5-bromo-4-chloro-3-indolyl-β-D-galactopyranoside (X-Gal) were in use.

Table 4: Antibiotics and supplements used in this study.

Supplement	Final concentration [µg/mL]	Stock solution [mg/mL]	Solvent	Treatment
Ampicillin (Amp)	50 – 100	100	70 % EtOH	-
Gentamycin (Gen)	10	50	H_2O_{bidest}	-
Kanamycin (Kan)	50	50	H_2O_{bidest}	-
Rifampicin (Rif)	25	25	100 % MeOH	-
Spectinomycin (Spec)	50	50	H_2O_{bidest}	-
Tetracycline (Tet)	5	5	70 % ETOH	-
IPTG	100	100	H_2O_{bidest}	Sterile filtering
X-Gal	50	50	DMF	Sterile filtering

3.3 Molecular biology techniques

All molecular cloning techniques, including restrictions, ligations and bacterial standard transformations, utilised in this work were done in general according to Green and Sambrook (2012) and according to the enzyme manufacturer's instructions, respectively. Restrictions were done using restriction enzymes commercially available by Thermo Fisher Scientific™ (Thermo Fisher Scientific™, Waltham, MA, USA) or provided by New England BioLabs® Inc. (New England BioLabs® Inc., Ipswich, MA, USA).

3.3.1 Plasmid preparations

Bacterial plasmid preparations were conducted with the Geneaid Presto™ Mini Plasmid Kit (Geneaid, New Taipei City, Taiwan) according to the manufacturer's instruction. Elution of plasmid DNA occurred in 50 µL H_2O_{bidest}. However, in some cases a procedure following the alkaline lysis plasmid preparation was performed according to Green and Sambrook (2012).

3.3.2 Electroporation of rhizobia

Transformation of rhizobia can be conducted using electroporation (Krysciak et al., 2014). The pBBR1MCS-5::P*traI_gfp*::P*ngrI_dsRed*::P*qsdR1_mCerulean* vector construct for monitoring phenotypic heterogeneity in *S. fredii* strains was transferred to selected strains via electroporation. For electrocompetent rhizobia cells, a fresh culture was inoculated in 50 mL YEM medium supplemented with the appropriate antibiotics and grown at 28 °C and 135 rpm until an optical density at 600 nm (OD_{600}) of 0.4-0.6 was reached. For all further steps, cells were kept on ice. Prior to cell harvest, incubation on ice for 30 min was conducted. Cell harvest was performed at 4 °C for 20 min at 4500 *g* in an Eppendorf centrifuge 5810 R (Eppendorf AG, Hamburg, Germany). After centrifugation, the supernatant was discarded, and the cells were washed four times with 4 mL of cold, sterile H_2O_{bidest}. An additional washing step with 1 mL of sterile 10 % (v/v) glycerol in dH_2O followed before the cells were resuspended in 1 mL of 10 % (v/v) glycerol. Aliquots of 100 µL were stored at -70 °C until use or directly utilised for electroporation.

For electroporation, the Gene Pulser Xcell™ Electroporation System and Gene Pulser® Electroporation Cuvettes 0.1 cm width (Bio-Rad, Hercules CA, USA) were used. Electrocompetent rhizobia cells were thawed on ice for 5 min, carefully mixed with 1-5 µL pure plasmid DNA eluted in dH_2O and incubated for 30 min on ice. After incubation, the mixture was transferred into an ice-cold cuvette, condensed water was removed, and cuvettes were subsequently put into the electroporator. For electroporation of rhizobia cells, the device was set to 200 Ω resistance, 25 µF condenser capacity and 2400 V current. After a short electric impulse occurred, the cuvette was put back onto ice for 10 min before cells were transferred into a sterile reaction tube, mixed with 1 mL of TY medium, and incubated for 24 h at 28 °C and 135 rpm before streaking onto selective plates. Clones growing on selective plates were analysed by CLSM.

3.4 Confocal microscopy to analyse phenotypic heterogeneity

To explore phenotypic heterogeneity in NGR234, the promoter fusion of three different genes was utilised and simultaneously analysed with confocal laser scanning microscopy (CLSM).

Focusing on the native promoter activity of NGR234s' AI-synthases, *traI* and *ngrI*, as well as QQ gene *qsdR1* expression, a single plasmid based triple promoter fusion was used to visualise all three gene activities in NGR234 (J. Grote, unpublished). In this construct, each promoter was fused to a specific fluorescing protein in order to distinguish promoter activity. The NGR234 *traI*-promoter controlled expression of a *gfp* (green fluorescence protein), NGR234 *ngrI*-promoter was fused to the gene coding for the red fluorescent protein *dsRed* and the NGR234 QQ-enzyme QsdR1 promoter regulated expression and production of *mCerulean*, a blue fluorescent protein.

Figure 4: Scheme of the triple promoter fusion with three fluorescent proteins to analyse phenotypic heterogeneity in NGR234. Monitoring of phenotypic heterogeneity in NGR234 was conducted by promoter fusion of NGR234 native AI-synthase promoters of *traI* to green fluorescent protein, *gfp*, and *ngrI* promoter fusion to *dsRed*. Promoter of QQ-gene *qsdR1* controlled expression of *mCerulean*, a blue fluorescent protein. All three promoter fusions were cloned together into the broad host range vector pBBR1MCS-5 (J. Grote, unpublished) and transformation of *S. fredii* strains was conducted by electroporation.

CLSM was performed with the Zeiss LSM800 with Airyscan, either using a Plan-Apochromat 63x/1.4 oil DIC M27 or a Plan-Apochromat 100x/1.4 oil DIC M27 objective (Carl Zeiss Microscopy GmbH, Jena, Germany). Detection of each fluorescence signal was performed consecutively. Microscope adjustments are indicated in Table 5. For the microscopy 3 mL of NGR234 cells were harvested at 7500 *g* for 3 min after incubation for either 24, 48, or 72 h; afterwards washed once with 1x PBS buffer and resuspended in 200 µL or 500 µL 1x PBS (Phosphate-buffered saline; diluted with sterile dH_2O from 10x PBS stock solution: 1.37 M NaCl, 27 mM KCl, 100 mM Na_2HPO_4, 18 mM KH_2PO_4, pH 7.4 according to Green and Sambrook (2012)). Washed cells were then transferred onto a cover slide for sedimentation for 45 minutes at room temperature (RT) and kept protected from light. Excessive liquid was carefully removed and an equal volume of 4 % para-formaldehyde solution (pH 6.9; Sigma-Aldrich, St. Louis MO, USA) was used to fix the cells. After fixation, the formaldehyde solution was removed by slow aspiration and 30-50 µL Mowiol® 4-88 (Sigma-Aldrich) were used to embed cells for microscopy. Until analysis, cells were kept dark and at 4 °C.

Table 5: Setting for CLSM. Imaging was conducted with the LSM 800 with Airyscan using the same general settings for all images taken to ensure comparability. Indicated are adjustments for each fluorescence protein. Detection wavelength of DsRed was set 600-700 nm to compensate for crosstalk with GFP.

Setting	dsRed	GFP	mCerulean
Excitation wavelength [nm]	561	488	405
Detection wavelength [nm]	600-700	506-600	400-506
Laser intensity [%]	10.0	10.0	15.0
Detector gain [V]	850	800	800
Detector digital gain	2.0	1.0	1.0
Pinhole [µm]	One airy unit		

3.4.1 Automated cell counting and intensity analysis

Analysing single cell images by hand, like quantifying numbers of cells and their fluorescence intensity (FI), is a process that is prone to human bias and errors. Therefore, in this work an automated workflow was established to ensure objectiveness as well as reproducible and consistent results regarding cell count and FI. For this purpose the free software CellProfiler 3.1.8. (Carpenter et al., 2006) was used and a pipeline adapted.

Before images were used for quantitative analysis, image processing occurred by adjusting grey values for each image separately with the ZenBlue 2.0 software (Carl Zeiss Microscopy GmbH, Jena, Germany) to ensure that fluorescence signals were distinguishable before background. In the software gamma value was set to 1.0 for all images. Tiff image format was chosen for export.

The parameters for the CellProfiler 3.1.8. cell analysis had to be determined by adjusting each parameter using exemplary images. The first step of the pipeline was to convert merged image files and single channel images to greyscale images employing the *ColorToGray* module. After the initial identification of bacterial cells (also referred to as *primary objects*) on greyscale images, their diameter was defined as 20-60 pixels as minimum and maximum size of cells. Cells that were only partially observable on the image were discarded. The lower and upper outlier fraction excluded signals too weak or too intense. Weak or intense signals were determined to set a threshold that uses a global robust background strategy.

Subsequent data analyses of CLSM images and output of the CellProfiler 3.1.8 pipeline was conducted using Microsoft Excel (Microsoft Corporation, Redmond WA, USA).

Images showing FI and conjunctive statistical analyses were generated using GraphPad Prism® 5.03 (GraphPad Software Inc., San Diego CA, USA).

3.5 Real-time qPCR

Real-time quantitative PCR (qPCR) is a versatile tool to monitor relative gene expression based on isolated mRNA samples that have to be reverse transcribed into cDNA before analysis (Horikoshi et al., 1992; Murphy et al., 1990; Noonan et al., 1990). However, qPCR further provides the possibility to examine relative plasmid copy numbers in bacteria. Applying the well-established '-ΔΔCt' calculation method (Livak and Schmittgen, 2001), the plasmid copy number can be determined in relation to chromosome numbers.

3.5.1 Copy number assays

The copy number of the symbiotic plasmid pNGR234*a* was analysed by qPCR. The NGR234 WT strain was compared to several NGR234 mutant strains or treatment groups. Bacteria were cultured as described in 3.2 in 50 mL of YEM medium and with appropriate antibiotics. Incubation at 28 °C was conducted for 96 h at 135 rpm before DNA cell harvest and DNA extraction. Cell harvest of 3 mL culture was performed in an Eppendorf Centrifuge 5424 R (Eppendorf AG, Hamburg, Germany) at 20,000 *g* and 4 °C for 3 min. For genomic DNA (gDNA) extraction, the Macherey-Nagel bacterial genomic DNA kit was utilised (Macherey-Nagel GmbH & Co KG, Düren, Germany). Extraction was done as recommended by the manufacturer. DNA concentration was checked with either a NanoDrop 2000 Spectrophotometer (Thermo Fisher Scientific™, Waltham, MA, USA) or the Implen NanoPhotometer® NP80 (Implen Inc., Westlake Village CA, USA). Each DNA sample was subsequently diluted to a final concentration of 50 ng/µL using H_2O_{bidest} and frozen at -20 °C until usage.

Table 6: Master mix for plasmid copy number qPCR. Applied Biosystems 2x SYBR Select Master Mix (Applied Biosystem, Thermo Fisher Scientific) was used for qPCR containing polymerase and buffer.

Component	Volume per reaction [µL]	Final concentration
2x SYBR Select Master Mix	8.0	1
Primer forward 100 pmol	0.4	2500 nM
Primer reverse 100 pmol	0.4	2500 nM
H_2O	6.8	-
DNA	0.4	1.25 ng/µL
Final Volume	16.0	-

For qPCR, the reaction setup as stated in Table 6 was prepared with the Applied Biosystems™ SYBR™ Select Master Mix (Applied Biosystems (Thermo Fisher Scientific)) for each used primer pair. Each sample was run in four technical replicates and three biological replicates. The prepared master mix, including either sample or no template control (NTC), was spread onto a Hard-shell® 96-Well PCR Plate (Bio-Rad, Hercules CA, USA) with 16 µL each well and sealed with the Microseal 'B' PCR Plate Sealing Film (Bio-Rad) before qPCR. The Bio-Rad CFX96™ Real-Time Detection System was used for the qPCR run and programmed as described in Table 7. Following the qPCR run, a melting curve was generated to ensure correct PCR template amplification.

For data analysis the Bio-Rad CFX Manager 3.1 software (Bio-Rad, Hercules CA, USA) was utilised. Each RT-qPCR run was analysed using NGR234 WT gDNA as a control group and mutant strain gDNA or treatment group was compared to NGR234 WT. The calculation threshold (Ct) was set manually for all targets. Each sample initially was examined regarding its replicate stability. Ensuring replicate stability, sample replicates varying more than 0.5 Ct values from median Ct value were excluded from analysis.

Table 7: Program utilised for qPCR analysis. The qPCR was run on BioRad CFX96 Touch™ Real-Time PCR Detection System (Bio-Rad Laboratories Inc). After elongation, a plate fluorescence read was conducted. To identify correct PCR products, a melting curve with a temperature increment of 0.5 °C for 5 seconds each and a fluorescence read after each step was generated.

Step	Time [s]	Temperature [°C|	Cycles
Initial denaturation	180	95	1
Denaturation	15	95	39
Primer annealing	20	60	
Elongation	20	72	
Analysis		Plate read	
Melt curve	5	65 →95 (+0.5 °C)	1
Analysis		Plate read	

A comparison of the relative plasmid copy number was conducted by using two reference genes that are encoded on the chromosome, C_03800 and *recA*. Furthermore, measurements of the expression of these chromosomal genes were used to normalise gene expression differences, comparing the control group and the treatment group. The ratio of chromosome gene expression and two target genes of

the symbiotic plasmid, *nifB* and *repA*, in the untreated NGR234 WT sample was used for normalisation. This way, expression ratios of the control and the treatment samples of the target genes *nifB* and *repA* could be compared, using the '-ΔΔCt' calculation method as implemented in the Bio-Rad CFX Manager 3.1 software (Bio-Rad). A relative value for the plasmid copies per chromosome was calculated.

3.5.2 Effect of spent growth medium of other rhizobia and soil bacteria on *S. fredii* symbiotic plasmid copy number

Bacteria secret a diverse range of molecules into their environment or culture medium, respectively. Investigating the influence of these secreted molecules of NGR234 itself or bacteria also living in the soil, spent medium was utilised during cultivation. For spent medium experiments, the NGR234 strains, *S. fredii* USDA257, *S. fredii* ANU265 as well as *Burkholderia glumae* PG1 WT and its QS system mutant strains (*B. glumae* PG2, PG3 and PG4 respectively) were cultivated as described in 3.2 for 96 h in 50 mL YEM or LB medium with appropriate antibiotics. Supernatant was harvested after 96 h by centrifugation at 4 °C and 4,500 *g* for 40 min with an Eppendorf Centrifuge 5810 R (Eppendorf AG). Centrifugation was followed by decantation and sterile filtration with a 0.2 µm sterile, non-pyrogenic, hydrophilic filter (Dominique Dutscher SAS) into a new sterile 50 mL Falcon tube (Sarstedt AG & Co. KG, Nürnbrecht, Germany). Supernatant was then mixed with fresh YEM medium at a ratio of 10 % (v/v) and fresh cultures of NGR234 WT and mutants of interest were inoculated at an OD_{600} of 0.04 into this spent-fresh-medium mixture and again were incubated for 96 h at 28 °C before gDNA was extracted as described in 3.5.1. Extracted gDNA was then utilised for qPCR analysis as described in 3.5.1 to verify plasmid copy number of NGR234 symbiotic plasmid pNGR234*a*.

3.6 Nodulation assay

Since NGR234 is a natural plant root symbiont, NGR234 mutant strains were tested on one of its host plants, *Vigna unguiculata* or cowpea, analysing the influence of mutation on plant symbiosis.

3.6.1 *Vigna unguiculata* growth, infection, and nodulation assay

Plant seeds were prepared according to Irmer et al. (2015) with modifications. First, surface sterilisation occurred by washing in 70 % (v/v) ethanol for 20 min at 28 °C and 130 rpm. Ethanol was decanted and seeds covered in 35 % (v/v) H_2O_2 (Carl Roth GmbH + Co. KG, Karlsruhe, Germany) and again agitated at 28 °C and 130 rpm for

10 min. Before placing the surface sterilised seed onto 0.5 % (w/v) TY plates (see 3.2.1) or 5 mM NOD (nodulation media) plates (see Table 8) covered with sterile filter paper, seeds were washed in sterile dH_2O three times and left to dry shortly under sterile conditions. On each plate 5-6 seeds were placed, each black eye facing downward. Sealed and tinfoil wrapped plates were incubated for 2-3 days at 28 °C without light. After germination occurred, tinfoil was partly removed but roots remained covered, moving pea seedlings to 16 h light, 8 h darkness, and growing at 24 °C and 60 % relative humidity. Furthermore, plates were set up with an angle of approximately 45°. This way, the seedlings incubated for 2-3 days. Before infection, the seed's testa (seed coat) was removed. NGR234 strains used for infection were grown in TY medium with 25 µg/mL rifampicin and as described in 3.2 to an OD_{600} of approximately 0.8. One millilitre of cells was harvested at 16,100 *g* for 1 min, washed twice with liquid NOD medium and finally resuspended in an equal volume of NOD medium. Of this infection solution, 50 µL per root were used to infect *V. unguiculata* plants by carefully dropping the solution with a pipet onto the root and filter paper lying under the pea seedlings. Infected plants were put back into the climate chamber (16/8 h light/dark, 24 °C) and further grown for 7 days before transferred into growth vessels (Weck, Wehr-Öflingen, Germany) that were loosely sealed with clamps. Growth vessels contained 75-100 mL 5 mM NOD medium (pH 6.5) solidified with 1.0 % agar-agar (w/v) (Carl Roth GmbH + Co. KG). Infected plants were then again grown for 52 days (after infection) at 24 °C and 16 h light. 52 days past infection (dpi), the plants and nodules were harvested. Nodules of each plant were counted, weighted, afterwards immediately frozen in liquid nitrogen, and stored at -70 °C for further analysis.

This assay was also performed using 0.25 strength Hoagland medium (Table 9) to check if composition of different media had an influence on nodule number or nodulation itself. Nevertheless, all media used here were low nitrogen media to promote and enable nodulation on *V. unguiculata* and infection with NGR234. A comparison of the two plant growth media is given in Table A. 1.

Table 8: NOD medium composition. The concentrations of stock solutions are indicated. For preparation of 1 L NOD medium containing 5 mM N, 1 mL of stock A, B1, B2; D and E as well as 0.5 mL of stock MOB1B5b and 4 mL of stock N are used and mixed with H_2O_{bidest}. The pH value was set to 6.5 with NaOH before autoclaving (Irmer et al., 2015).

Stock solution	Component	Concentration [g/L]	Final Concentration [mM]
Stock A	$CaCl_2$ x $2H_2O$	147	1
Stock B1	KH_2PO_4	68	0.5
Stock B2	K_2HPO_4	58	0.333
Stock D	Na/Fe III EDTA	7.58	0.02065
Stock E	$MgSO_4$ x $7H_2O$	61.5	0.25
Stock MOD1B5b	$MnSO_4$ x $7H_2O$	10	0.0296
	$ZnSO_4$ x $7H_2O$	3	0.0052
	H_3BO_3	3	0.0243
	KI	0.75	0.0023
	Na_2MoO_4 x $2H_2O$	0.25	0.0005
	$CuSO_4$ x $5H_2O$	0.25	0.0005
	$CoCl_2$ x $6H_2O$	0.25	0.0005
Stock N	KNO_3	126.39	5

Table 9: Hoagland medium composition. Final concentrations are indicated for an 0.25 strength solution (Hoagland and Arnon, 1950).

Component	Final concentration [mM]
$MgSO_4 \times 7H_2O$	2
$Ca(NO_3)_2 \times 4H_2O$	5
KNO_3	5
NH_4NO_3	1
KH_2PO_4	1
$FeCl_3 \times 6H_2O$	0.0597
EDTA	0.1026
H_3BO_3	0.0463
$MnCl_2 \times 4H_2O$	0.0091
$ZnSO_4 \times 7H_2O$	0.0008
$CuSO_4 \times 5H_2O$	0.0002
$H_2MoO_4 \times H_2O$	0.0005

4 Results

4.1 Phenotypic heterogeneity in *S. fredii* NGR234

Monitoring of single cell gene expression can expand our knowledge regarding regulatory networks, interaction patterns and phenotypic heterogeneity of single cell bacteria in an isogeneic population. In this work single cell analysis by CLSM was implemented to track and compare promoter activity of *S. fredii* NGR234 AI-synthases *traI* and *ngrI* as well as *qsdR1*, coding for a metallo-β-lactamase. In a single plasmid based triple promoter construct each of these promoters were fused to a specific fluorescent protein-coding gene, *gfp, dsRed* or *mCerulean* (Figure 4)*,* to simultaneously observe all three gene expression patterns.

4.1.1 Automated cell counting and fluorescence analysis

An automated cell counting, and image analysis software pipeline was established (3.4.1). In Table 10 final settings of the automated pipeline for cell counting and fluorescence analysis of NGR234 WT and mutant single cells containing the construct pBBR1MCS-5::P*traI_gfp::*P*ngrI_dsRed::*P*qsdR1_mCerulean* are shown (Table 10). The pipeline was specifically adjusted to cells of *S. fredii*.

Table 10: Parameters utilised for counting bacteria and measuring intensity. Parameters of CellProfiler 3.1.8 pipeline for counting bacterial cells of CLSM images and calculating FI of cells in all three channels (dsRed, GFP, and mCerulean). Cells were characterised as *Primary objects* for which a typical diameter [pixels] was determined. *Bacteria* shows the setting for combined counting and calculation of all three channels.

Function	Setting	Primary object			
		Bacteria	**dsRed**	**GFP**	**mCerulean**
Identification of bacteria	Diameter	20-60			
	Lower outlier fraction	0.050	0.065	0.065	0.065
	Upper outlier fraction	0.050	0.050	0.050	0.050
	Threshold method	global, robust background			
	Variance method	standard deviation			
	Number of deviations	1.00	3.00	3.00	3.00
	Threshold smoothing scale	1.3488			
	Threshold correction factor	1.00	2.00	1.00	1.00
	Lower bound threshold	0.010	0.018	0.018	0.018
	Upper bound threshold	1.00	1.00	1.00	1.00
Separation of cells	Declumping	intensity			
Object overlay	Opacity	0.3			

To analyse the cells, first CLSM images were exported as tiff-files. Bacteria were then characterised as *primary object*. The determination of the average diameter of the bacteria cells and outlier fractions was the first step to identify cells to be analysed by the program. It should be noted that this diameter does not represent cell size in µm, but all values use arbitrary units or pixels. In general, threshold values and all other values determined for cell counting and FI analyses were set by verification of results of the CellProfiler 3.1.8. pipeline after each run and continuous optimisation. This was done using images with a limited number of cells. Less restricted settings for the overall identification of bacterial cells (Table 10, column *Bacteria*) were established to account for overlaying cells with varying fluorescent intensities. Since identification of cells or objects was performed on CLSM images showing fluorescently labelled promoter expression, objects of interest had higher light intensities compared to the background. This precondition is optimal for using the threshold method *global, robust background* chosen in this analysis. It enables the program to distinguish the fluorescing cells from a dark background. *Lower and upper outlier fraction* refer to the darkest and brightest pixels respectively that are not considered for analysis to account for artefacts that may

influence the FI measurements. As variance methods, *standard deviation* and variance values for each fluorescence channel were selected. The *Threshold smoothing scale* value as well as the *Threshold correction factor* were not changed compared to default settings. *Lower and upper bounds on threshold* were set to adjust for images where no fluorescence signal would be detectable. Determining these values can be conducted by measuring background intensity. In images with nearly no fluorescence signal, false positive signals could be detected if no *lower bounds on threshold* have been set. Based on changes in FI, *Declumping* of objects was performed by the CellProfiler 3.1.8 program. Fluorescence signals of neighbouring cells may overlap but show variances in their intensities. This phenomenon can be used to distinguish overlapping or neighbouring cells. An output image with overlays of identified objects was created at the end of cell analysis. *Opacity* value represents the transparency of the overlay in the created output.

After identification of all bacteria by creating a grey image of the merged fluorescence channel images, individual channel images were analysed. This allowed identification of vital bacteria in total, independent of single promoter activity, and each sub-set of bacteria expressing one or more promoters. Identification of bacteria as *primary objects* in single channel images was performed as described above. Parameters were set according to values given in Table 10 for the individual fluorescent channels. Applying more restrictive thresholds to the identification of single fluorescing channel objects was chosen to prevent false classification of signals as cells.

Objects that had been identified were analysed and measured with the CellProfiler 3.1.8 pipeline. Therefore, object intensities and total area occupied by objects were measured. CellProfiler 3.1.8 automatically executed several calculations during intensity measurements. For example, *Integrated Intensity, Mean Intensity, Median Intensity* or *Standard Deviation of Intensity* were evaluated for each previously identified object. The area occupied by *primary objects* was determined by implementing the *Measure Image Area Occupied* pipeline module. This module automatically reports the *Area Occupied* and *Total Area* of predefined objects. An overview of all CellProfiler 3.1.8 modules used and settings therein is shown in Figure A. 1 (chapter 7.1.1). All measurements were exported as a comma-separated values (.csv) file and further analysis was performed with Microsoft Excel. Images of FI were generated using GraphPad Prism® 5.03.

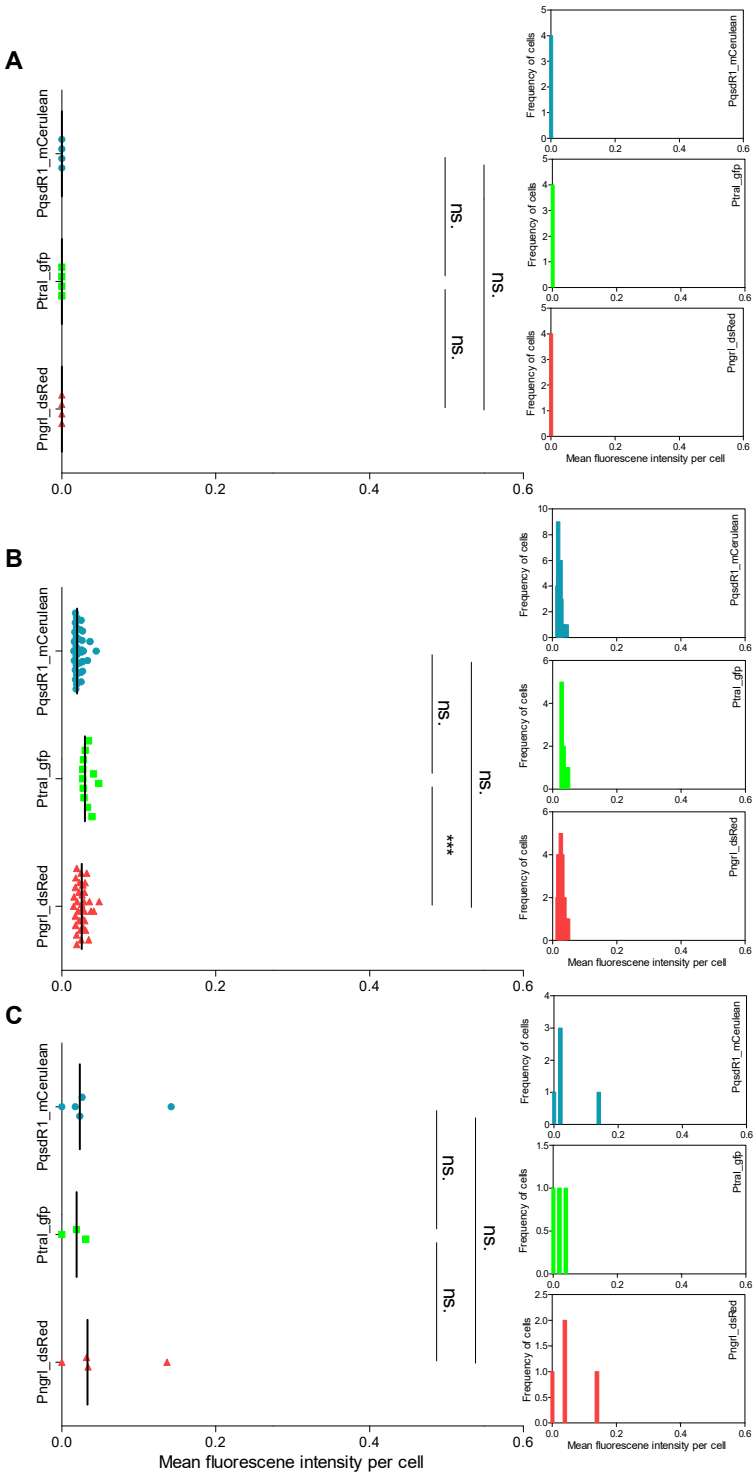

Figure 5: Mean FI of *S. fredii* NGR234 carrying the empty vector control. NGR234 WT with the empty vector control pBBR1MCS-5. Mean FI per single cell is shown on the left. On the right frequencies of cells showing distinct fluorescence intensities are given. Bacteria were grown in YEM medium with appropriate antibiotics. Cultivations were conducted at 28 °C and 135 rpm for 24, 48 or 72 h. **A:** Mean fluorescence after 24 h. **B:** Mean fluorescence after 48 h. **C:** Mean fluorescence after 72 h.

Transforming different strains of *S. fredii* NGR234 and ANU265 with one construct containing promoter fusions of both AI-synthases of NGR234 and one of its QQ lactonases, presented the opportunity to not only investigate phenotypic heterogeneity of these genes and their expression in one isogeneic population of NGR234 cells: It enabled the observation of their interaction, how µ-proteins in NGR234 or the complete loss of one replicon, the symbiotic plasmid pNGR234*a,* affects the expression of these genes. Population level studies reflect on general expression patterns in a specific population and can generate an understanding for underlying regulatory processes.

Analysing NGR234 transformed with an empty pBBR1MCS vector was used as a control for the cell counting and identification program established in this study. Only very few cells were identified by the implemented cell counting pipeline in the merged fluorescent images. Cells that were identified, were measured to show very low levels of fluorescence for each fluorescent protein fused to its respective NGR234 native promoter (see Figure 5).

4.1.2 Phenotypic heterogeneity in *S. fredii* NGR234 WT

CLSM was performed to analyse single cell and population-wide expression of the promoters of the QS AI synthases P*traI* and P*ngrI* as well as the QQ metallo-β-lactamase P*qsdR1*, in NGR234. Each of these promoters had been fused to a specific fluorescent protein and cloned into a single broad host range vector. This vector, the pBBR1MCS-5::P*traI_gfp::*P*ngrI_dsRed::*P*qsdR1_mCerulean*, enabled the simultaneous observation of the promoter expression. As seen in the CLSM images, parallel promoter activity of more than one promoter can lead to the formation of new merged colours. In order to give an impression how overlaid colours are represented, a ternary diagram in R studio was generated. It should be noted that the used colours cannot be transferred directly onto the CLSM images. However, the ternary plot may provide guidance in analysing merged colours (see Figure 6).

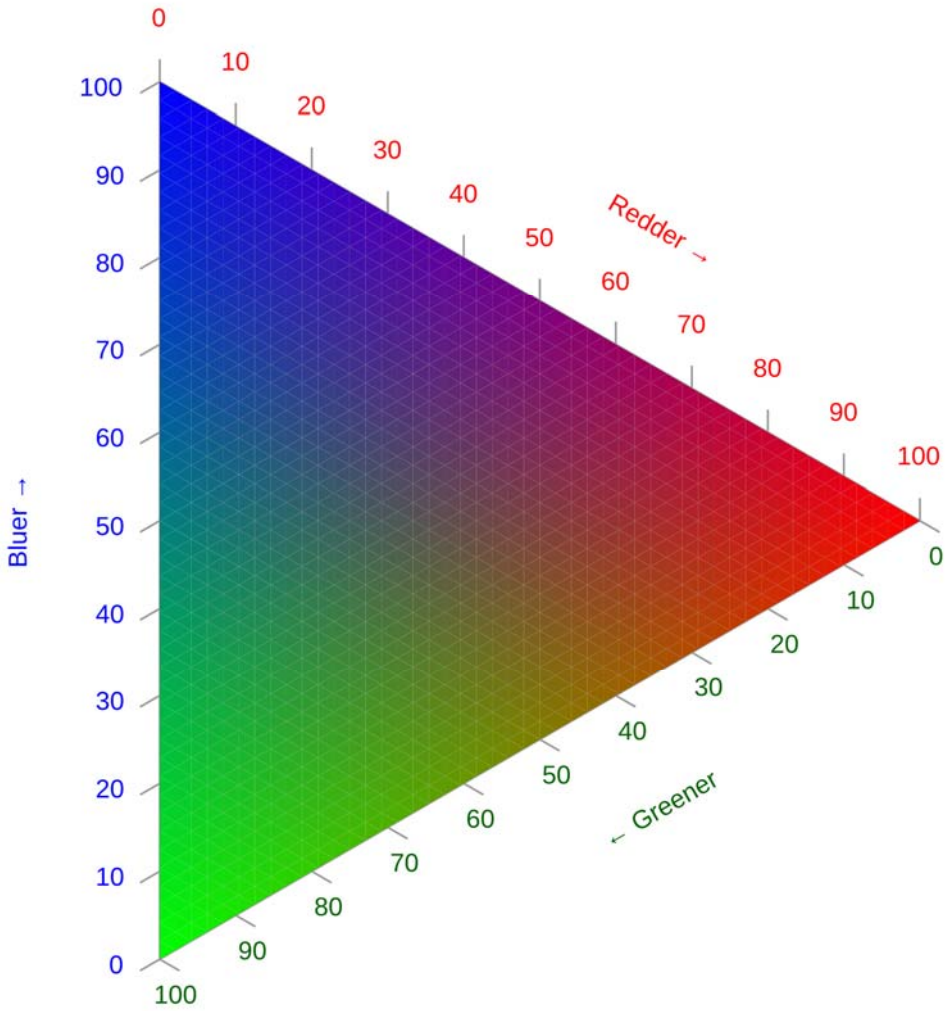

Figure 6: Ternary plot generated with R Studio using the *Ternary plot* package. The plot represents exemplary colour merging of red, green, and blue as used for display of different fluorescing signals in CLSM images. It can serve as a model to make an easier classification of how mixed promoter signals fused each to either red, green, or blue fluorophore may overlay in CLSM images and create a new merged colour. Each corner of the plot represents a single promoter expression of one promoter fusion to the respective fluorophore. The ternary plot does not strictly reflect mixed colours of images. The ternary plot was kindly provided by Dr. Güllert.

Investigating CLSM images taken after 24, 48, and 72 h of NGR234 WT showed cells in all stages of growth experienced phenotypic heterogeneity. Figure 7 represents one example of a NGR234 WT population after 48 h of growth (for growth conditions see 3.2). Clearly visible is the spatial distribution of fluorescent signals from left to right. Cells on the left side appear to express higher ratios of the *ngrI* promoter that is fused to the red fluorescent protein dsRed (see Figure 7A). On the right side the GFP (green) and mCerulean (blue) fluorescence signals dominate, representing activity of the *traI* and the *qsdR1* promoters, respectively. Nevertheless, the majority of cells displayed

multiple intermediate or mixed expression signals, indicated by merged fluorescence colour signals. These cells express two to three of the promoters of interest in parallel. Interestingly, this is not only the case for the two QS promoters, P*traI* and P*ngrI*, but also for the QQ promoter P*qsdR1*. This indicates concurrent expression of QS and QQ signals in one cell as well as on a population level.

Single cell phenotypic heterogeneity can be easily identified by examining the magnified region in Figure 7 B-E. Figure 7 B represents the merged fluorescence signal of the indicated section (white rectangle) in Figure 7 A. Simultaneously promoter expression of all three promoter constructs can be observed in nearly all cells. Cells showing an orange colour indicate a high expression level of P*ngrI_dsRed* and lower levels of P*traI_gfp* expression, whereas cells shown in yellow express both AI synthase promoters in nearly equal amounts (red and green merged to orange or yellow respectively (see Figure 6)). Single cells can be found that only express one of the three monitored promoters (see Figure 7 B-E encircled cells in green and blue). Overall, this exemplary image shows how heterogeneous the expression of QS AI synthases *traI* and *ngrI* is. The parallel expression of the QQ gene *qsdR1* is regulated heterogeneously in NGR234 WT. Furthermore, heterogeneous levels of promoter activity for each individual promoter were detectable. Some single cells showed high promoter activity, whereas adjacent cells only had mid to low levels of fluorescence, representing mid to low levels of promoter activity. These differences in fluorescence signals correlate with the phenotypic heterogeneity of P*traI*, P*ngrI* and P*qsdR1* expression (Figure 7).

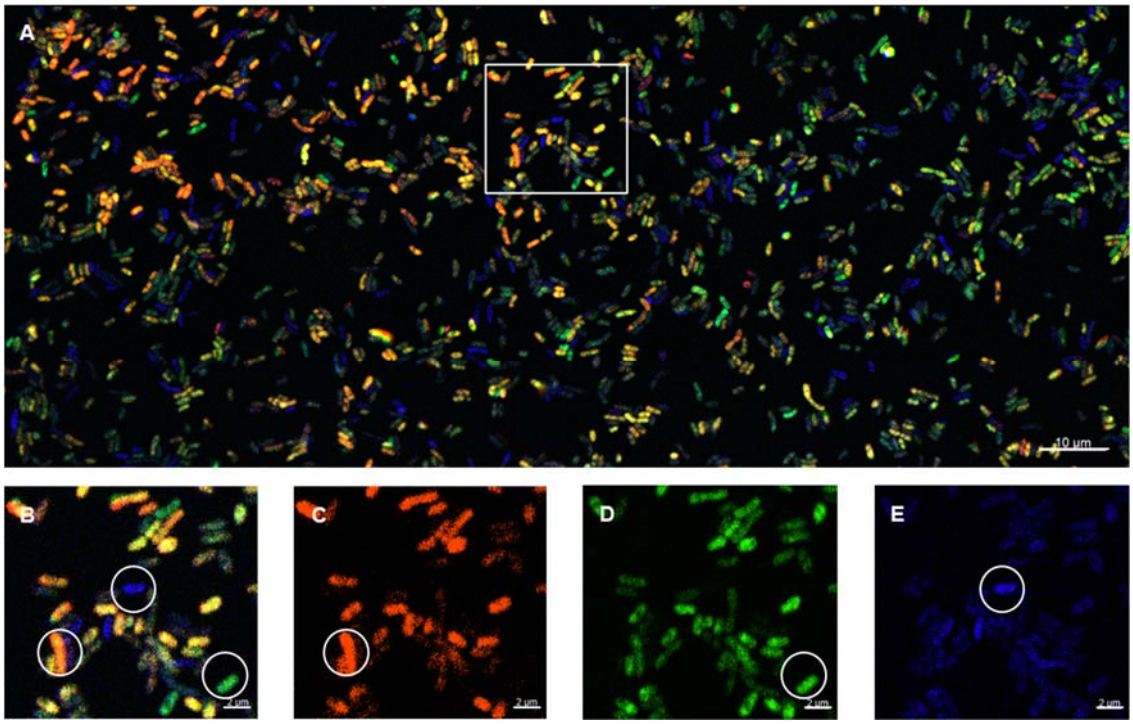

Figure 7: Phenotypic heterogeneity in *S. fredii* NGR234 WT analysed by CLSM. *S. fredii* NGR234 WT containing the pBBR1MCS-5::P*traI_gfp*::P*ngrI_dsRed*::P*qsdR1*_mCerulean vector. Incubation for 48 h in YEM medium with appropriate antibiotics at 28 °C and 135 rpm. Scale bar in section A represents 10 µm, scale bar in B-E represent 2 µm. **A:** Merged fluorescence image. Rectangle marks area magnified in Figure 7 B-E. Differential expression pattern on population level can be observed. Cells in the upper left quadrant show a higher expression of P*ngrI_dsRed*, whereas cells in the far right showed very weak P*ngrI* expression. On the other hand, expression of P*traI_gfp* and P*qsdR1_mCerulean* are the highest in cells on the right. This indicates micro-environmental influences on the QS and QQ genes in NGR234. **B:** The magnified region shown in A., merged channels. White circles highlight cells that prominently express one promoter or even show just one promoter activity at all. In general, a high degree of phenotypic heterogeneity of P*ngrI*, P*traI* and P*qsdR1* can be observed on a single cell level. **C:** Red fluorescent detection channel showing P*ngrI_dsRed* expression in most of the cells. However, phenotypic heterogeneity can be observed in cells in direct contact with each other. Therefore, not only micro-environmental effects can cause phenotypic heterogeneity in NGR234. **D:** Expression of P*traI_gfp* is very prominent and spread throughout the entire population. Nevertheless, differences in expression levels can be observed on a single cell level, representing phenotypic heterogeneity. **E:** Fluorescence channel detecting *mCerulean* expression. Expression of the promoter of QQ gene *qsdR1* is detectable in almost all cells but weak. Few cells show high levels of P*qsdR1_mCerulean* expression. Furthermore, most cells seem to express QS and QQ genes simultaneously.

Examination of the phenotypic heterogeneity in NGR234 WT over time further offers the opportunity to observe cells shifting their gene expression and how the respective ratios of expression change over time. In Figure 8 NGR234 WT cells containing the pBBR1MCS-5::P*ngrI_dsRed::*P*traI_gfp::*P*qsdR1_mCerulean* construct are shown after 24, 48 and 72 h. Each row represents one independent sample of NGR234 WT cells at the indicated timepoint (A-E, F-J and K-O), columns show designated fluorescence channels. Remarkably, a high degree of phenotypic heterogeneity can be observed. The initial growth phase (24-48 h) allows the observation of cells highly expressing the QS PtraI promoter (Figure 8 B and D, G, and I). After 72 h of growth, cells experience a

more homogeneous expression of P*traI*, even though, some single cells show no expression of P*traI_gfp* at all (Figure 8 L and N). Expression of *PngrI_dsRed* was very low in the examined cells after 24 h (Figure 8 B and C), but increased after 48 h in nearly all cells to a similar level (Figure 8 G and H). In the cells expressing P*ngrI_dsRed*, the promoter activity tends to be more homogeneous overall, but heterogeneity can be observed on cells expressing P*ngrI* at all (Figure 8 G and H, L and M). During all timepoints, a low but detectable expression of P*qsdR1* could be observed (Figure 8 B and E, G and J, L and O). This basal yet persistent expression of this QQ gene may indicate a regulatory function in NGR234 WT. Parallel expression of QS and QQ genes was observable during all growth phases (Figure 8 B, G and L).

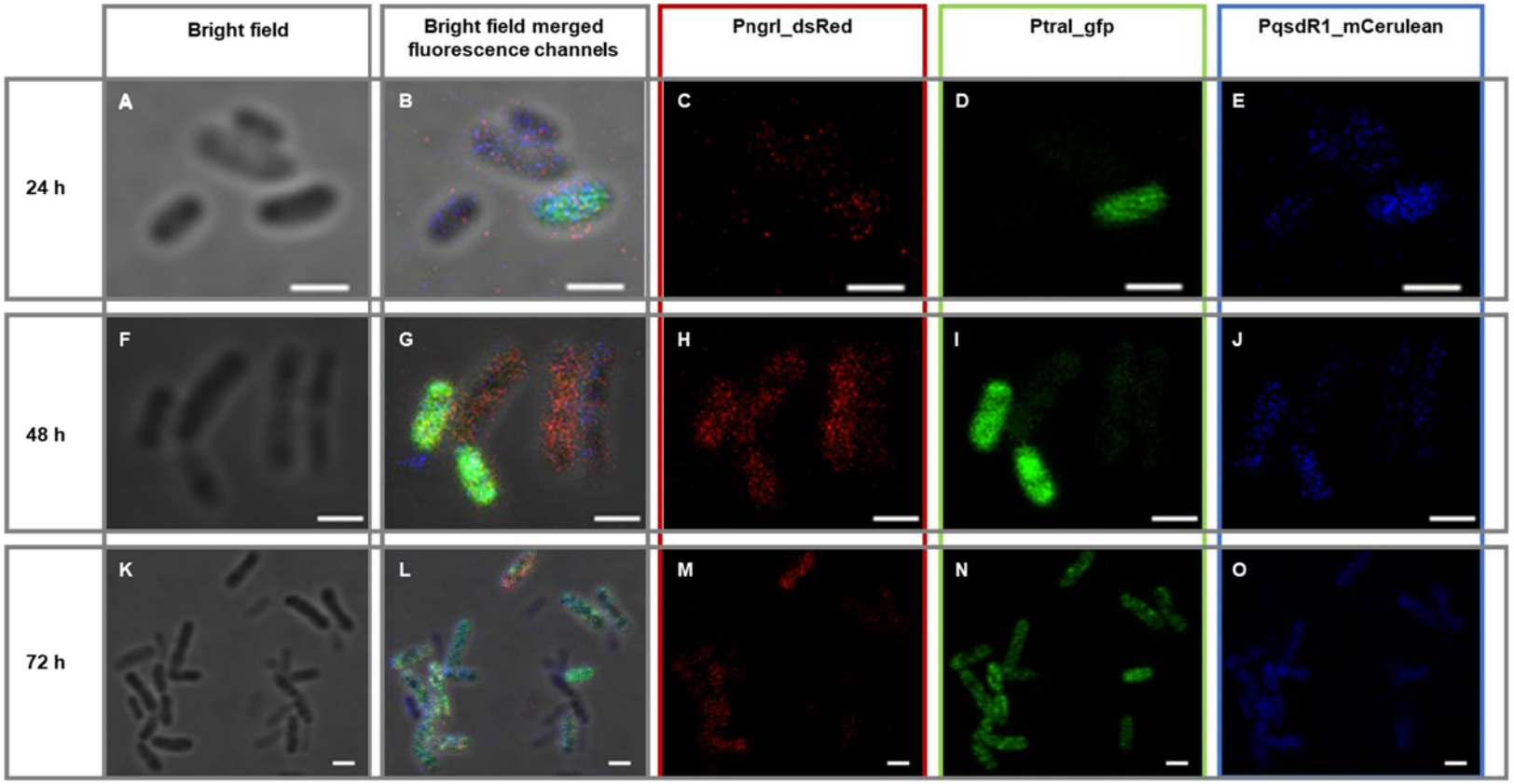

Figure 8: Phenotypic heterogeneity in *S. fredii* NGR234 WT over time. NGR234 WT cells showing phenotypic heterogeneity in CLSM analysis. Cells contain the pBBR1MCS-5::P*ngrI_dsRed*::P*traI_gfp*::P*qsdR1_mCerule*an promoter construct to analyse the expression of AI synthases and QQ gene expression in one cell in parallel. Scale bar represents 1 µm**. A-E**: NGR234 WT cells after 24 h incubation. **F-J**: NGR234 WT cells after 48 h of incubation**. K-O:** NGR234 WT cells after 72 h incubation. From left to right: bright field image, bright field image overlaid with merged fluorescence signals, red fluorescence signals representing PngrI_dsRed expression, green fluorescence signals representing P*traI_gfp* expression and blue fluorescence expression representing PqsdR1_mCerulean expression. Phenotypic heterogeneity was most prominent after 48 h of growth for PtraI promoter activity. During later growth stages (72 h), expression activity of PtraI was more homogeneous. Activity of PqsdR1 was weak but observable over all time points. Expression activity of PngrI showed its peak after 48 h.

By analysing the full set of CLSM images for NGR234 WT cells with the CellProfiler 3.1.8 pipeline, the mean integrated fluorescence intensity per cell (MIFISC) was calculated. This value represents the average integrated FI or the signal per analysed image divided per total number of cells analysed for the respective fluorescence channel and image. Results per image were again averaged and standard deviation was calculated. This enables the overall analyses of all CLSM images taken for one genotype and a comparison of values between genotypes, considering the differences in the number of total cells that have been observed.

In Table 11 values of the MIFISC are given for NGR234 WT. Overall, mean fluorescence was highly variable for each timepoint and in general. Due to the relatively low number of cells analysed after 24 h, MIFISC was the highest at this timepoint while also showing the highest level of standard deviation. This indicates an increased level of phenotypic heterogeneity in NGR234 WT cells after 24 h. Decreasing levels of standard deviation over time represent an increase of homogenous expression of the analysed promoter activity. It is notable that most detected cells highly expressed P*traI_gfp* compared to P*ngrI_dsRed* expression, indicating a more prominent role of *traI* AI synthase in NGR234 WT cells independent of time.

Table 11: MIFISC of *S. fredii* NGR234 WT. The mean integrated fluorescence intensity per cell was calculated. The mean value of integrated fluorescence was divided by the total number of cells analysed.

P*ngrI_dsRed*			**P*traI_gfp***			**P*qsdR1_mCerulean***			
Mean value	Std. dev.	No. of cells	Mean value	Std. dev.	No. of cells	Mean value	Std. dev.	No. of cells	Incubation time [h]
7.76	6.36	270	9.35	7.68	310	22.32	42.27	318	24
3.77	4.48	1,432	3.50	3.64	1,640	6.01	10.30	1,202	48
1.71	1.11	1,977	0.98	0.76	3,019	1.10	0.99	2,521	72

Looking at each cell individually, as well as on a population level provided the opportunity to further deepen the knowledge of how single cell gene expression shapes population-wide response. Every detected single cell was analysed regarding its mean FI and plotted for each individual fluorescence channel (Figure 9 left). In this way the whole range of FI of a NGR234 WT population can be shown. Additionally, it gives an overview of how minimal and maximal FI differ from the FI median (black bar) and

mean of the population. Secondly, Figure 9 shows distribution of cells regarding their individual FI (Figure 9, histogram right side). Independent of the timepoint of analysis, a high variability and heterogeneous expression of the three monitored promoters could be observed. Comparing the population median values, significant differences between individual promoter activities were partially detectable.

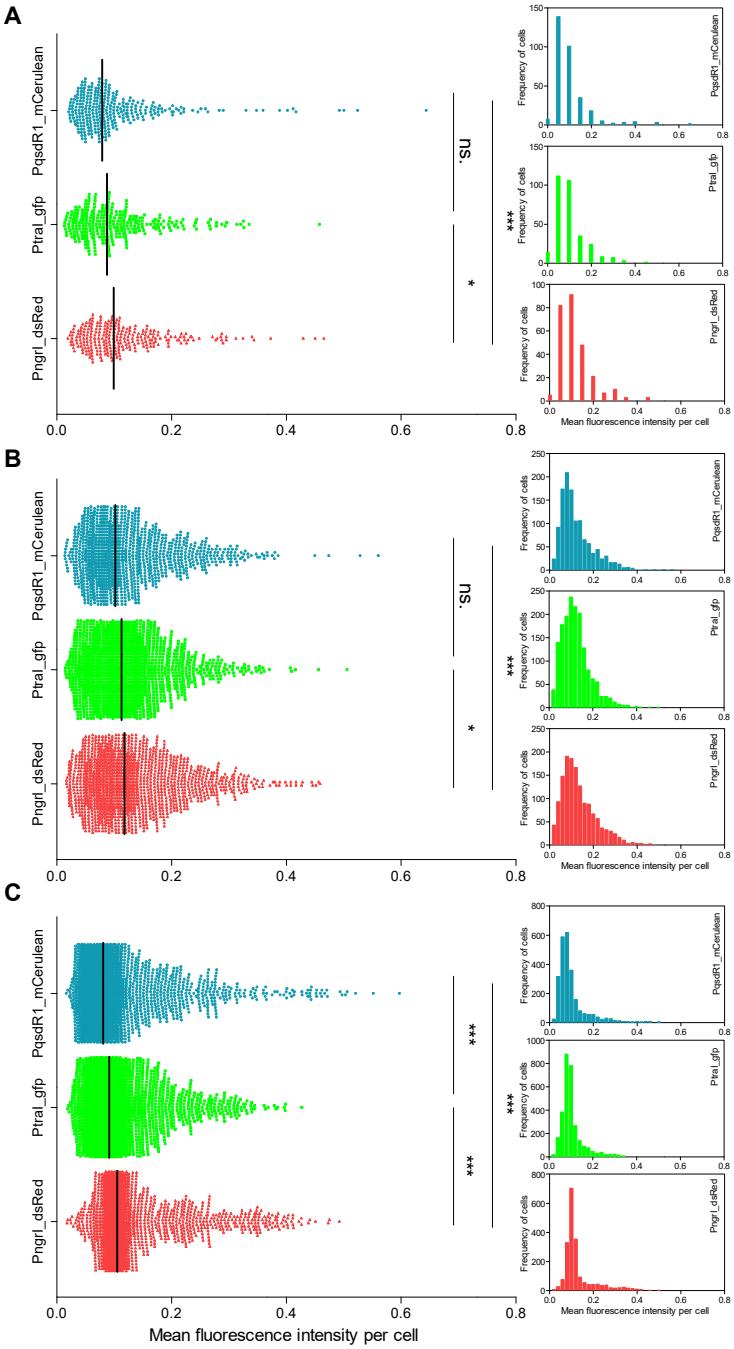

Figure 9: Phenotypic heterogeneity in *S. fredii* NGR234 WT. Mean FI per single cell is shown on the left. On the right frequencies of cells showing distinct FI are given. Bacteria were grown in YEM medium with appropriate antibiotics. Cultivations were conducted at 28 °C and 135 rpm for 24, 48 or 72 h. Cells carrying the pBBR1MCS-5::P*traI_gfp*::P*ngrI_dsRed*::P*qsdR1_mCerulean* vector. For analysing significance, an unpaired t-test was performed, and significance levels are depicted as asterisk ($p \leq 0.05$ shown by one asterisk (*), $p \leq 0.01$ shown by two asterisks (**)). If values did not differ significantly, it was indicated by ns. (not significant). **A:** NGR234 WT population after 24 h of growth. Median values for each fluorophore differ significantly from P*ngrI_dsRed* based fluorescence. Median FI per cell is lower than 0.2 AU (arbitrary units) and only few cells show higher intensities. **B:** NGR234 WT population after 48 h of growth. Median values of mean FI per cell increased for each fluorophore compared to 24 h. Populations of NGR234 WT show a high degree of heterogeneous expression for each of the tagged promoters as shown in the frequency histogram. **C:** NGR234 WT population after 72 h of cultivation. Mean FI per cell shifted back and decreased again compared to timepoints measured before.

Considering the median values for all three FI at the indicated timepoints, shifts of gene expression of each gene of interest can be observed. Table 12 lists the population-wide median, as well as the minimum and maximum values for FI for each promoter. Although minimal and maximal intensities were very similar over time and partially comparable between the fluorescence channels, the population median varied over time. After 48 h of incubation all median FI had reached their maximum and decreased again towards 72 h. The shift of the median FI represents a population-wide increase or decrease of FI and therefore promoter activity. Even though there seems to be a high degree of phenotypic heterogeneity and variability on a population level, general gene expression changed towards a common pattern.

Table 12: Median FI per cell analysed in *S. fredii* NGR234 WT. Median FI (median) was determined over all cells measured separately for each timepoint (24, 48 and 72 h) and promoter fusion. Minimum (Min.) and maximum (Max.) values for mean FI are given to show the range of observed FI and therefore promoter activity. Total number of the cells that were analysed is given (No. of cells). Regardless of the timepoint observed, the NGR234 WT population experienced a broad distribution of expression intensities of the respective promoter fusion. All promoters showed the highest median activity after 48 h.

P*ngrI_dsRed*				P*traI_gfp*				P*qsdR1_mCerulean*				
Median	Min.	Max.	No. of cells	Median	Min.	Max.	No. of cells	Median	Min.	Max.	No. of cells	Incubation time [h]
0.0993	0.019	0.465	270	0.0873	0.013	0.458	310	0.0786	0.021	0.643	318	24
0.1176	0.016	0.458	1,432	0.1129	0.015	0.505	1,640	0.1018	0.014	0.560	1,202	48
0.1052	0.017	0.492	1,977	0.0911	0.019	0.427	3,019	0.080	0.016	0.597	2,521	72

4.1.3 Phenotypic heterogeneity in *S. fredii* ANU265 WT

The strain *S. fredii* ANU265 is a derivative of NGR234 that was heat-cured of its symbiotic plasmid and that is no longer able to nodulate its host plants or fixate nitrogen. This strain was used to examine if the loss of the pNGR234*a* symbiotic plasmid has an influence on the expression of the QS AI-synthases expression and how QQ gene activity may be altered.

Monitoring the promoter activity of P*traI*, naturally encoded on the missing pNGR234*a* plasmid, P*ngrI* and P*qsdR1, S. fredii* ANU265 was transformed with the pBBR1MCS-5::P*traI_gfp::*P*ngrI_dsRed::*P*qsdR1_mCerulean*. Analysing CLSM images of ANU265 showed rather high expression levels of P*traI_gfp* compared to NGR234 WT after 24 h

growth. The expression levels after 48 h and 72 h decreased again and were lower or equal to NGR234 WT levels. Nevertheless, P*traI_gfp* was actively expressed in most ANU265 cells after 48-72 h (Figure 10 A). This exemplary image of ANU265 after 72 h of incubation indicates that the QS systems in NGR234 may experience cross talk, since the AI synthase *traI* and the respective regulator genes are not present in ANU265, but P*traI* promoter activity was detectable. In Figure 10 B and D, phenotypic heterogeneity in ANU265 cells was recognisable. Expression of P*ngrI* and P*qsdR1* promoter fusions could be observed as well, but compared to P*traI_gfp* expression, expression levels were clearly decreased (Figure 10 B-E).

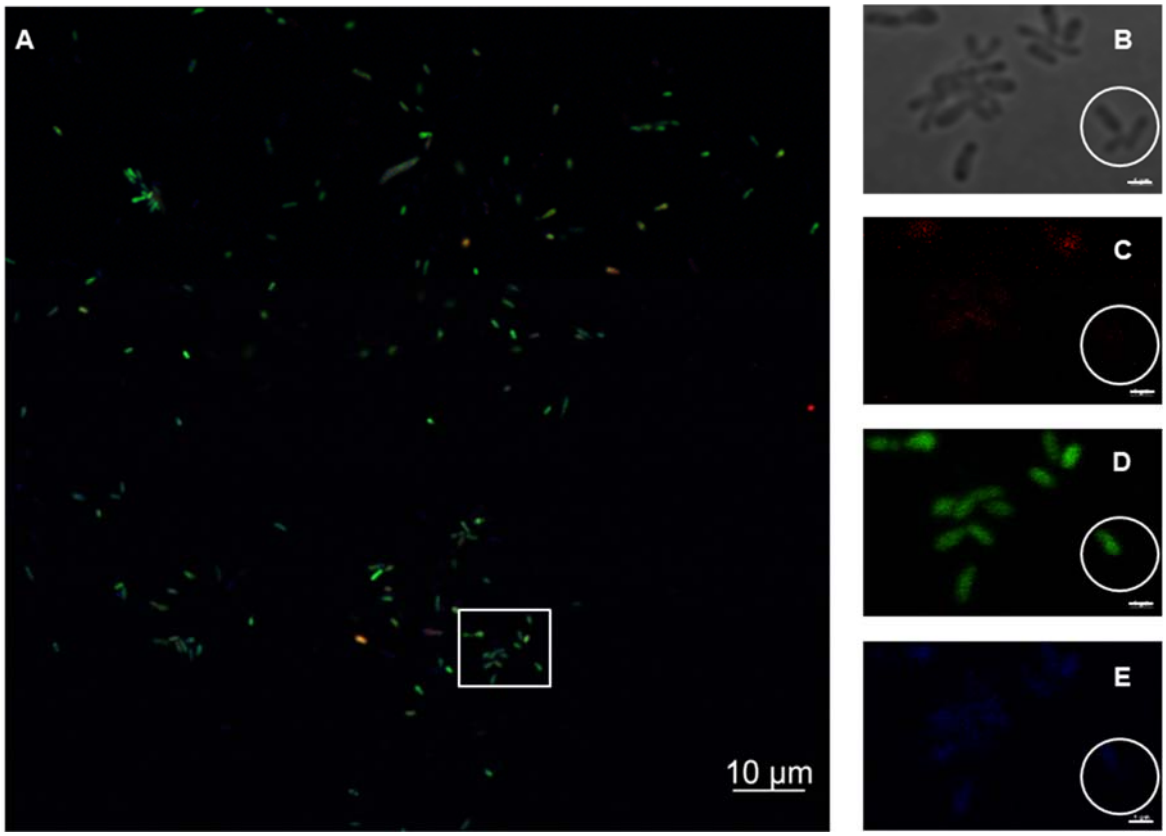

Figure 10: Phenotypic heterogeneity in *S. fredii* ANU265 WT analysed by CLSM. *S.fredii* ANU265 WT containing the pBBR1MCS-5::P*traI_gfp*::P*ngrI_dsRed*::P*qsdR1_mCerulean* construct. Incubation conducted for 72 h in YEM medium with appropriate antibiotics at 28 °C and 135 rpm. The scale bar in section A represents 10 µm, sections B-E scale bar represents 1 µm. **A:** Merged fluorescence channel image. Only single cells showed detectable red fluorescence representing the activity of the P*ngrI*, whereas most cells express P*traI_gfp*. Expression of P*qsdR1_mCerluean* was less prominent compared to P*traI* activity, but almost all cells expressed the promoter on a low level. Rectangle marks area magnified in B-E. **B:** Brightfield images of magnified cells marked in A. **C:** Red fluorescent detection channel showing only diffuse and weak signal for P*ngrI_dsRed* expression. **D:** Most cells identified in the brightfield channel displayed P*traI_gfp* signal, but few cells showed no *gfp* expression at all. **E:** Fluorescence channel detecting P*qsdR1_mCerulean* expression. Cells expressing *traI* promoter also show signals for P*qsdR1* expression activity.

As already stated above, expression levels of P*traI_gfp* in ANU265 differed over time, as well as the promoter activities of the other examined promoters. Comparing

ANU265 cells after 24, 48 and 72 h, it can be observed that the expression of P*ngrI_dsRed* is most distinct after 24-48 h and only low after 72 h (Figure 11 C, H and M). The P*qsdR1_mCerulean* signal was detectable at all timepoints and the intensity slowly increased over time (Figure 11 E, J and O). Phenotypic heterogeneity regarding different levels of expression could be identified at all timepoints, but few cells showed expression of only a single promoter (Figure 11 B, G and L).

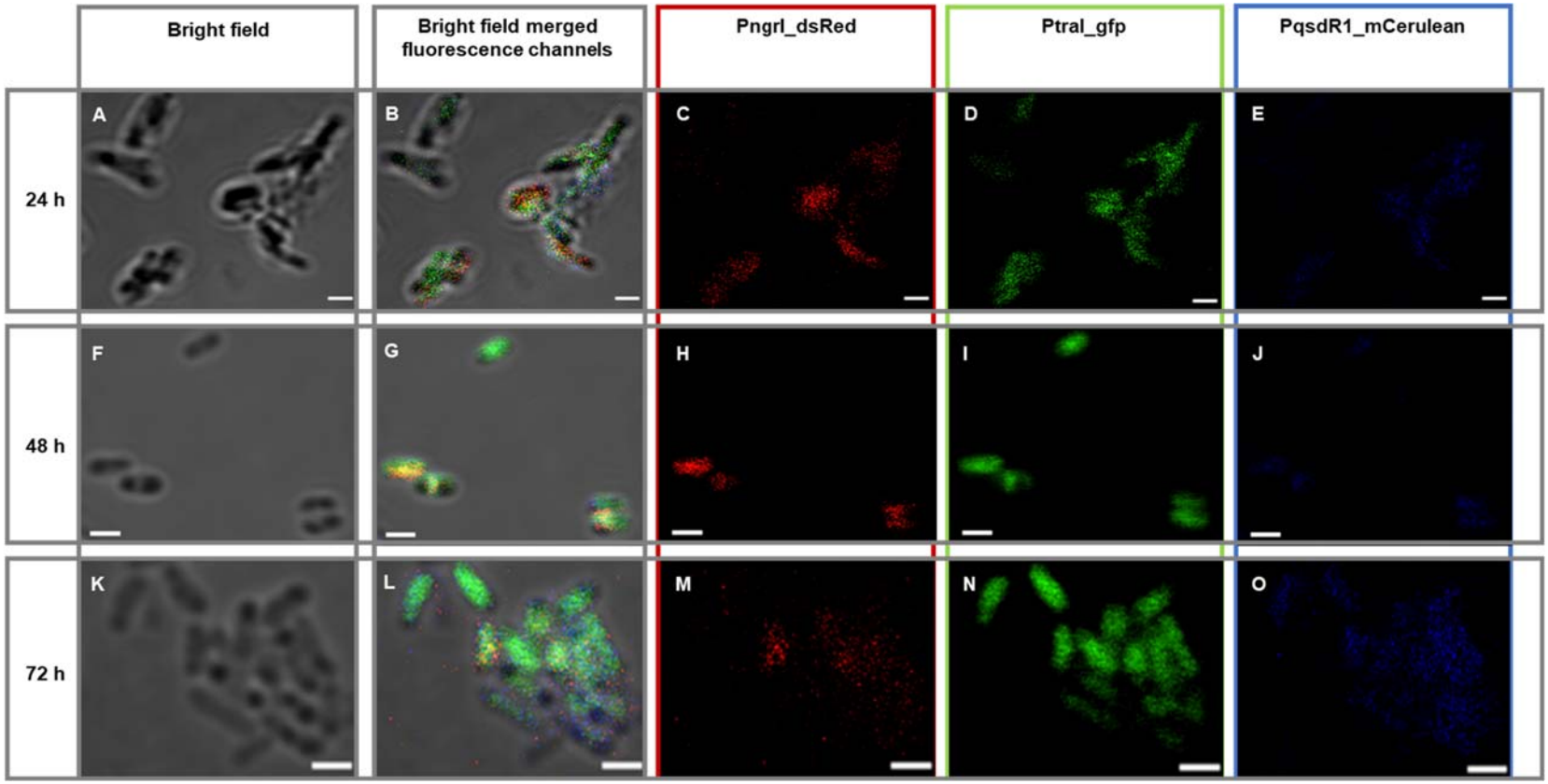

Figure 11: Phenotypic heterogeneity in *S. fredii* ANU265 over time. ANU265 WT cells showing phenotypic heterogeneity in CLSM analysis. Cells contain the pBBR1MCS-5::P*ngrl_dsRed::*P*tral_gfp::*P*qsdR1_mCerulean* promoter construct to analyse the expression of AI synthases and QQ gene expression in one cell in parallel. Scale bar represents 1 µm. **A-E:** ANU265 WT cells after 24 h incubation. **F-J:** ANU265 WT cells after 48 h of incubation. **K-O:** ANU265 WT cells after 72 h incubation. From left to right: bright field image, bright field image overlaid with merged fluorescence signals, red fluorescence signals representing P*ngrl_dsRed* expression, green fluorescence signals representing P*tral_gfp* expression and blue fluorescence expression representing P*qsdR1_mCerulean* expression.

Looking at the MIFISC revealed that most cells had low promoter activities after 24 h. Compared to NGR234 WT, mean values and standard deviation for each promoter were reduced. This indicates a diminished level of phenotypic heterogeneity and gene expression of the observed QS and QQ genes. On the other hand, the MIFISC was considerably higher after 48 and 72 h for PngrI_*dsRed* and PqsdR1_*mCerulean* in contrast to NGR234 WT. FI of PtraI_*gfp* was enhanced, but not as prominent as in the WT (Table 13). In addition, in Table 13 the overall shift of cells expressing PtraI_*gfp* is displayed, since after 48-72 h most cells could be detected in this channel.

Table 13: MIFISC of *S. fredii* ANU265 WT. The mean integrated FI per cell was calculated. The mean value of integrated fluorescence was divided by total number of cells analysed.

P*ngrI_dsRed*			**P*traI_gfp***			**P*qsdR1_mCerulean***			
Mean value	Std. dev.	No. of cells	Mean value	Std. dev.	No. of cells	Mean value	Std. dev.	No. of cells	Incubation time [h]
2.82	1.51	1,351	4.10	4.09	1,216	2.67	0.61	1,200	24
17.58	19.83	419	4.65	4.51	770	51.49	70.24	350	48
20.22	25.31	304	1.58	1.16	1,298	17.71	24.53	262	72

Mean FI on single cell basis is depicted in Figure 12. First, the high level of FI after 24 h was noticeable (Figure 12 A, left side). Generally, all three promoter fusion constructs showed a high degree of phenotypic heterogeneity but balanced distribution of FI on a population level (Figure 12 A, right side). After 48 and 72 h of growth, this equal distribution shifted towards lower median FI. However, few cells still had notably high fluorescence signals (Figure 12 B and C). The shift of median FI on population level can also be observed analysing the respective histograms (Figure 12 B and C, right side). Furthermore, Figure 12 shows the significant division of the median FI of P*traI* and P*qsdR1* regulated fluorophore expression over time.

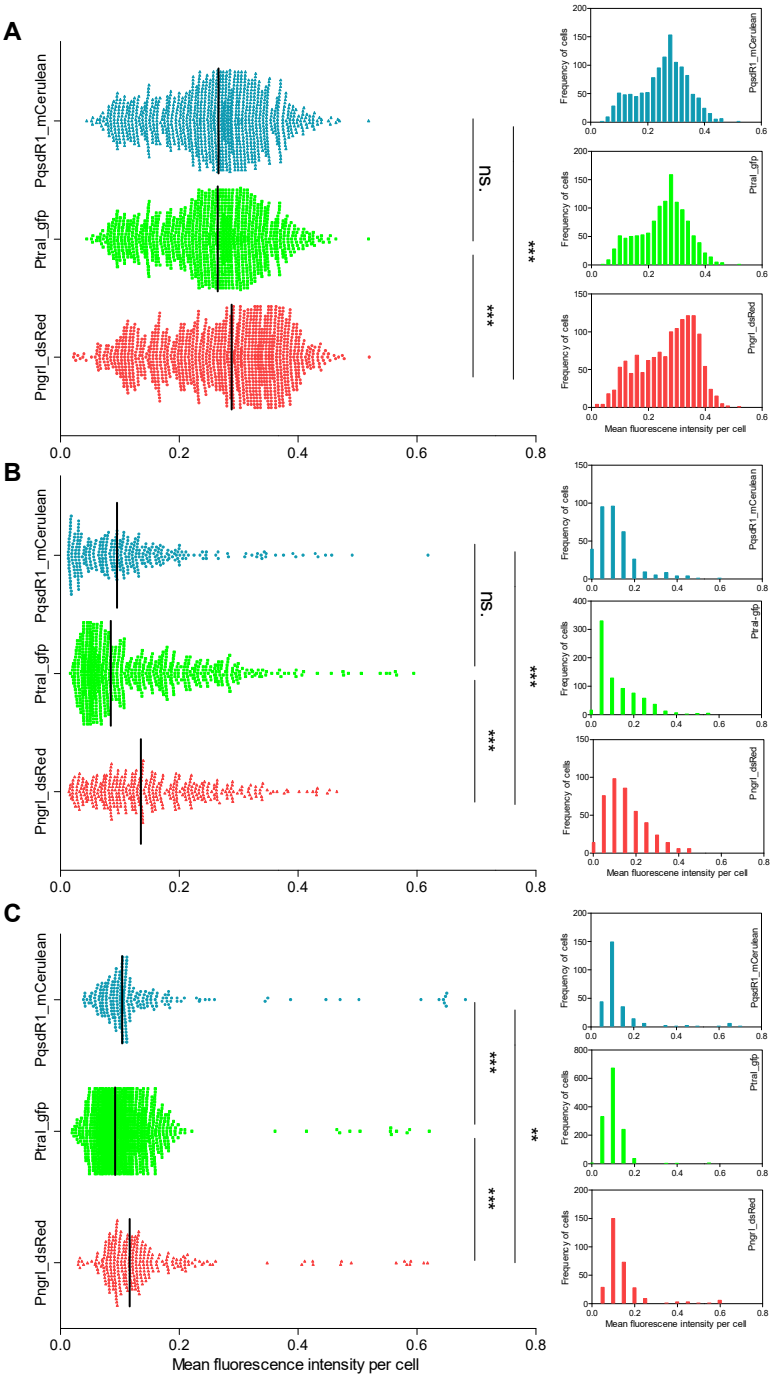

Figure 12: Phenotypic heterogeneity in *S. fredii* ANU265. The mean FI per single cell is shown on the left. On the right, the frequencies of cells showing distinct fluorescence intensities are given. Analysing significance, an unpaired t-test was performed, and significance levels are depicted as asterisk ($p \leq 0.05$ shown by one asterisk (*), $p \leq 0.01$ shown by two asterisks (**)). If values did not differ significantly it was indicated by ns. (not significant). Incubation at 28 °C and 135 rpm in YEM medium supplemented with appropriate antibiotics. The ANU265WT containing the vector pBBR1MCS-5::P*traI_gfp*::P*ngrI_dsRed*::P*qsdR1_mCerulean*. **A:** ANU265 WT population after 24 h growth. Cells show a high range of phenotypic heterogeneity on the population level for all three promoters. The median values for mean FI per cell are very similar (black bars). **B:** ANU265 WT population after 48 h of growth. **C:** ANU265 WT population after 72 h growth. The population median for mean FI shifted towards lower intensities for all three promoter activities. The population is less phenotypic heterogenic, but some cells showed distinctly higher FI.

The overall higher median FI after 24 h can be seen in Table 14. All three promoter fusions do not differ in the maximum of FI after 24 h but P*ngrI_dsRed* significantly varies in median and minimal fluorescence. Values for median FI per cell decreased considerably from 24 to 48 h and remained on this level until 72 h of growth. Even though all FI shifted following the same pattern, differences between median intensities increased additionally to further divergence of minimal and maximal fluorescence signals (Table 14).

Table 14: Median FI per cell analysed in *S. fredii* ANU265 WT. The median FI (median) was determined over all cells measured separately for each timepoint (24, 48 and 72 h) and promoter fusion. Minimum (Min.) and maximum (Max.) values for mean FI are given to show the range of observed FI and therefore promoter activity. The total number of cells that were analysed is given (No. of cells). Regardless of the timepoint observed, the ANU265 WT population experienced a broad distribution of expression intensities of the respective promoter fusion. All promoters showed the highest median activity after 24 h, whereas some cells showed absolute maximum fluorescence after 72 h.

P*ngrI_dsRed*				P*traI_gfp*				P*qsdR1_mCerulean*				
Median	Min.	Max.	No. of cells	Median	Min.	Max	No. of cells	Median	Min.	Max.	No. of cells	Incubation time [h]
0.2881	0.022	0.519	1,351	0.2648	0.044	0.518	1,216	0.2659	0.044	0.518	1,200	24
0.1354	0.014	0.465	419	0.0846	0.016	0.594	770	0.0952	0.013	0.618	350	48
0.1164	0.029	0.617	304	0.0921	0.019	0.621	1,298	0.1038	0.038	0.681	262	72

4.1.4 Phenotypic heterogeneity in *S. fredii* NGR234 Δ*repX*

RepX is a µ-protein encoded on the symbiotic plasmid of NGR234 and lays within the intergenic region of *traI* and the *repABC* operon, near the origin of replication. The deletion of this gene led to the total loss of the symbiotic plasmid in NGR234 (Petersen, 2019). The deletion mutant *S. fredii* NGR234 Δ*repX* was transformed with the pBBR1MCS-5::P*traI_gfp::*P*ngrI_dsRed::*P*qsdR1_mCerulean* promoter construct, to investigate the influence of the deletion of this µ-protein on the gene expression of these three genes.

In Figure 13 a CLSM image of NGR234 Δ*repX* after 48 h of growth is shown. Most cells in the observed area displayed a high P*traI_gfp* expression, represented by the green fluorescence signal in the image (Figure 13 A). In a few cells single blue fluorescence signals could be detected, reflecting P*qsdR1_mCerulean* expression. Even fewer cells were actively expressing P*ngrI_dsRed* promoter fusion (Figure 13 A, purple cells). These cells all displayed parallel activity of P*qsdR1* fused to *mCerulean* and P*ngrI*

fused to *dsRed,* and therefore were depicted as purple (Figure 13 C and E). In the following exemplary image, no cells showed sole expression of P*ngrI_dsRed.*

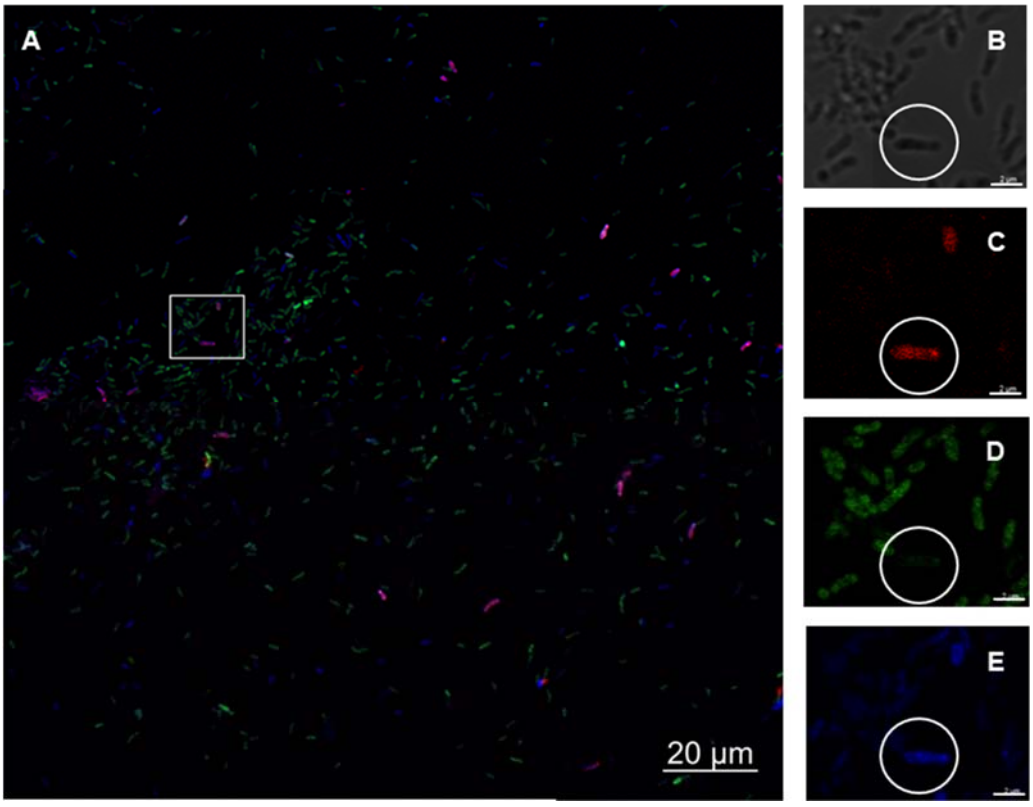

Figure 13: Phenotypic heterogeneity in *S. fredii* NGR234 Δ*repX* analysed by CLSM. *S. fredii* NGR234 *ΔrepX* containing the pBBR1MCS-5::P*traI_gfp*::P*ngrI_dsRed*::P*qsdR1_mCerulean* construct. Incubation was conducted for 48 h in YEM medium with appropriate antibiotics at 28 °C and 135 rpm. The scale bar in section A represents 20 µm, and in sections B-E 2 µm. **A:** Merged fluorescence channels image. Green-fluorescing cells are dominating, representing promoter activity of *traI.* Few cells were expressing *dsRed*, indicating P*ngrI* activity. Expression activity of P*qsdR1* was less prominent compared to P*traI*, but almost all cells expressed the fluorophore regulated by the respective promoter on a low level. Cells appearing violet experienced parallel expression activity of P*ngrI* and P*qsdR1*. The rectangle marks the area magnified in B-E. **B:** Brightfield images of magnified cells marked in A. **C:** Red fluorescent detection channel, few cells showing distinct signals for P*ngrI_dsRed* expression. **D:** Most cells identified in the brightfield channel showed a P*traI_gfp* signal, but few cells showed no *gfp* expression at all. **E:** Fluorescence channel detecting P*qsdR1_mCerulean* expression.

Following the expression patterns of the AI-synthases and the metallo-β-lactamase promoter over time indicated a decreased P*ngrI* activity after 24 h, when compared to the NGR234 WT and only very few cells expressed the P*ngrI_dsRed* construct (Figure 14 B and C). After 48 h, distinct fluorescence of dsRed could be detected in single cells, also simultaneously expressing P*traI* and P*qsdR1* (Figure 14 G-J, L-O). The same could be observed for P*qsdR1*-regulated expression. Though the overall expression was lower, the *qsdR1* promoter was active in most cells at 24 h (Figure 14 B and E). The number of cells showing only expression of P*qsdR1_mCerulean* seemed to increase over time (Figure 14 B, G and L). When examining the expression of

P*traI_gfp* it was noticeable that not all cells showed an active promoter, leading to observable phenotypic heterogeneity at all timepoints (Figure 14 B, D, G, I, L and N).

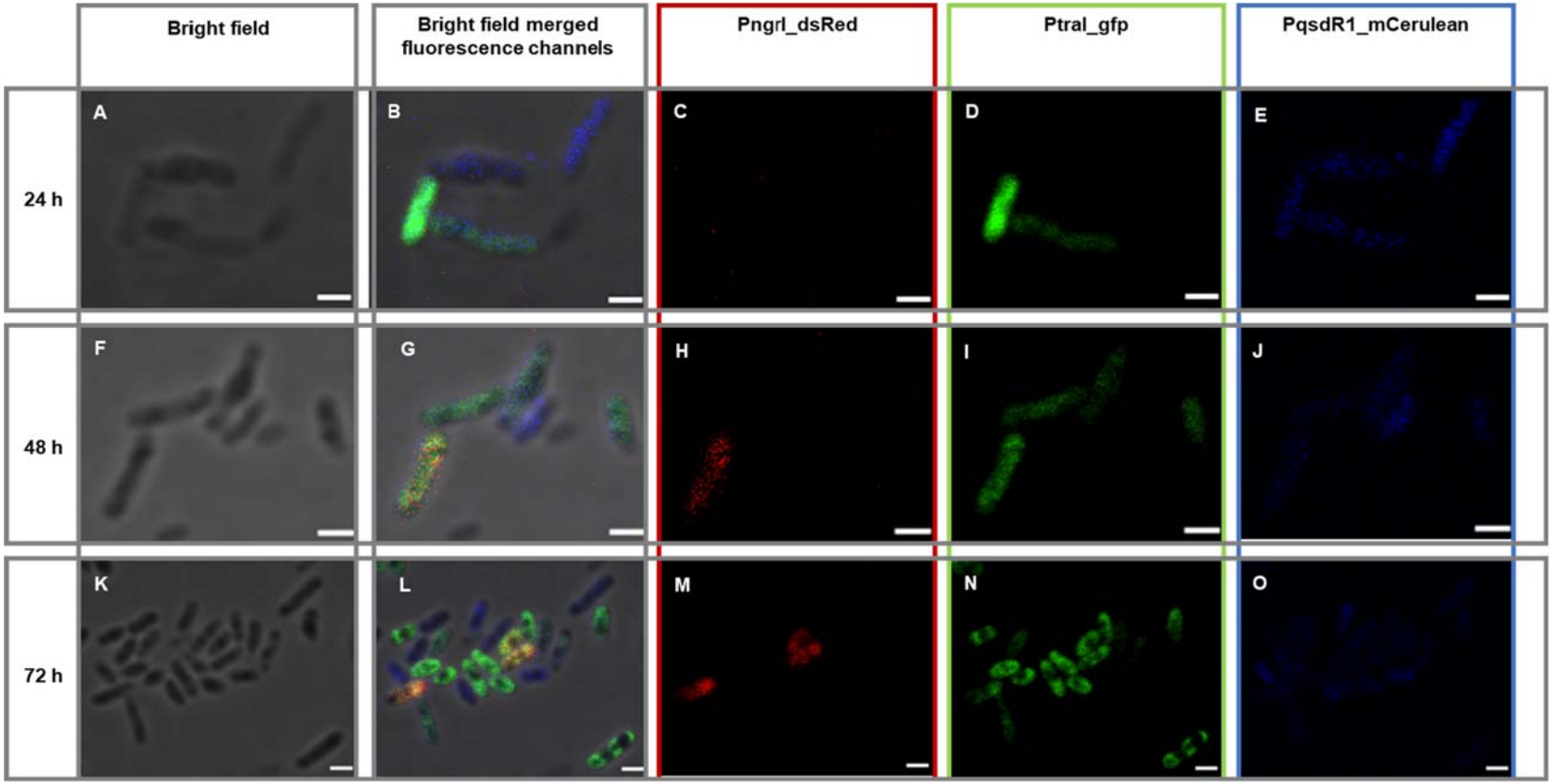

Figure 14: Phenotypic heterogeneity in *S. fredii* NGR234 Δ*repX* over time. NGR234 Δ*repX* cells showing phenotypic heterogeneity in CLSM analysis. Cells contain the pBBR1MCS-5::P*ngrI_dsRed*::P*tral_gfp*::P*qsdR1_mCerulean* promoter construct to analyse the parallel expression of AI synthases and QQ gene expression in one cell. Scale bar represents 1 µm. **A-E:** NGR234 Δ*repX* cells after 24 h of incubation. **F-J:** NGR234 Δ*repX* cells after 48 h of incubation. **K-O:** NGR234 Δ*repX* cells after 72 h of incubation. From left to right: bright field image, bright field image overlaid with merged fluorescence signals, red fluorescence signals representing PngrI_*dsRed* expression, green fluorescence signals representing P*tral_gfp* expression and blue fluorescence expression representing PqsdR1_*mCerulean* expression.

Analysing the MIFISC for NGR234 Δ*repX* (Table 15), values for P*ngrI_dsRed* were increased at all timepoints, especially after 48 h. On the other hand, the mean value for P*traI_gfp* FI was lower over the whole period observed, but after 72 h it was again more aligned with the NGR234 WT level. Compared to the NGR234 WT, the P*qsdR1_mCerulean* MIFISC was decreased in early stages of population growth but increased after 72 h above WT level.

Table 15: MIFISC in *S. fredii* NGR234 Δ*repX*. The mean integrated FI per cell was calculated. The mean value of integrated fluorescence was divided by the total number of cells analysed.

P*ngrI_dsRed*			**P*traI_gfp***			**P*qsdR1_mCerulean***			
Mean value	Std. dev.	No. of cells	Mean value	Std. dev.	No. of cells	Mean value	Std. dev.	No. of cells	Incubation time [h]
8.28	8.86	441	1.45	0.97	496	0.89	0.69	780	24
21.15	21.50	506	1.82	1.97	2,316	2.11	1.59	1,581	48
3.50	1.95	323	0.77	0.74	1,162	1.38	0.86	482	72

When looking at all analysed cells and the mean FI over time, a shift from a similar expression intensity of the *traI* and *ngrI* promoter to significantly diverting promoter activities could be observed (see Figure 15).

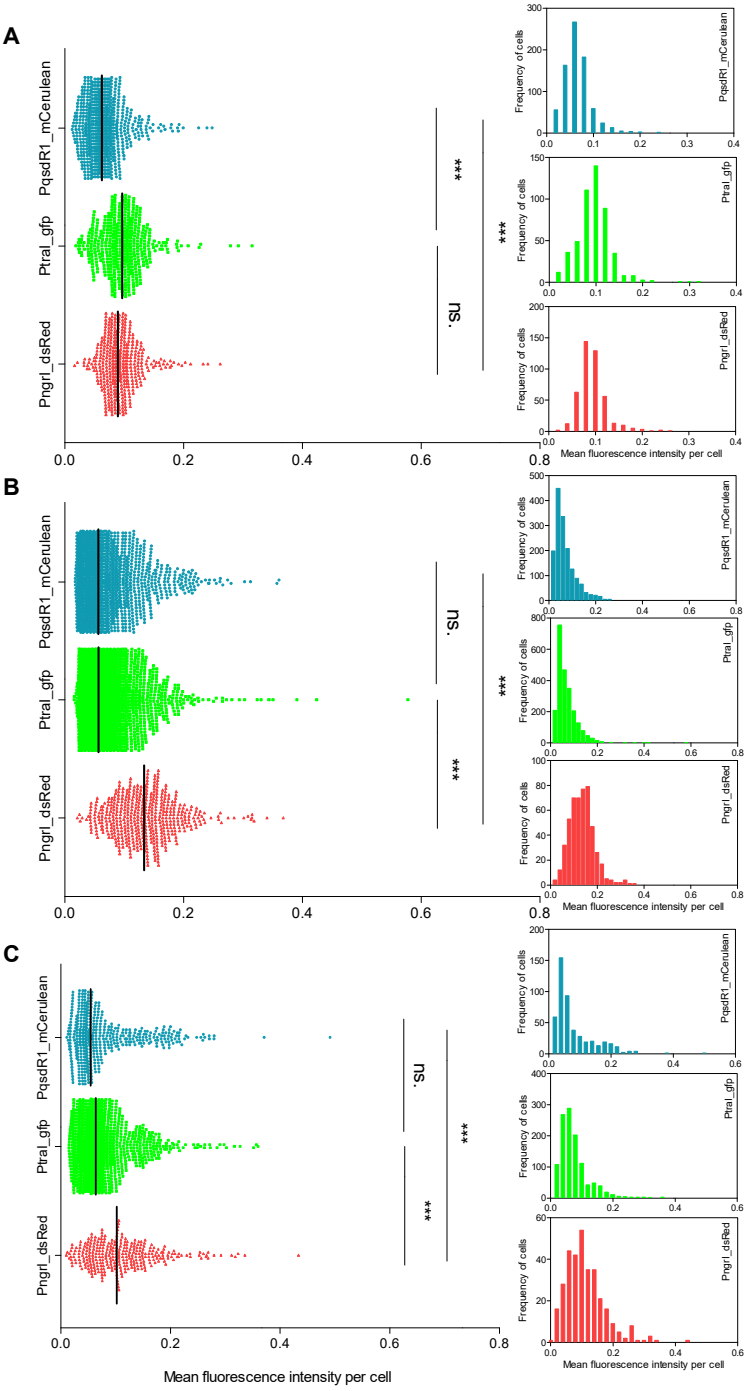

Figure 15: Phenotypic heterogeneity in *S. fredii* NGR234 Δ*repX*. The mean FI per single cell is shown on the left. On the right, frequencies of cells showing distinct FI are given. Incubation was conducted at 28 °C and 135 rpm in YEM medium supplemented with appropriate antibiotics. NGR234 Δ*repX* containing the pBBR1MCS-5::P*traI_gfp*::P*ngrI_dsRed*::P*qsdR1_mCerulean* construct. Analysing significance, an unpaired t-test was performed, and significance levels are depicted as asterisk ($p \leq 0.05$ shown by one asterisk (*), $p \leq 0.01$ shown by two asterisks (**)). If values did not differ significantly it was indicated by ns. (not significant). **A:** NGR234 Δ*repX* population after 24 h growth. Most cells showed a lower mean FI than 0.1 for P*qsdR1_mCerulean* expression. FI for P*ngrI_dsRed* and P*traI_gfp* were more balanced. **B:** NGR234 Δ*repX* population after 48 h growth. **C:** NGR234 Δ*repX* population after 72 h growth. The population median (black bar) for mean FI shifted towards lower intensities for all three promoters. The population was less phenotypic heterogenic, but some cells showed a distinctly higher FI.

As indicated by black bars in Figure 15, median FI of all promoter fusions shifted over the observed period. The values for median FI are shown in Table 16. Both P*ngrI*- and P*qsdR1*-controlled expression slowly increased from 24 to 72 h. However, promoter activity of P*traI* represented by GFP fluorescence had a peak after 48 h.

Table 16: Median FI of *S. fredii* NGR234 Δ*repX*. The median FI (median) was determined over all cells measured separately for each timepoint (24, 48 and 72 h) and promoter fusion. Minimum (Min.) and maximum (Max.) values for mean FI are given to show the range of observed FI and therefore promoter activity. The total number of cells that were analysed is given (No. of cells). Regardless of the observed timepoint, the NGR234 Δ*repX* population experienced a broad distribution of expression intensities of the respective promoter fusion. The promoter activity of P*ngrI* was highest after 48 h, P*traI* regulated GFP showed the maximum median FI after 24 h and the P*qsdR1*-controlled fluorophore expression was highest after 24 h.

P*ngrI_dsRed*				**P*traI_gfp***				**P*qsdR1_mCerulean***				
Median	Min.	Max	No. of cells	Median	Min.	Max.	No. of cells	Median	Min.	Max.	No. of cells	Incubation time [h]
0.0897	0.016	0.262	441	0.0967	0.019	0.315	496	0.0625	0.013	0.2484	780	24
0.1336	0.0212	0.368	506	0.0568	0.016	0.577	2,316	0.0567	0.018	0.361	1,581	48
0.1019	0.010	0.434	323	0.0637	0.015	0.360	1,162	0.0542	0.011	0.491	482	72

4.1.5 Phenotypic heterogeneity in *S. fredii* NGR234 Δ*NGR_a01725+*

The small ORF NGR_a01725 located on the symbiotic plasmid was deleted and the respective deletion mutant was transformed with the promoter construct pBBR1MCS-5::P*traI_gfp::*P*ngrI_dsRed::*P*qsdR1_mCerulean* to investigate the influence on QS and QQ, as well as phenotypic heterogeneity of this small ORF.

In Figure 16 a CLSM image of NGR234 ΔNGR_a01725+ after 72 h of growth is shown. Most cells expressed the QQ promoter of QsdR1 metallo-β-lactamase, fused to the gene of the blue fluorescent protein *mCerulean* (Figure 16 A). Only a few cells showed clear expression activity of P*traI* and P*ngrI*, visible as green and reddish cells in the merged image and in the single channel images (Figure 16 A, C-E). In general, the expression regulated by the two QS AI synthase promoters seemed only to be present in some cells. Furthermore, NGR234 ΔNGR_a01725+ experienced low levels of phenotypic heterogeneity. These cells expressed the *traI* and *ngrI* promoter controlled fluorescing proteins in parallel with the QQ promoter regulated *mCerulean* (Figure 16 B-E encircled cells).

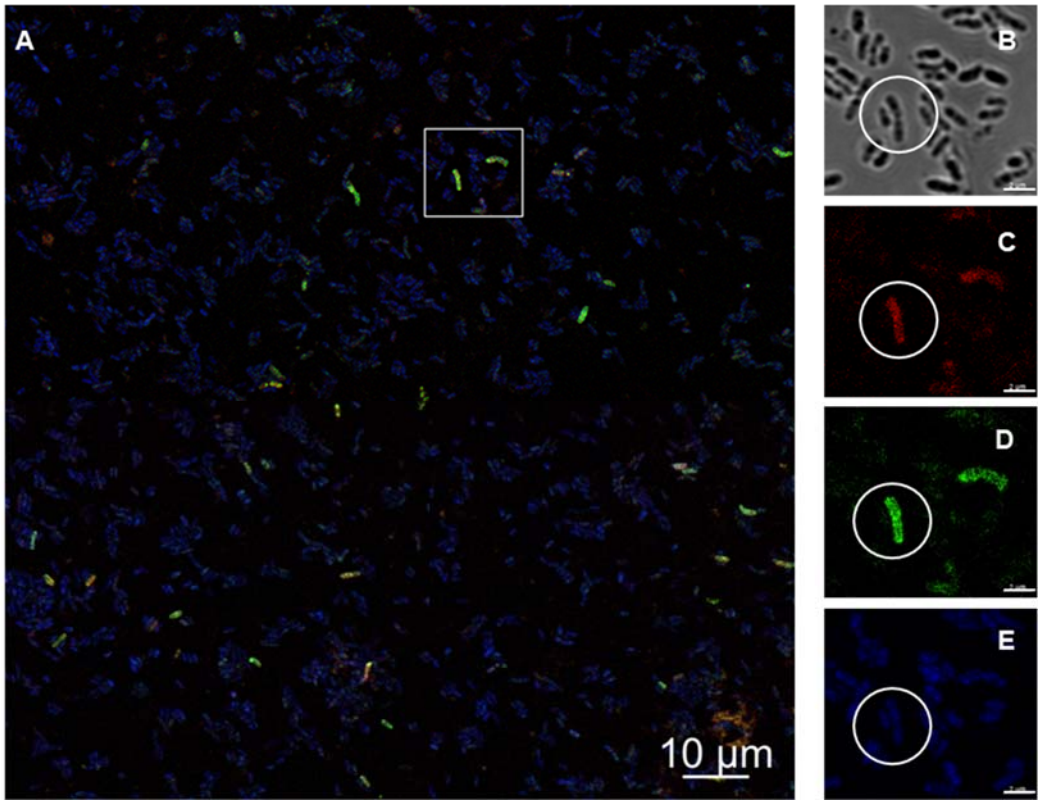

Figure 16: Phenotypic heterogeneity in *S. fredii* NGR234 ΔNGR234_a01725+ analysed by CLSM. *S. fredii* NGR234 ΔNGR234_a01725+ containing the promoter construct pBBR1MCS-5::P*traI_gfp::*P*ngrI_dsRed::*P*qsdR1_mCerulean*. Incubation conducted for 48 h in YEM medium with appropriate antibiotics at 28 °C and 135 rpm. Scale bar in A represents 10 µm, scale bar in sections B-E represents 2 µm. **A:** Merged fluorescence channels image. Blue fluorescing cells were dominating, representing promoter activity of *qsdR1*. Only few cells were observed weakly expressing *dsRed*, indicating low P*ngrI* activity. Expression activity of P*traI* was less prominent compared to P*qsdR1* controlled gene activity, but some cells expressed the *gfp* regulated by the *PtraI* promoter distinctly. Rectangle marks area magnified in B-E. **B:** Brightfield images of magnified cells marked in A. **C:** Red fluorescent detection channel, few cells showing distinct signals for P*ngrI_dsRed* expression. **D:** Most cells identified in the brightfield channel showed a P*traI_gfp* signal but few cells show no *gfp* expression at all. **E:** Fluorescence channel detecting *mCerulean*. Encircled cell showed parallel promoter activity of all three promoters.

Following the expression patterns of QS and QQ gene promoters further confirmed that most cells had detectable signals for all three promoters after 24-48 h (Figure 17 B, G, and L). When looking at the single channel images, it could be observed that nearly all cells showed similar fluorescence levels for each respective fluorescing protein. This indicated a low level of phenotypic heterogeneity (Figure 17 C-E, H-J and M-O). During the late stages of growth after 72 h, fewer cells could be detected expressing the *dsRed* or *gfp* regulated by the QS promoters. However, QQ promoter activity was still clearly visible in the majority of the cells (Figure 17 L and O).

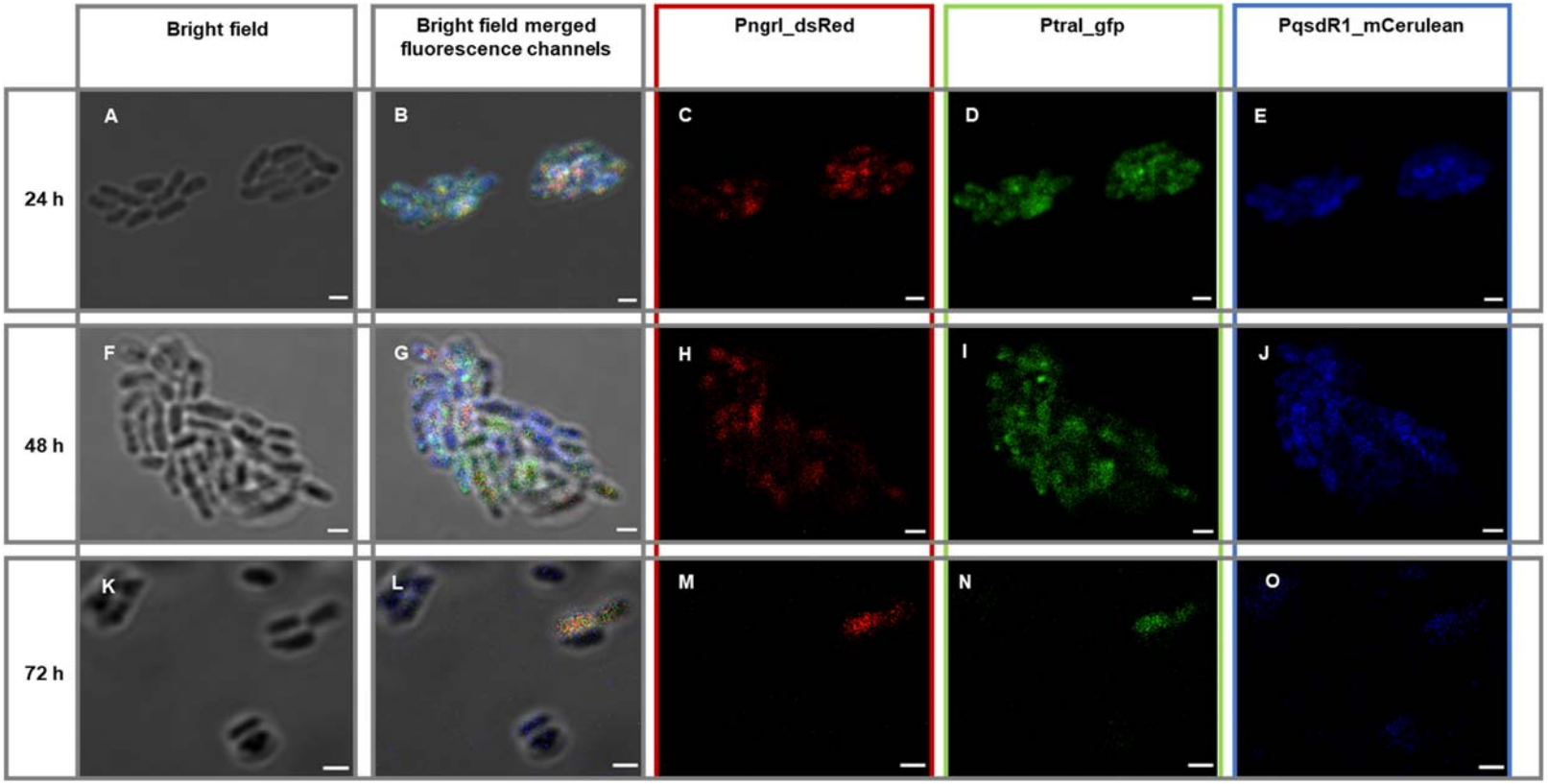

Figure 17: Phenotypic heterogeneity in *S. fredii* NGR234 ΔNGR234_a01725+ over time. NGR234 ΔNGR234_a01725+ cells showing phenotypic heterogeneity in CLSM analysis. Cells contain the pBBR1MCS-5::P*ngrI_dsRed*::P*traI_gfp*::P*qsdR1_mCerulean* promoter construct to analyse the parallel expression of AI synthases and QQ gene expression in one cell. The scale bar represents 1 µm in A-E and K-O, 2 µm in F-J. **A-E:** NGR234 ΔNGR234_a01725+ cells after 24 h incubation. **F-J:** NGR234 ΔNGR234_a01725+ cells after 48 h incubation. **K-O:** NGR234 ΔNGR234_a01725+ cells after 72 h incubation. From left to right: bright field image, bright field image overlaid with merged fluorescence signals, red fluorescence signals representing P*ngrI_dsRed* expression, green fluorescence signals representing P*traI_gfp* expression and blue fluorescence representing P*qsdR1_mCerulean* expression.

All analysed images were used to count cells, measure their FI and to calculate the MIFISC. In Table 17 the MIFISC for NGR234 ΔNGR_a01725+ is given. The number of cells in total that showed visible expression of the respective promoters did not differ between the *ngrI* and *qsdR1* promoters at 24 h. However, less cells were found to express the *traI* promoter after 24 h. Over time, an increasing number of cells showed QQ promoter activity, whereas the numbers of cells activating either one QS promoter also increased, but on a much lower level. In general, the MIFISC was higher or similar to that of NGR234 WT, except for the mCerulean FI after 24 h. Here NGR234 ΔNGR_a01725+ had a lower MIFISC value but more cells in total were detected.

Table 17: MIFISC in *S. fredii* NGR234 ΔNGR234_a01725+.The mean integrated FI per cell was calculated. The mean value of integrated fluorescence was divided by the total number of cells analysed.

P*ngrI_dsRed*			P*traI_gfp*			P*qsdR1_mCerulean*			
Mean value	Std. dev.	No. of cells	Mean value	Std. dev.	No. of cells	Mean value	Std. dev.	No. of cells	Incubation time [h]
43.71	126.39	757	10.97	15.62	578	9.50	13.15	758	24
21.15	41.91	1,317	8.92	10.02	1,842	7.01	11.15	2,442	48
11.49	10.74	940	8.52	14.48	4,576	1.48	2.27	8,309	72

In Figure 18 each analysed single cell was plotted. Foremost, the shift of a population with less phenotypic heterogeneity after 24 h (Figure 18 A) towards a high degree of phenotypic heterogeneity after 48 h (Figure 18 B) was most prominent. Even though the level of phenotypic heterogeneity shifts during the observed period, as well as the population median FI (black bar), all subpopulations showed significant differences comparing median FI. Around 24 and 48 h of growth, a directed distribution of FI for each promoter was observed (Figure 18 A and B right-hand side). Towards the end of the observed period, the mean FI of cells became more balanced again, especially for P*ngrI_dsRed* (Figure 18 C). Phenotypic heterogeneity had its peak after 48 h for all three promoters, showing a wide range of mean FI. This was also true for the population median, indicating a population-wide increase of promoter activity and again a decline after 72 h. Interestingly, NGR234 ΔNGR_a01725+ formed two subpopulations after 72 h in regard of its P*traI* expression activity, represented by a clear cut in the histogram (Figure 18 C right-hand side).

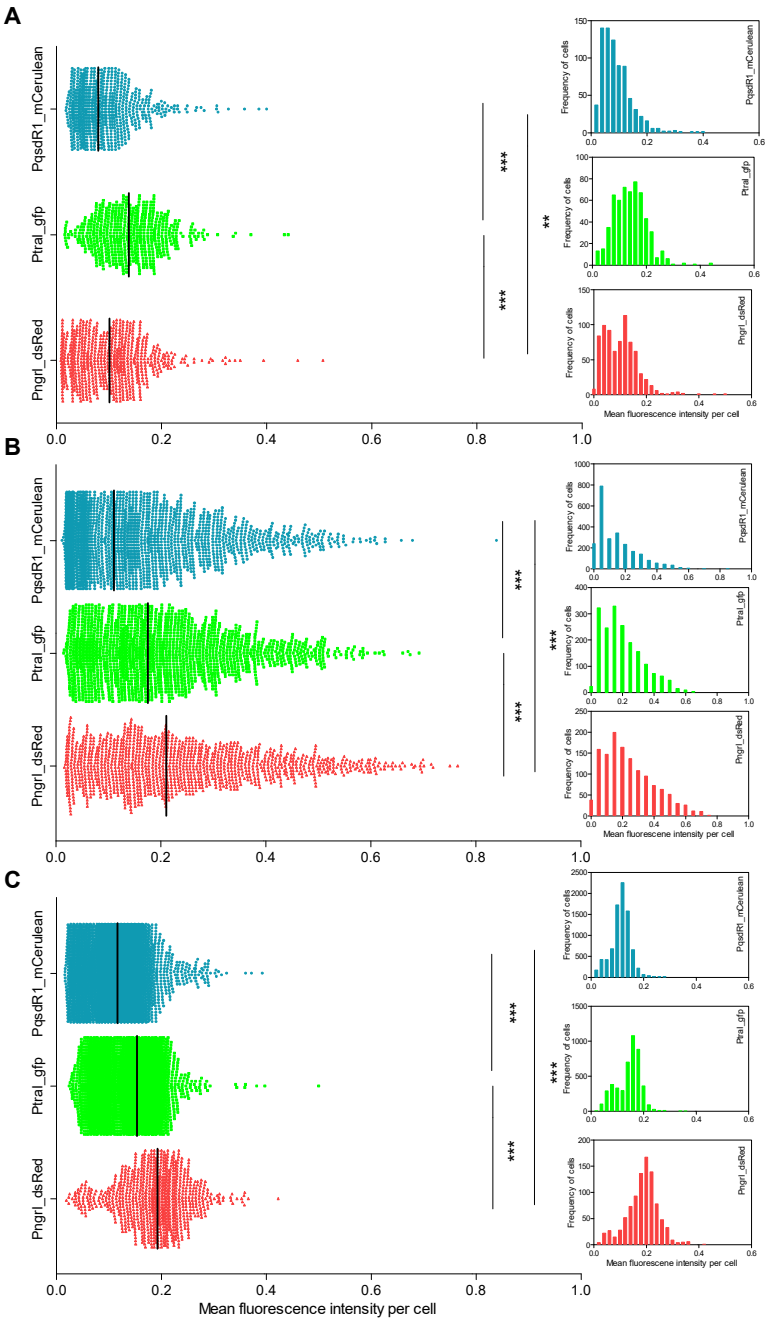

Figure 18: Phenotypic heterogeneity in *S. fredii* NGR234 ΔNGR234_a01725+. The mean FI per single cell is shown on the left. On the right, frequencies of cells showing fluorescence intensities are given. Incubation was conducted at 28 °C and 135 rpm in YEM medium supplemented with appropriate antibiotics. ΔNGR234_a01725+ containing the pBBR1MCS-5::P*traI_gfp*::P*ngrI_dsRed*::P*qsdR1_mCerulean* construct. Analysing significance, an unpaired t-test was performed, and significance levels are depicted as asterisk ($p \leq 0.05$ shown by one asterisk (*), $p \leq 0.01$ shown by two asterisks (**)). **A:** NGR234 ΔNGR234_a01725+ population after 24 h growth. The median values for mean FI per cell were very similar for fluorescence regulated by P*qsdR1* and P*ngrI* (black bars). **B:** NGR234 ΔNGR234_a01725+ population after 48 h growth. The population experienced a broad distribution of FI, representing phenotypic heterogeneity. **C:** NGR234 ΔNGR234_a01725+ population after 72 h growth. Population median for mean FI shifted towards lower intensities for all three promoters compared to 48 h. Population was less phenotypic heterogenic, but some cells showed distinct higher FI.

The median FI is listed in Table 18. Comparing the median values over time shows shifts of the FI for each promoter fusion on population level. As already described above, all FI median values increased from 24 h to 48 h and decreased after 72 h. All values were higher for NGR234 ΔNGR_a01725+ compared to the NGR234 WT median values with exception of the 24 h values of P*ngrI_dsRed* and P*qsdR1_mCerulean* that were similar to WT levels. Looking only at the minimum and maximum numbers of the mean FI, revealed less differences between the promoter activities and the timepoints, but indicated that the overall population FI had shifted while minimal and maximum fluorescence changed more slowly.

Table 18: Median FI *S. fredii* NGR234 ΔNGR234_a01725+. The median FI (median) was determined over all cells measured separately for each timepoint (24, 48 and 72 h) and promoter fusion. Minimum (Min.) and maximum (Max.) values for the mean FI are given to show the range of observed FI and therefore promoter activity. The total number of cells that were analysed is given (No. of cells). Regardless of the timepoint observed, NGR234 ΔNGR234_a01725+ population experienced a broad distribution of the expression intensities of the respective promoter fusion. Promoter activities of P*ngrI* and P*traI* were highest after 48 h. P*qsdR1* expression rate was highest after 72 h.

P*ngrI_dsRed*				P*traI_gfp*				P*qsdR1_mCerulean*				
Median	Min.	Max	No. of cells	Median	Min.	Max.	No. of cells	Median	Min.	Max.	No. of cells	Incubation time [h]
0.1008	0.008	0.507	757	0.1378	0.016	0.441	578	0.0795	0.018	0.400	758	24
0.2104	0.016	0.765	1,317	0.1753	0.0147	0.692	1,842	0.1102	0.011	0.839	2,442	48
0.1931	0.019	0.423	9,40	0.1536	0.024	0.500	4,576	0.1162	0.016	0.392	8,309	72

4.1.6 Relative comparison of fluorescence intensities in *S. fredii* NGR234 WT and mutant strains

Since the mean integrated FI, the median FI and minimum and maximum FI were analysed for each NGR234 strain individually, differences between the WT and the mutant strains cannot easily be seen. Therefore, mean integrated FI and median FI of each strain were normalised against NGR234 WT fluorescence levels for each timepoint. This way a direct comparison was possible. Figure 19 shows the relative MIFISC in comparison to NGR234 WT. ANU265, lacking the symbiotic plasmid, had a promoter activity almost two-thirds lower after 24 h, but drastically enhanced after 48 to 72 h, showing a more than 4-11 times (4-11x) higher relative MIFISC compared to NGR234 WT (Figure 19 A, dark red). Like ANU265, NGR234 Δ*repX* has no symbiotic plasmid. In contrast to ANU265, NGR234 Δ*repX* showed very similar levels of P*ngrI* activity in relation to NGR234 WT. However, expression levels of P*ngrI_dsRed* were

much higher after 48 h in NGR234 Δ*repX* (5.6x) and less enhanced, but still clearly increased compared to NGR234 WT (2.0x) expression after 72 h (Figure 19 A, light red). NGR234 ΔNGR_a01725+ on the other hand, could be observed to have an elevated relative MIFISC over the whole observed period. The deletion of the small ORF NGR_a01725+ lead to a constant raise of P*ngrI* promoter activity compared to NGR234 WT levels (Figure 19 A, red; 5.6x, 5.6x, 6.7x).

Analysing the relative differences of P*traI_gfp* expression between the WT and mutant strains did not show distinct changes in fluorescence levels but for NGR234 ΔNGR_a01725+. The relative MIFISC was higher at all times, increased levels ranging from only 1.2x at 24 h to 2.5x after 48 h and 8.7x after 72 h respectively (Figure 19 B, green). Only ANU265 WT showed higher fluorescence levels (compared to NGR234 WT) besides NGR234 ΔNGR_a01725+, but to a much lower degree (Figure 19 B, dark green). Expression of P*traI_gfp* was around 6 times lower in NGR234 Δ*repX* after 24 h. Expression slightly increased over time (2-1.2x lower) but did not reach WT levels (Figure 19 B, light green).

The QQ promoter P*qsdR1_mCerulean* construct clearly had a reduced activity in all strains analysed at 24 h. NGR234 Δ*repX* and ANU265 had a decline of 25-8x of promoter activity when set in relation to NGR234 WT (Figure 19 C, light and dark blue). ANU265 recovered after 48 h and expression activity increased just below of NGR234 WT conditions. At 72 h P*qsdR1* promoter activity increased and was 16x higher compared to the NGR234 WT. NGR234 Δ*repX* on the other hand, had no change in expression at 48 h. After 72 h P*qsdR1* regulated fluorescence exceeded WT expression intensity about 1.2x. NGR234 ΔNGR_a01725+ showed higher levels of expression of P*qsdR1_mCerulean* after 24 h compared to ANU265 and NGR234 Δ*repX* but still was 2.3x below WT level. *QsdR1* promoter regulated fluorescence in NGR234 ΔNGR_a01725+ was reduced to only one-tenth of NGR234 WT after 48 h before rising to 1.3x expression intensity at 72 h (Figure 19 C, blue).

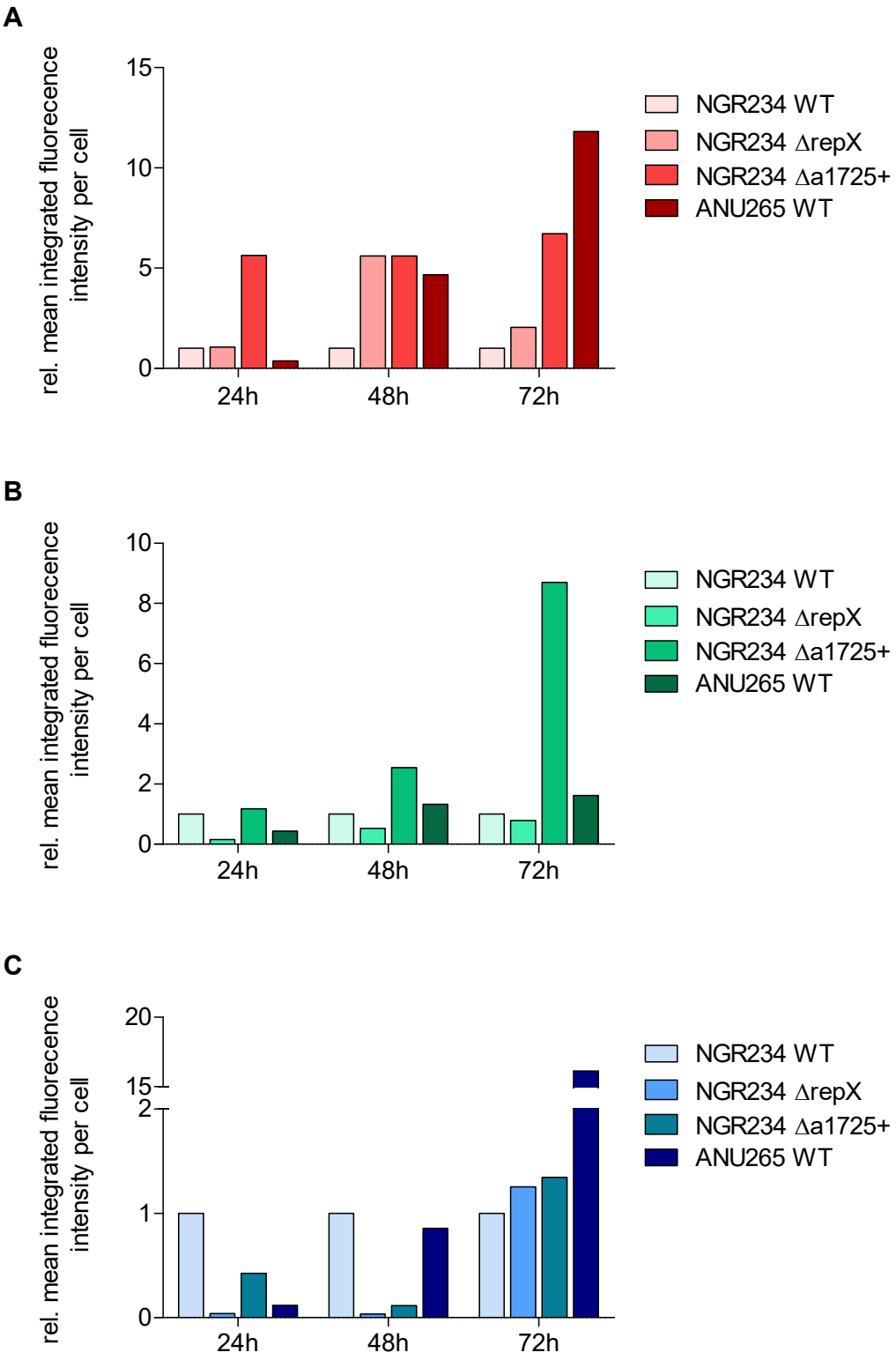

Figure 19: Relative MIFISC in *S. fredii* NGR234 mutants compared to NGR234 WT. MIFISC after 24, 48 and 72h normalised to NGR234 WT levels for each timepoint. The MIFISC analysed with the CellProfiler 3.1.8 pipeline of three independent replicates for each genotype and timepoint. Promoter fusion on the pBBR1MCS-5::P*ngrI_dsRed*::P*traI_gfp*::P*qsdR1_mCerulean* plasmid. Incubation at 28 °C and 135 rpm in YEM medium supplemented with appropriate antibiotics. **A:** Relative MIFISC of P*ngrI_dsRed*. **B:** Relative MIFISC of P*traI_gfp*. **C:** Relative MIFISC of P*qsdR1_mCerulean*.

The examination of population median FI for each promoter fusion is shown in Figure 20. It could be observed that the overall population median FI after 24 h for P*ngrI_dsRed* did not differ between NGR234 WT, NGR234 ΔNGR_a01725+ and NGR234 *ΔrepX* (Figure 20 A). ANU265 WT revealed a distinctly increased median FI after 24 h. After 48 h and 72 h only NGR234 ΔNGR_a01725+ showed a higher median FI compared to the remaining strains.

Even though median values for P*traI_gfp* were somewhat more scattered, the general pattern was the same as observed for PngrI_*dsRed* (Figure 20 B). ANU265 median FI was increased after 24 h but aligned after 48 h with the median values of NGR234 WT and NGR234 *ΔrepX* (Figure 20 B). Again, only NGR234 ΔNGR_a0175+ showed a clearly elevated median FI.

Comparing the median FI of P*qsdR1_mCerulean,* the values for all strains except for ANU265 adjusted around the NGR234 WT. ANU265 showed, as already observed for the other two promoter fusions, an increased promoter activity, but aligned with NGR234 WT after 48 h.

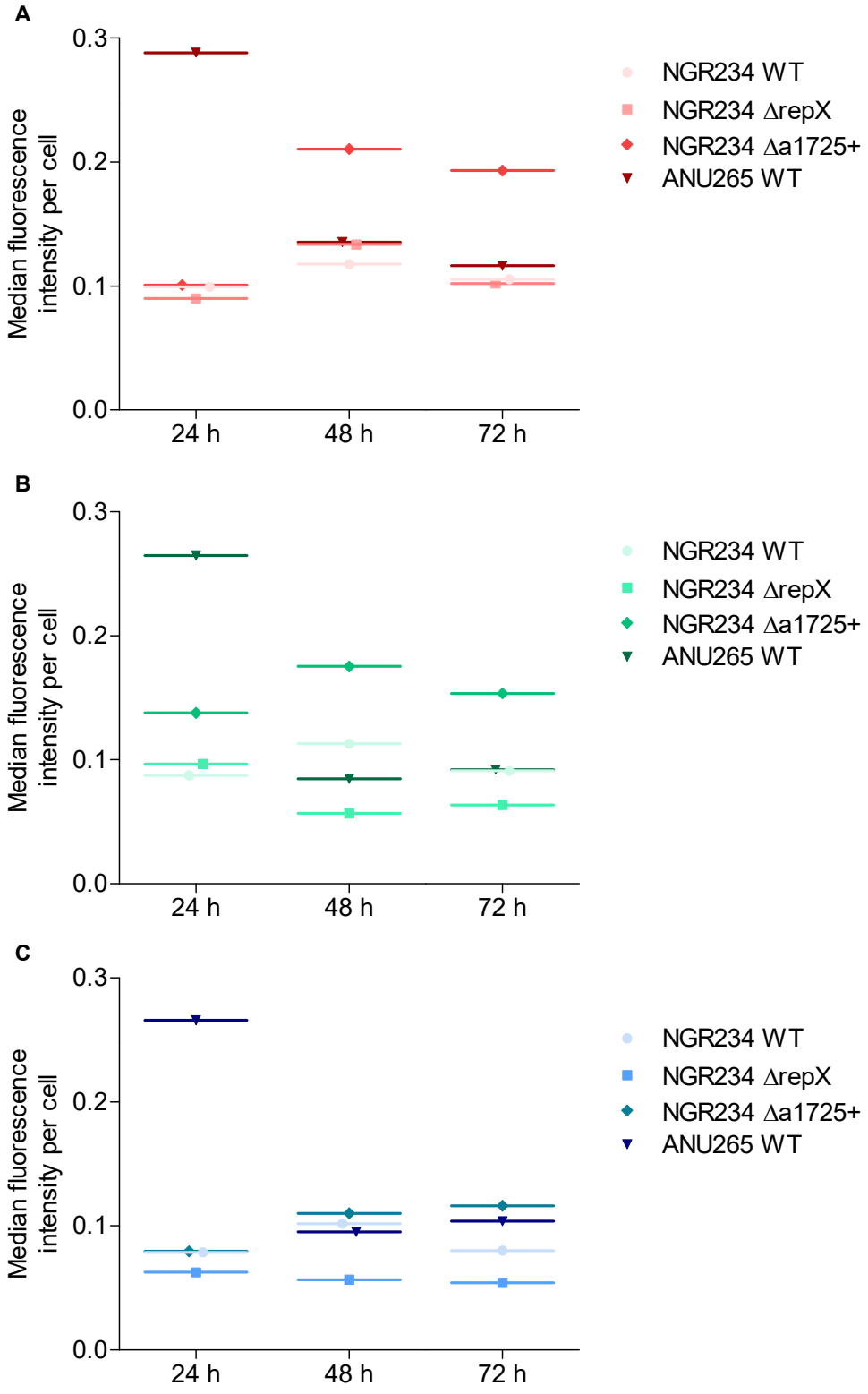

Figure 20: Median FI of *S. fredii* NGR234 mutants and NGR234 WT. The median FI after 24, 48 and 72h. The median FI of all was cells analysed with the CellProfiler 3.1.8 pipeline of three independent replicates for each genotype and timepoint. Promoter fusion on the pBBR1MCS-5::P*ngrI_dsRed*::P*traI_gfp*::P*qsdR1_mCerulean* plasmid. Incubation was performed at 28 °C and 135 rpm in YEM medium supplemented with appropriate antibiotics. **A:** Median FI of P*ngrI_dsRed*. **B:** Median FI of P*traI_gfp*. **C:** Median FI of P*qsdR1_mCerulean*.

4.2 Copy number variations of pNGR234*a*

The symbiotic plasmid of NGR234 was observed to be affected in its plasmid copy number (in relation to the number of chromosomes) due to the absence of AI. Therefore, the effect of spent culture medium of different NGR234 AI deletion mutants and closely related species, such as *S. fredii* USDA257 and ANU265, on NGR234s' symbiotic plasmid copy number was analysed. Investigation of the plasmid copy number was conducted by qPCR. Two sets of primers, *repA* and *nifB,* were used to measure the number of the symbiotic plasmid (Table 2). Simultaneously, two primer sets were used to amplify and measure the copies of two genes encoded on the chromosome as a reference, *recA* and NGR_c03800 (Table 2). The results of gene expression of the latter two were used to normalise for fluctuations in gene expression that were not caused by copy number effects.

In Figure 21 the results of the qPCR analyses are shown. Without any pre-treatment NGR234 WT plasmid copy was set to 1, whereas the NGR234 Δ*ngrI*Δ*traI* copy+ mutant had a 3-4x higher copy number of its symbiotic plasmid. Addition of NGR234 WT spent medium during incubation completely quenched this effect and NGR234 Δ*ngrI*Δ*traI* copy+ pNGR234*a* stabilised at one copy per chromosome. Repeating this experiment with the ANU265 strain, lacking the pNGR234*a* and therefore the respective *traI* AI synthase gene, yielded very similar results to the no-treatment control. Both genes, *nifB* and *repA,* are encoded on the symbiotic plasmid, indicating increased plasmid copies. Using spent medium of the very closely related strain USDA275 resulted again in elevated plasmid copy numbers in the NGR234 Δ*ngrI* Δ*traI* copy+ mutant, even though, NGR234 WT copy numbers were not changed compared to the control. A further increase of plasmid copies was observed when incubation of the NGR234 Δ*ngrI*Δ*traI* copy+ mutant strain was conducted using spent medium of either NGR234 Δ*ngrI* or NGR234 Δ*traI copy*+ (Δ*traI c*+). After 96 h of incubation in YEM medium that was diluted with 10 % (v/v) spent medium of these two strains, a further increase in total symbiotic plasmid copy number was observable. The NGR234 WT control showed no altered copy number during growth under the same conditions (Figure 21).

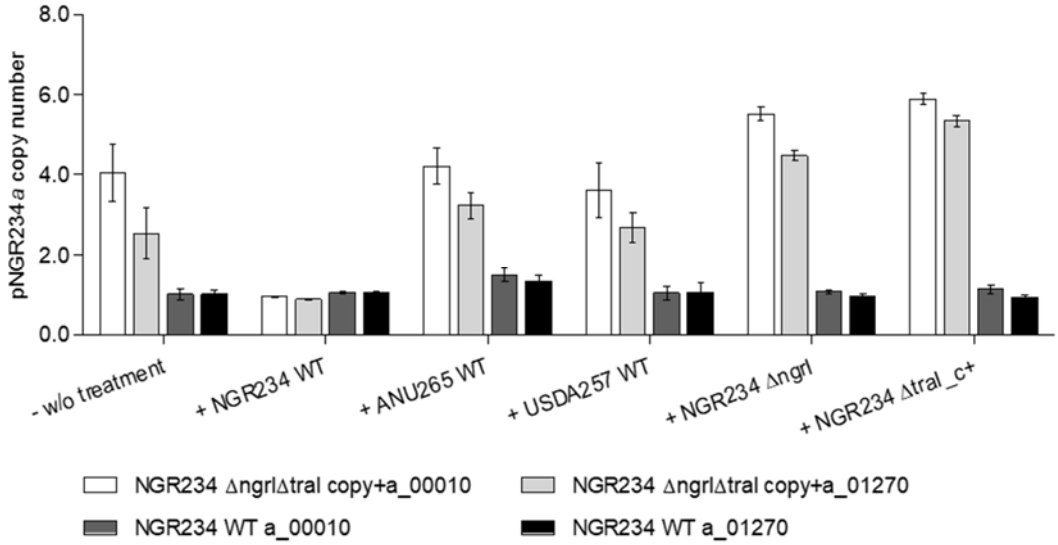

Figure 21: Influence of *S. fredii* strains on NGR234s' symbiotic plasmid copy number. Cultures for spent medium were grown in YEM medium for 96h at 28 °C and 135 rpm with appropriate antibiotics. To clear the supernatant, cultures were centrifuged for 40 min at 4,500 *g* and 4 °C and filtration with a 0.2 µm filter followed. Fresh cultures of either *S. fredii* NGR234 WT or *S. fredii* NGR234 Δ*ngrl* Δ*traI* copy+ were inoculated in YEM medium at an OD_{600} of 0.04 and with addition of 10.0 % (v/v) spent medium and 25.0 µg/mL rifampicin. Analysed genes: a_00010 (*repA*), a_01270 (*nifB*). Without treatment (w/o treatment). NGR234 Δ*traI copy+* (Δ*traI c+)*.

To analyse if the supernatants and the respective metabolites, such as AI of other soil-living bacteria, had an influence on NGR234 plasmid copy number, spent medium of the β-Proteobacteria *Burkholderia glumae* PG1 was used as described above. The *B. glumae* PG1 strain has three AI synthases systems, *bgaI1-3*. Deletion mutants of each of these AI synthases were also used for these supernatant experiments (Figure 22). The incubation with supernatant of *B. glumae* PG1 together with the NGR234 Δ*ngrl*Δ*traI* copy+ strain, lead to decreased numbers of the symbiotic plasmid in the mutant, whereas *B. glumae* PG1 WT supernatant had little to no effect on the NGR234 WT (Figure 22, '+ B. glumae WT'). Using spent medium of the Δ*bgaI1* AI deletion mutant resulted in highly raised symbiotic plasmid copies (5-8x) in the NGR234 Δ*ngrl*Δ*traI* copy+ strain. A similar effect was seen in the NGR234 WT. However, the effect in the NGR234 WT was not as distinct as in the NGR234 copy+ mutant. By using the single deletion mutants of the remaining two AI synthases in *B. glumae*, Δ*bgaI2* and Δ*bgaI3*, for the spent medium experiments and analysing the plasmid copy number of pNGR234*a*, similar effects as with the B*. glumae* PG1 WT could be observed. Both AI deletion mutants lowered the plasmid copy number of the NGR234 copy+ mutant and had a somewhat reducing effect on the NGR234 WT copy number as well. However, this effect was much less pronounced (Figure 22).

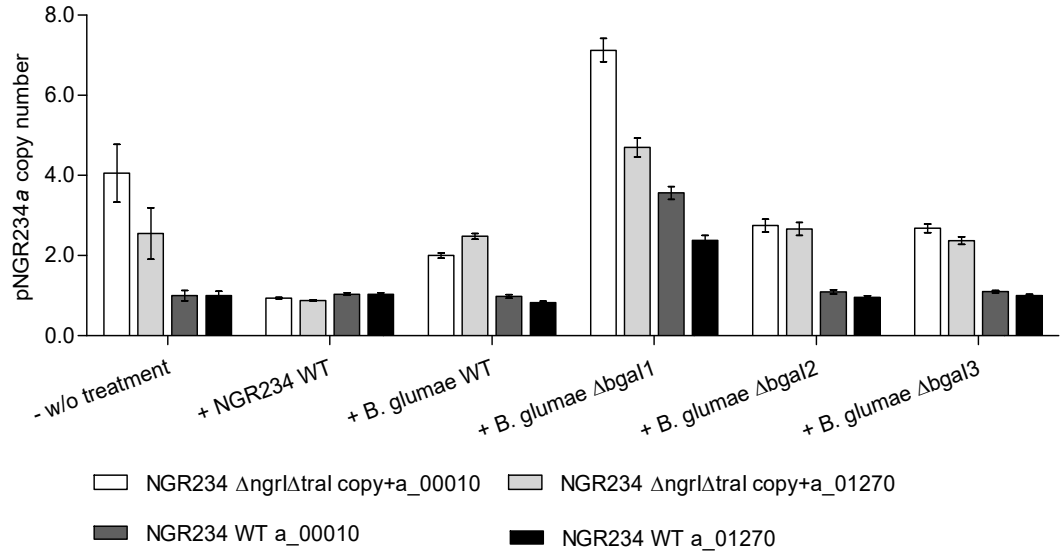

Figure 22: Influence of *B. glumae* PG1 and its AI mutants on the copy number of the symbiotic plasmid in *S. fredii* NGR234. B. glumae cultures for spent medium were grown in LB medium for 96 h at 28 °C and 135 rpm with appropriate antibiotics. To clear the supernatant, cultures were centrifuged for 40 min at 4,500 *g* and 4 °C and filtration with a 0.2 µm filter followed. Fresh cultures of either NGR234 WT or *S. fredii* NGR234 Δ*ngrl*Δ*traI* copy+ were inoculated in YEM medium at an OD_{600} of 0.04 and with addition of 10.0 % (v/v) spent medium and 25.0 µg/mL rifampicin. Analysed genes: a_00010 (*repA*), a_01270 (*nifB*). Without treatment (w/o treatment).

4.3 Nodulation of *Vigna unguiculata* with NGR234

Since NGR234 is known for its broad host range regarding nodulation of plants, nodulation experiments were conducted to investigate the potential effect of the pNGR234*a* plasmid copy number on nodulation and host-symbiont interaction. As a plant host, the *Fabaceae Vigna unguiculata* was chosen. Experiments were conducted at and in cooperation with the group of Prof. Dr. D. Ober at the Christian-Albrechts University of Kiel.

4.3.1 Nodulation efficiency

Nodulation efficiency testing was performed by infection of *V. unguiculata* with NGR234 WT, NGR234 Δ*ngrl*Δ*traI* copy+, NGR234 ΔNGR_a1725, NGR234 Δ*repX* and ANU265 WT. NGR234 WT was used as a positive control for correct execution of inoculation, whereas infection with ANU265 WT, lacking the symbiotic plasmid, was used as a negative control. NGR234 ΔNGR_a01725, in contrast to ΔNGR_a01725+ used in the CLSM experiments, represents a mixed culture of cells containing the symbiotic plasmid and cells that lost the respective plasmid. The duality of this strain was identified after conducting the nodulation experiments.

V. unguiculata beans were surface sterilised and germinated on either NOD or Hoagland medium agar plates as described before (see chapter 3.6). After inoculation, plants were grown for 57 days at controlled conditions in a climate chamber (for settings refer to 3.6.1). In total, 41 plants were examined in two independent experiments. Seven plants were excluded from analysis, because they did not grow after inoculation. It should be noted that 3/7 plants that were excluded had been inoculated with the NGR234 Δ*ngrI*Δ*traI* copy+ mutant, 2/7 infected with the NGR234 Δ*ngrI*Δ*traI* strain and 2/7 plants were inoculated with the NGR234 WT. Only one plant inoculated with NGR234 Δ*ngrI*Δ*traI* copy+ developed nodules that could be analysed. Plants inoculated with the copy+ strain stayed small in comparison to plants infected with other strains. In Figure 23 the plants and the roots after inoculation with either of the above-mentioned strains are shown. All plants inoculated with the strains still harbouring the symbiotic plasmid of NGR234 could induce nodule growth on the host plant (Figure 23 A-E NGR234 WT, G-L NGR234 Δ*ngrI*Δ*traI*, M-O NGR234 ΔNGR_a1725+). ANU265 WT and the NGR234 Δ*repX* deletion mutant were unable to induce any growth of nodules on their natural host plant, *V. unguiculata*, confirming the loss of their symbiotic plasmid pNGR234*a* (Figure 23 P and Q).

When comparing the two different growth media, Hoagland and NOD, both allowed successful infection, plant growth and nodulation. No observable differences between the media used could be shown. However, since the sample size for each medium and genotype was small these results can only be regarded as preliminary and need further examination.

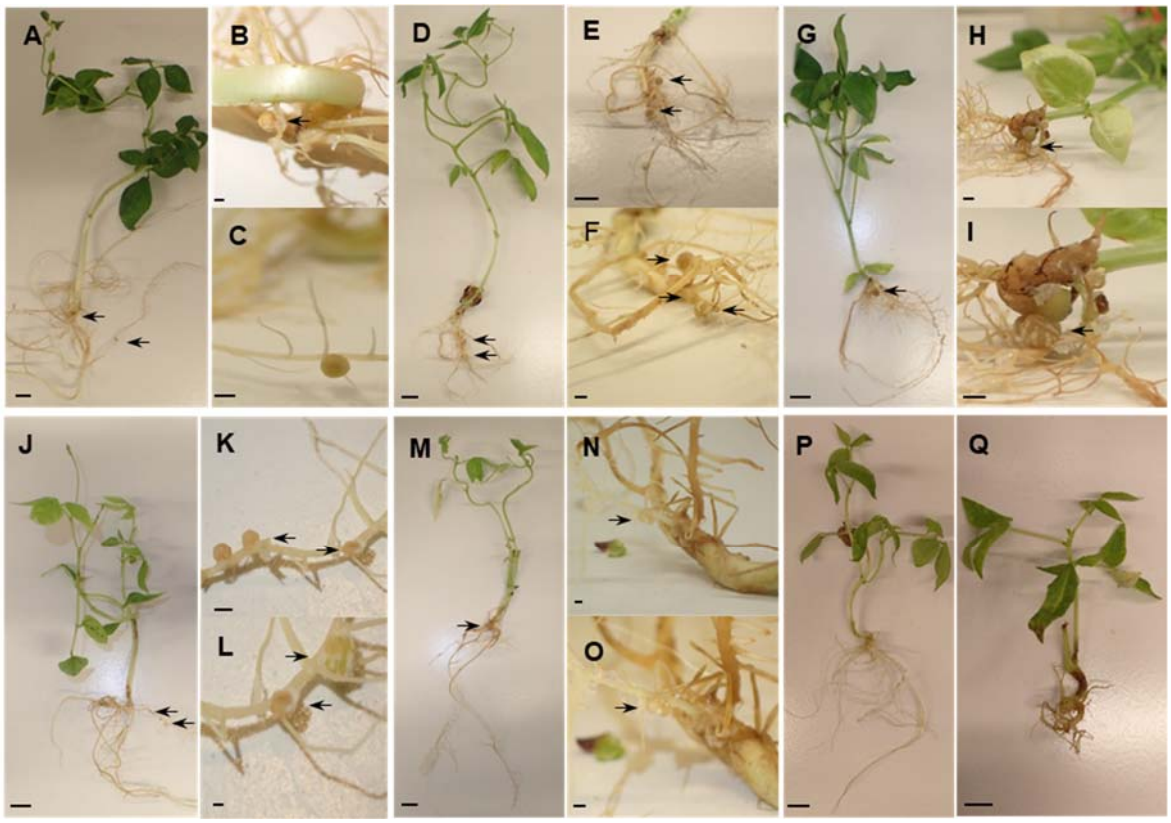

Figure 23: *Vigna unguiculata* plants infected with *S. fredii* NGR234 WT and mutant strains. Plants were either grown in 0.25x Hoagland medium (H) or in NOD medium (NOD) solidified with 1 % (w/v) agar. The harvest of the nodules was conducted 57 days past infection (dpi), nodules were weighed and stored at -70 °C until further use. **A-C:** Infection with NGR234 WT on H. **D-F:** Infection with NGR234 WT on NOD. **G-I:** Infection with NGR234 Δ*ngrl*Δ*traI* on H. **J-L:** Infection with NGR234 Δ*ngrl*Δ*traI* on NOD. **M-O:** Infection with NGR234 ΔNGR_a01725+ on NOD. **P:** Infection with NGR234 Δ*repX* on NOD resulting in no nodules due to loss of the symbiotic plasmid. **Q:** Infection with ANU265 WT on NOD resulting in no nodules due to the lack of the symbiotic plasmid.

Analysing the total number of root nodules on each plant after infection, a wide range of the total nodule number was observed, regardless of the strain used for infection (Figure 24). Plants infected with NGR234 WT showed 2-8 nodules per plant. The NGR234 Δ*ngrl*Δ*traI* mutant produced comparable amounts of nodules. Since only a small number of plants was analysed for the NGR234 Δ*ngrl*Δ*traI* copy+ and the NGR234 ΔNGR_a01725+, limited conclusions can be drawn from the number of nodules. Nodulation using either of these two strains was possible and plants showed a low number of nodules, but this complied with observations made of the NGR234 WT. By analysing the given data, mutations in these strains seem to decrease the number of nodules (Figure 24). Since NGR234 Δ*repX* and ANU265 were not able to induce any nodule growth, no nodules could be analysed for these two strains regarding nodule weight.

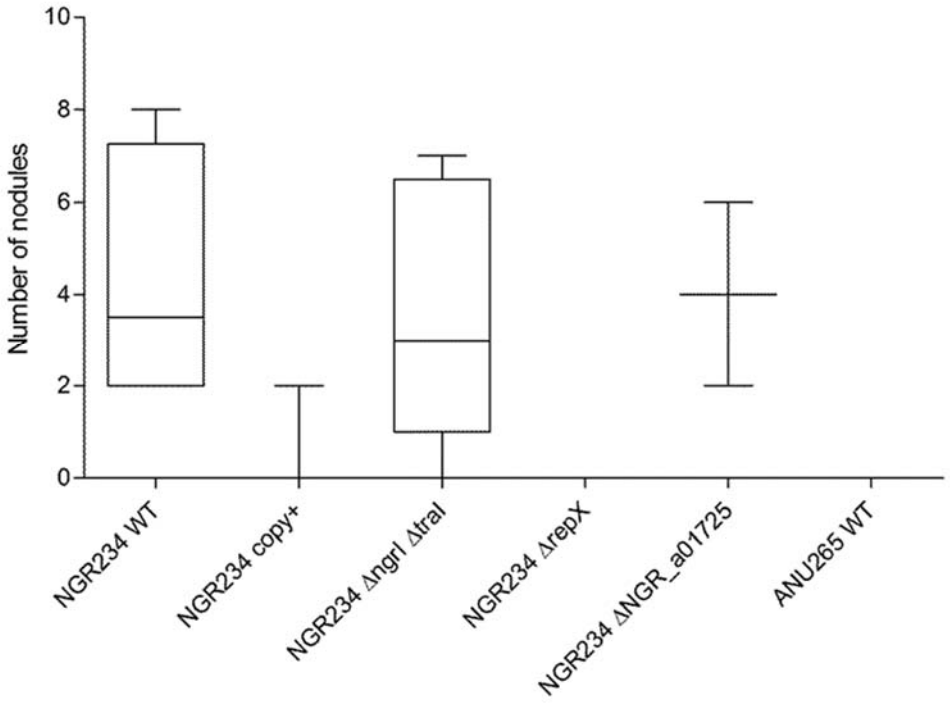

Figure 24: Number of root nodules induced by *S. fredii* NGR234 strains on *Vigna unguiculata.* The boxplots shown, indicate the number of root nodules induced on NGR234's host plant *V. unguiculata* 57 dpi. *V. unguiculata* plants inoculated with the NGR234 WT developed the highest number of nodules on one plant. Plants infected with either NGR234 *ΔrepX* or ANU265 WT did not develop any nodules at all, confirming the lack of the symbiotic plasmid pNGR234*a.* QS system knock-out mutants, NGR234 Δ*ngrI*Δ*traI* copy+ and NGR234 Δ*ngrI*Δ*traI,* were able to nodulate the host plant. Analysing significance, an unpaired t-test was performed, but no significant differences regarding nodule number was seen. Boxes of the boxplots represent the central 50 % of all values, with whiskers including the lowest and upper-most 25 % each. Bar shown in the box represents the median.

Looking at the weight of each of the found nodules some differences could be observed between the weight of nodules induced by the NGR234 WT and the mutant strains (Figure 25). The nodule weight of plants inoculated with the NGR234 Δ*ngrI*Δ*traI* mutant was significantly lower compared to the NGR234 WT formed nodules. The same could be observed for nodules formed by the NGR234 Δ*ngrI*Δ*traI* copy+ strain. However, this result must be examined with care since only a limited number of nodules and plants could be analysed. Two nodules found on plants inoculated with NGR234 Δ*ngrI*Δ*traI* were regarded as outliers indicated by two dots. A highly increased weight of these two nodules was measured compared to other nodules induced by the same strain. Nodules on plants inoculated with NGR234 ΔNGR_a1725 showed a tendency of being smaller or lighter compared to NGR234 WT nodules, but no significant differences were observed (Figure 25).

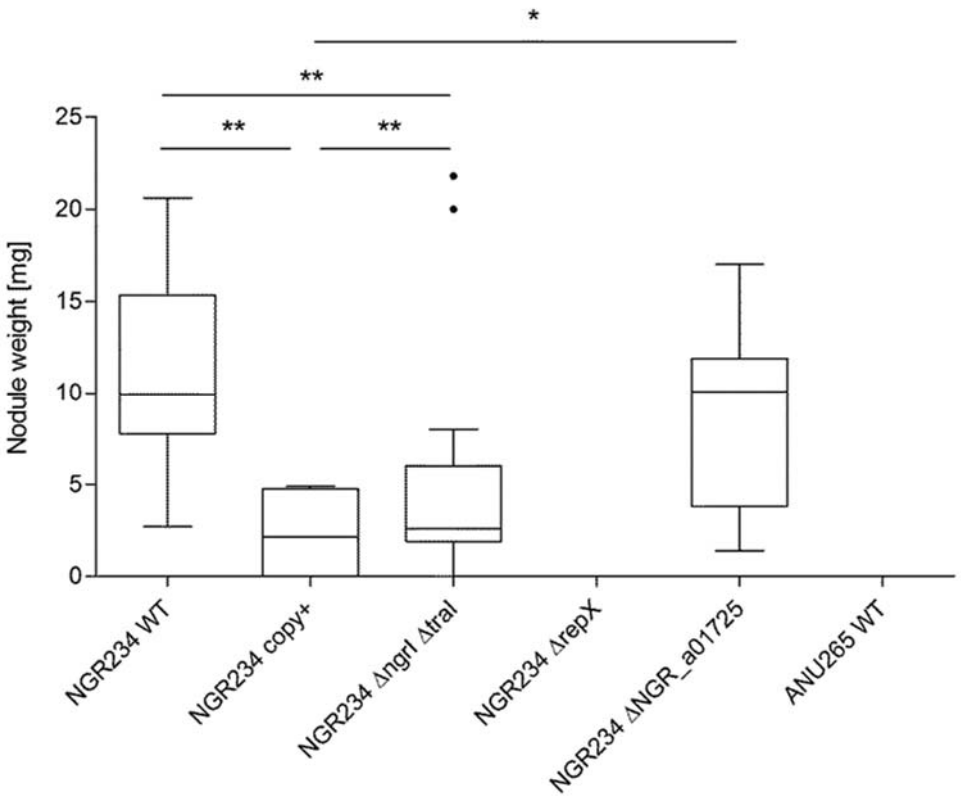

Figure 25: Root nodule weight of *Vigna unguiculata* root nodules induced by *S. fredii* NGR234 strains. The root nodule weight is shown in mg of nodules formed by NGR234's natural host plant *V. unguiculata* 57 dpi. Significant differences in nodule weight were observed, depending on which NGR234 strain was used to infect the *V. unguiculata* plant. Plants inoculated with NGR234 WT exhibited nodules with the highest weight per nodule. QS deletion mutants, NGR234 Δ*ngrI*Δ*traI* copy+ (NGR234 copy+) and NGR234 Δ*ngrI*Δ*traI,* showed significantly lower nodule weight compared to the WT. Comparing the nodule weight of NGR234 copy+ nodules and nodules induced by the NGR234 ΔNGR_a01725 strain, a significant shift in weight was observed. Analysing significance, an unpaired t-test was performed, and significance levels are depicted as asterisk above boxplots ($p \leq 0.05$ shown by one asterisk (*), $p \leq 0.01$ shown by two asterisks (**)). If values did not differ significantly no indication was included. Boxes of the boxplots represent the central 50 % of all values, with whiskers including the lowest and upper-most 25 % each. Bar shown in the box represents the median. Outliers are indicated as dots.

5 Discussion

5.1 Phenotypic heterogeneity

Phenotypic heterogeneity is a phenomenon in bacteria that has been studied just recently. Understanding how the expression of a gene in each single cell forms the population's answer to a specific environmental cue came into focus when methods were available for researchers to track the response of single cells. Here, the effect of deleting two µ-proteins that were just recently discovered (Grote et al., 2016; Petersen, 2019), RepX and NGR_a01725, was analysed and how this lack of such small ORFs modulates phenotypic heterogeneity of QS AI synthase and QQ gene expression in NGR234. Since deletion of the small ORF *repX* leads to a total loss of the symbiotic plasmid, the influence of complete plasmid loss on phenotypic heterogeneity in ANU265 and NGR234 Δ*repX* was further examined. Using the fusion of the *traI*, *ngrI* and *qsdR1* promotors to different fluorescent proteins, enables the visualisation of phenotypic heterogeneity in the population by plotting single cells according to their mean FI.

All NGR234 genotypes analysed here were observed to heterogeneously regulate both AI synthases, *traI* and *ngrI* (see Figure 7 and Figure 8). This pattern was in accordance with the observation made in earlier studies with the NGR234 WT (Grote et al., 2014). Since QS is foremost thought to be a tool for bacteria to monitor their population density, a homogeneous expression would be expected. This would allow bacteria to truly reference the level of AI molecules to population density. However, if single cells are producing more, less, or even no AI molecules, signal intensity only reflects a proportion of the population. A previous study reasoned that the observed phenotypic heterogeneity in *S. fredii* and its close relative *S. meliloti* QS systems is modulated by different internal and external factors (see Figure 26) (Baumgardt et al., 2014, 2016; Bettenworth et al., 2019; Fetzner, 2014; Gao et al., 2015a; Grote et al., 2014, 2016; He et al., 2003; Krol and Becker, 2011; Krysciak et al., 2011; McIntosh et al., 2009; Schäper et al., 2016) and may reflect a variety of division of labour. This division of labour could strengthen the overall population fitness, since not all cells would need to produce costly AI in equal amounts, but all could benefit from the transported information (Bettenworth et al., 2019). Even though not all cells produce AI, the QS signal can trigger population-wide responses to environmental cues. There are many theories as to why bacteria express certain genes heterogeneously besides division of labour: stochastics of intra-cellular compounds, micro-environmental differences – even

though this would be expected to be neglectable in a well-mixed laboratory culture – nutrient availability, host signals, employing different survival strategies (*e.g.* bet hedging), and using QS signals as a way to measure diffusion rates (Ackermann, 2015; Bettenworth et al., 2019; Grote et al., 2014; Schreiber et al., 2016).

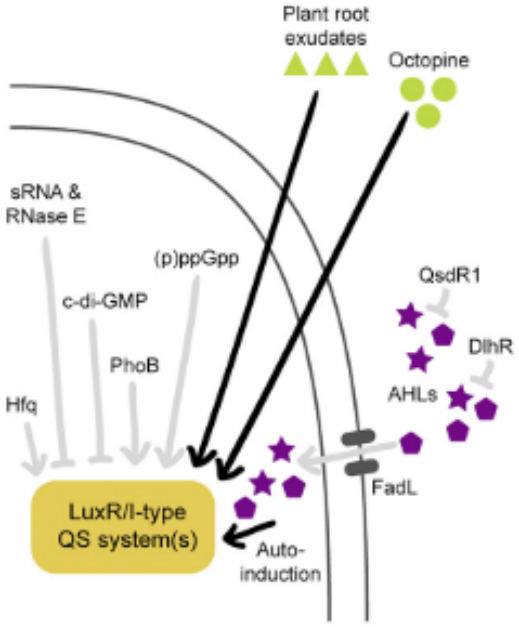

Figure 26: Quorum sensing modulating factors in *S. fredii* and *S. meliloti.* The expression of the LuxR/I-type QS system in *S. fredii* and *S. meliloti* is modulated by several factors. AHL-AI molecules (purple) induce the expression of the respective QS system. QQ enzymes like QsdR1 and DlhR degrade the AI molecules and thereby modify the QS signaling. External factors that influence QS in *Sinorhizobium* are plant derived signals like root exudates or octopine. Internal factors shaping the expression of LuxR/I-type QS systems in *Sinorhizobium* have been linked to nutrient availability. In *S. meliloti* carbon and nitrogen levels influence the expression of the QS regulator gene *sinR*. This is regulated by the guanosine pentaphosphate ((p)ppGpp) synthase *relA*. Phosphate starvation is sensed via the PhoB regulator, leading to an increase in *sinR* expression. QS expression is decreased during the exponential growth phase which is controlled by cyclic diguanylate (c-di-GMP). RNase E degradation of *sinI* RNA was also shown after binding of a small RNA (sRNA). Adapted from Bettenworth et al. (2019).

The genotypes used in this study, namely NGR234 WT, NGR234 Δ*repX*, NGR234 ΔNGR_a01725+ and ANU265, showed considerable phenotypic heterogeneity for the activity of the analysed gene promoters P*traI*, P*ngrI* and P*qsdR1*. This observation indicates that phenotypic heterogeneity of QS AI synthases and the metallo-β-lactamase QsdR1 can be viewed independently of the two examined μ-proteins encoded on the symbiotic plasmid. Phenotypic heterogeneity in general was not strongly influenced by any factor encoded on pNGR234*a,* since neither ANU265 nor NGR234 Δ*repX* harbour the mentioned plasmid. In the past, it was shown that high levels of externally provided AI, as well as plant derived compounds, could quench the degree of heterogeneously expressed QS genes and lead to a more homogeneous expression (Grote et al., 2014). This leads to the conclusion that low levels of AI, as

expected when one AI synthase is missing, favour phenotypic heterogeneity. The results here further underline this observation for ANU265, presenting a high degree of phenotypic heterogeneity (see Figure 12). ANU265 showed a broad range of varying FI after 24 and 48 h, with the population-wide median FI at 24 h being three times higher compared to the NGR234 WT (see Figure 20). Since ANU265 was cured of its symbiotic plasmid (Morrison et al., 1983), this de-regulated early QS and QQ activation could be caused by factors encoded on the respective plasmid and therefore missing. Another possible reason for the high diversity of P*traI* and P*ngrI* promoter activity in ANU265 could be, that the missing AI synthase *traI,* leaving only *ngrI* as AI source, leads to very low AI levels and therefore stimulates phenotypic heterogeneity as mentioned above. Reasoning against low AI levels as a main stimulating factor for phenotypic heterogeneity are results shown for NGR234 Δ*repX* (see Figure 15). This genotype was also cured of its symbiotic plasmid after deletion of the small ORF *repX* (Petersen, 2019) and exhibits less pronounced levels of phenotypic heterogeneity indicating that AIs are not the only factors in NGR234 to modulate phenotypic heterogeneity of the QS AI synthases and the QQ *qsdR1* gene. There have been reports in other bacteria showing heterogeneity independently of QS AI concentration (Pradhan and Chatterjee, 2014). Deletion of the ORF encoding for the µ-protein NGR234 ΔNGR_a01725+ leads to a high diversity of FI, representing heterogeneously expressed QS and QQ genes after 48 h (see Figure 18). Micro-proteins have only recently come into focus and have been discovered to regulate many cellular processes in bacteria like spore formation, cell division or signal transduction (Storz et al., 2014). Therefore, it can be speculated that the µ-protein NGR_a01725, encoded on the symbiotic plasmid, may influence phenotypic heterogeneity in NGR234 and shifts the whole level of population-wide expression to higher levels as well (see Figure 20). Even though the underlying regulation mechanisms are not yet fully understood.

However, in this study the degree of observed phenotypic heterogeneity regarding expression intensity of the analysed promoter fusions was affected depending on the genotype, indicating some sort of secondary effect on the degree of phenotypic heterogeneity and the monitored genes. The median FI of each genotype (see Figure 20 A-C) reflects how the population-wide expression level of the specific monitored genes was, without being too sensitive to extreme outliers. Altering NGR234's genetic background, by either deleting small ORFs like NGR234 ΔNGR_a01725+ or Δ*repX,* had an influence on how the population regulated AI synthases and a QQ gene and thereby shifted the level of phenotypic heterogeneity. Even though the deletion of the

μ-proteins or the complete loss of pNGR234*a* may not strongly influence gene expression on a population level, it influences the expression levels on the single cell level. This leads to a less pronounced shift in the expression on a population level.

One limitation of these kind of analyses – and all together the determination of phenotypic heterogeneity in bacteria – is the artificial laboratory setting in which these experiments take place. NGR234, being a soil bacterium, naturally encounters a broad range of other soil bacteria, especially in the rhizosphere. These organisms, along with plants that may serve as hosts, are modulating the environment and compete for resources. Plant roots constantly secret organic compounds into the soil in order to balance their intra-cellular pH value. Thereby, plants modulate the pH values of the soil in the rhizosphere (Hinsinger et al., 2016). In a study using *Pseudomonas aeruginosa* and *Yersinia pseudotuberculosis*, the influence of pH of the growth medium on AI concentrations was analysed. It was shown that AI were less stable at higher pH values compared to neutral or even acidic conditions (Yates et al., 2002). The natural concentration of AI by NGR234 in the rhizosphere may therefore differ when compared to the laboratory cultures analysed here. Since it is reasonable that the concentration of AI influences phenotypic heterogeneity of the respective genes as discussed above, the conducted analysis may only partially reflect conditions in the soil. Another factor affecting AI concentrations and phenotypic heterogeneity are other bacteria dwelling in the soil together with NGR234. In a co-cultivation experiment, two potable water bacteria, *Enterobacter sp.* and *Pseudomonas sp.* were grown together. In co-cultivation both bacteria experienced a decrease of phenotypic heterogeneity for the observed features, indicating that phenotypic heterogeneity in natural communities may not be as prominent as expected (Heyse et al., 2019). In the future, experiments on how bacteria mutually shape their phenotypic heterogeneity in nature should be performed.

A second interesting observation made in this study refers to the simultaneous activity of QS and QQ genes on the population level and especially on the single cell level. It may not seem to be efficient to express QS signal producing synthases and enzymes that degrade these signals simultaneously. QQ and the expression of its associated genes has been studied in a broad range of bacteria. The plant pathogen *A. tumefaciens* that harbours a *tral/traR* QS system like NGR234, was shown to degrade its own QS signal (Grandclément et al., 2015). The expression of QQ genes modulates the QS response during tumour growth and while population density is low. This prevents untimely and costly expression of the conjugational transfer machinery (Khan and Farrand, 2009). This is also in line with findings that NGR234 showed

growth inhibition in response to the TraI AI, 3-oxo-C_8-HSL (He et al., 2003). An overshooting early QS response would therefore lead to growth inhibition, making it reasonable why NGR234 co-expresses QS and QQ genes. Another possible and rather simple reason for parallel expression of QS and QQ genes may be the re-use of resources (Grandclément et al., 2015). All analysed genotypes were observed to express QS and QQ at the same time. This could hint towards a regulatory background independent of the symbiotic plasmid itself and the µ-proteins encoded thereon. Overall, this may explain the seemingly costly parallel expression of QS and QQ genes in NGR234 as observed here.

Employing single cell analysis and measurements gave the opportunity to shape the understanding on how single cell expression forms population response. It has become clear that cells experience a broad range of expression intensities, and that the degree of phenotypic heterogeneity is more diverse than expected.

5.2 Copy number variations in *S. fredii* NGR234

The copy number of low copy plasmids in bacteria has to be controlled and regulated in order to ensure stable plasmid maintenance. Plasmids of the *repABC* family, such as the symbiotic plasmid of NGR234, have their genes arranged in an operon structure for replication and plasmid segregation (Cevallos et al., 2008; Pinto et al., 2012). Its expression is governed via the *repA* promoter, a non-coding RNA in the intergenic region of the *repB* and *repC* ORF and by inhibition of the initiator protein, RepC, by RepA and RepB. These mechanisms lead to a low copy number. In NGR234 the plasmid copy number of the symbiotic plasmid equals one plasmid per chromosome (Grote et al., 2016). In the same study it was shown that deletion of both AI synthases resulted in an upregulation of the plasmid copy number of pNGR234*a,* as well as in an upregulation of nearly all genes encoded thereon (Grote et al., 2016). However, this effect was further analysed and it was revealed that the small ORF *repX,* direct divergently adjacent to the deleted *traI* ORF, had an influence on the symbiotic plasmid copy number (Petersen, 2019). To further characterise this effect, the NGR234 *ΔngrIΔtraI* copy+ mutant was grown with spent culture supernatant of other *S. fredii* strains and NGR234 mutants. Results of a higher plasmid copy number of pNGR234*a* could be reproduced as described before when no treatment was applied (Grote et al., 2016). The following analyses here showed that the copy number of the symbiotic plasmid in NGR234 could be rescued by addition of spent culture supernatant of NGR234 WT, but not by supernatant originating of the closely related

strains ANU265 and USDA257. Using the supernatant of the single AI synthase deletion mutants of NGR234 did even promote the observed copy number effect in the NGR234 *ΔngrIΔtraI* copy+ mutant (see Figure 21). These results indicate that the NGR234 symbiotic plasmid copy number is either partially regulated by some factor that can be secreted and influences plasmid copy number of other cells, or that the ratio of TraI and NgrI derived AI produced by NGR234 might have an effect on the symbiotic plasmid copy number. This could explain why the supernatant of other closely related species and the AI single deletion mutants could not quench the observed plasmid copy number effect by not producing AI in the respective ratio as NGR234. For *A. tumefaciens* an influence of AI on its plasmid copy number was already shown. In this plant pathogen, an increasing concentration of 3-oxo-C_8-HSL AI leads to an increase in the plasmid copy number (Pappas and Winans, 2003b). A similar observation was made for *R. leguminosarum* and its respective symbiotic plasmid pRL1JI. Elevated levels of AI not only induced conjugational transfer genes, but also stimulated expression of the *repABC* operon and thereby resulted in a higher plasmid copy number (McAnulla et al., 2007). In contrast to NGR234, the *R. leguminosarum* genome encodes for at least four AI synthases. Each of these QS systems influences different processes like growth and biofilm formation, nodulation or plasmid transfer (Lithgow et al., 2000; Rodelas et al., 1999; Wisniewski-Dyé and Downie, 2002). In NGR234, so far only two QS systems have been identified. As these QS systems regulate many genes and biological functions in NGR234 (Krysciak et al., 2014), altering the AI ratio and concentration may lead to a misbalance in plasmid copy number regulation. To overcome this imbalance and re-establish normal levels of AI for a possible normal functioning and communication with potential host plants, the copy number of the symbiotic plasmid may be altered. The up-regulation of the plasmid copy number and the corresponding gene transcription, may also be influenced by selective pressure on NGR234 to provide a potential host with growth promoting factors and therefore enhance its probability to establish successful symbiosis. Low amounts of AI and its degradation products have been shown to promote plant growth, whereas high concentrations have shown contrary effects (Palmer et al., 2014). In another study it was described that AHL could induce Ca^{2+} spiking in root cells of *Arabidopsis thaliana* (Song et al., 2011). Ca^{2+} spiking is known to be a general signal in plant cells, regulating a diverse set of genes and is also involved in signalling during symbiosis initiation (Oldroyd and Downie, 2008; Tuteja and Mahajan, 2007). Furthermore, a recent study presented evidence that bacterial communities and their AI are affecting plant responses to AI themselves (Veliz-Vallejos et al., 2020). First, AI signals are

perceived not only directly from symbiotic bacteria in the rhizosphere but detecting all AI signals produced by other near bacteria. Secondly, by altering signals by QQ. For example, NGR234 was shown to encode for five QQ enzymes (Krysciak et al., 2011). *A. tumefaciens* has been found to degrade its own QS signal, in order to suppress premature conjugation plasmid transfer (Grandclément et al., 2015). A similar process may also be applicable for NGR234 and its host infection. Thirdly, a study revealed that a host plant, upon receiving its symbiont-specific AHL signal 3-oxo-C_{14}-HSL, upregulated the expression of early nodulation genes important for successful symbiosis (Veliz-Vallejos et al., 2020). These results could explain why NGR234 relies on producing AI in a certain concentration and ratio and elevates its plasmid copy number to compensate for missing QS signals. This may be another link of QS to symbiosis and how bacterial signalling influences the plant response. However, in NGR234 the lack of AI and the impaired expression of the small ORF *repX* induced an up-regulation of almost all genes encoded on the symbiotic plasmid, leading to its increased copy number. It is thought to support higher metabolic rates of bacteriods in nodules (Jones et al., 2007). This effect is not fully understood, but the results presented here further indicate that the observed plasmid copy number effect was not only caused by a lack of AI. Hence, additional factors like RepX might play a role in plasmid copy number regulation besides the established regulation networks. A former study was able to show that rhizobia in indeterminate nodules can increase their genome copies and increase their cell size before differentiating into bacteriods during nodulation (Jones et al., 2007). Increasing the plasmid copy number, may be regulated by RepX in NGR234 and thereby providing a way for NGR234 to achieve these higher metabolic rates for symbiotically relevant genes.

In a second experiment, the influence of other bacteria, their AI and secreted compounds on NGR234's plasmid copy number was analysed (see Figure 22). The soil bacterium *B. glumae* PG1 was utilised as a model organism, being a soil dwelling plant pathogen. NGR234 WT and the NGR234 *ΔngrIΔtraI* copy+ mutant were grown with culture supernatant of *B. glumae* PG1 and its respective AI deletion mutants (Gao et al., 2015b), to gain a better understanding on how different AI influence the plasmid copy number in NGR234. The AI synthase BgaI1 is thought to produce a 3-oxo-C_8-HSL, while BgaI2 probably synthesises a 3-oxo-C_{10}-HSL and BgaI3 most likely corresponds to either a C_{10}-AHL or a 3-oxo-C_{12}-HSL (Gao et al., 2015b). The *B. glumae* PG1 WT and the single AI synthase mutant strains *B. glumae ΔbgaI2* and *ΔbgaI3* had a quenching effect on the increased copy number of pNGR234*a* in the

NGR234 *ΔngrIΔtraI* copy+ mutant and no effect on the NGR234 WT. Cultivation of NGR234 using spent medium of the *B. glumae Δbgal1* AI deletion mutant that no longer produced a putative 3-oxo-C_8-HSL AI, even had an increasing effect on both NGR234 strains, regarding their symbiotic plasmid copy number. Interestingly, these findings show that NGR234 cannot only sense, but does also respond to QS signals of other soil bacteria, altering its own gene expression. Since the *B. glumae* PG1 WT supernatant had a quenching effect, similar to the NGR234 WT supernatant, it can be speculated that the ratio of 3-oxo-C_8-HSL and long chain AHL like 3-oxo-C_{10}-HSL or 3-oxo-C_{12}-HSL may influence the NGR234 copy number. It may be possible that the ration of *B. glumae* PG1 AI resembles NGR234s' own AI ratio and thereby was able to slightly quench the copy number effect. When this ratio was disturbed and no 3-oxo-C_8-HSL by *B. glumae* PG1 was supplied, the copy number could not be rescued. This inter-species sensing is also known for other bacteria and was already speculated to interfere with *R. leguminosarum* QS (Miller and Bassler, 2001; Williams et al., 2007; Wisniewski-Dyé and Downie, 2002). A rather useful example of cross-species detection of QS AHL signals can be found in *A. tumefaciens* and *Chromobacterium violaceum.* When utilising AI synthases deficient reporter strains, these bacteria have been regularly used to screen for AI signals of other bacteria in TLC assays (Gao et al., 2015b; Krysciak et al., 2014; Shaw et al., 1997). The question remains if bacteria with multiple QS systems can encode another message, besides population density, in the ratio of the AI they produce to transport information to either their own population, other bacteria or their respective host. This has to be further investigated and analysed.

5.3 Nodulation

S. fredii NGR234 has a remarkable host range and can nodulate over 120 plant genera (Pueppke and Broughton, 1999). The influence of QS on its nodulation efficiency and how µ-proteins may alter nodulation in NGR234 was analysed to gain insights on how these factors modulate nodulation. The ability to nodulate the NGR234 host plant *Vigna unguiculata* was investigated using NGR234 WT, NGR234 *ΔngrIΔtraI copy+,* NGR234 *ΔngrIΔtraI,* NGR234 Δ*repX,* NGR234 ΔNGR_a01725 and AN265 WT. As mentioned before, ANU265 and NGR234 Δ*repX* have both been cured of their symbiotic plasmid. For both strains, no nodule formation could be observed being in line with previous reported results (Morrison et al., 1983; Petersen, 2019). All other strains were observed to produce nodules on their host plant *V. unguiculata* (see Figure 23). This is in accordance with results reported by other studies for the NGR234 AI synthase deletion mutants, where nitrogen fixing nodules were formed on the same

host plant (Krysciak et al., 2014). However, when EPS deficient NGR234 strains were used to infect another host plant of NGR234, *Leucaena leucocephala,* only compromised non-fixing nodules could be found. The addition of exogenous supplied EPS was able to restore nodule formation (Djordjevic et al., 1987). These contrasting results highlight that symbiosis between host plant and rhizobia is very specific and multiple factors come together. For other rhizobia, a connection between QS and symbiosis was shown. In *S. meliloti,* QS was observed to be essential for symbiosis establishment. Nevertheless, in a review a list of rhizobia was compiled, stating that not for all species a functioning QS system is needed during symbiosis (Calatrava-Morales et al., 2018). Even though QS systems might not influence symbiosis directly, a deficient QS may affect other processes that are essential during symbiosis. EPS for example have been reported to support biofilm formation on roots and can play a role in symbiosis (Calatrava-Morales et al., 2018; Deakin and Broughton, 2009). In NGR234, the reception of plant signals was shown to alter the composition of produced polysaccharides (Fraysse et al., 2002). Flagellar expression, down regulated in the NGR234 single QS mutants (Krysciak et al., 2014), has been reported to influence symbiosis in some rhizobia (Calatrava-Morales et al., 2018). Looking at the nodule type formed by NGR234 on *V. unguiculata* and *L. leucocephala* plants, revealed that one host plant, *Vigna* spp*.,* forms determinate nodules upon NGR234 infection and the other, *Leucaena* spp*.,* indeterminate nodules (Li et al., 2013). Since NGR234 is a broad host range strain, forming either determinate or indeterminate nodules, regulated by the host plant, QS may not play a crucial role in establishment of symbiosis with *V. unguiculata,* as shown here and in other studies (Krysciak et al., 2014). Other symbioses will need further research to elucidate the whole picture of NGR234's broad host range.

Results presented here referring to the number and weight of root nodules can only indicate tendencies, since numbers of tested plants did not reflect a broad sample size. However, the numbers of formed nodules observed for the tested genotypes of NGR234 can give a first impression if and how AI deletion or μ-proteins can influence the nodule number (see Figure 24) and weight (see Figure 25). The root nodule numbers seemed not to be significantly influenced by deletion of both AI synthases, neither utilising the deletion mutant with an elevated plasmid copy number of its symbiotic plasmid, nor the AI synthase mutant strain without plasmid copy number effect. This may not be surprising, since the number of nodules is regulated by the host (Schauser et al., 1999; Stougaard, 2000). If rhizobia remain capable of establishing

symbiosis, the total number of root nodules should remain stable (Figure 24). The nodule weight of harvested nodules showed higher deviations between the genotypes used for infection. Here, the AI synthase deletion mutants, with or without increased copy numbers of their symbiotic plasmid, were observed to have lighter nodules. In contrast, the deletion of the small ORF NGR234 ΔNGR_a01725 had no significant effect (Figure 25). Smaller and lighter nodules may indicate compromised nitrogen fixation compared to nodules induced by the NGR234 WT. However, fixation rates and nitrogenase activity were not measured. In the future, it will be interesting to investigate, if nodules of QS impaired NGR234 cells can fixate nitrogen as efficiently as their respective WT in *V. unguiculata.* In their review, Rolfe and Gresshoff stated that plants can sense whether nodules are functioning or not and, as a consequence, stop the nutritional flow towards these nodules (Rolfe and Gresshoff, 1988). It may be speculated that nodules of the NGR234 mutant strains, having smaller nodules due to impaired nitrogen fixation, may receive less nutrients by the host plant than the NGR234 WT strain.

5.4 Outlook

Rhizobia plant interaction and symbiosis constitutes a finely tuned and complex communication. There are many factors affecting this signal exchange. In this study, further insights could be gained, if QS modulates symbiosis with *V. unguiculata* and how newly identified plasmid borne μ-proteins of NGR234s symbiotic plasmid may influence symbiosis efficiency. Furthermore, bacterial phenotypic heterogeneity regarding QS and QQ genes was analysed, shedding a light on how single cells shape population-wide responses. In the future, work remains to further deepen our understanding on how these processes are interlinked and how host and symbiont shape their mutual gene expression.

Regarding phenotypic heterogeneity in NGR234, it will be interesting to explain, if this phenomenon can be observed in mixed bacterial communities and how it could be shaped by other bacteria. Therefore, experiments as conducted by Heyse and colleagues could be utilised, to analyse the development of NGR234 phenotypic heterogeneity when co-cultivated with other soil bacteria (Heyse et al., 2019). Phenotypic heterogeneity has been observed to be modulated by plant root exudates (Grote et al., 2014). As these plant signals lead to a more homogeneous expression pattern of AI synthases, it will be interesting, if this effect also alters the ratio and total levels of secreted AI. Extracting AI from NGR234 cultures cultivated with either

flavonoids, or plant root exudates may provide another link of QS and symbiosis. These results can broaden our understanding of the natural function of phenotypic heterogeneity in NGR234 and maybe even in bacteria in general. Co-cultivation may also be a useful tool to gain a better understanding, if NGR234 AI synthase mutants and other mutant strains tested here, really are not impaired in their nodulation efficiency, when compared to other competing rhizobia. Even though NGR234 *ΔngrIΔtraI,* its symbiotic plasmid copy+ variant (NGR234 *ΔngrIΔtraI copy+)* and the respective single AI synthase deletion mutants have been shown to nodulate their host plant *V. unguiculata,* it remains unclear if competitiveness of NGR234 may not be decreased. Lowered EPS production and flagellar expression represent two factors influencing symbiosis. EPS are crucial for some other rhizobia to establish symbiosis in the first place (Calatrava-Morales et al., 2018). It will be interesting to analyse, if decreased EPS and flagellar expression enhance or dampen NGR234's competitiveness.

A lot of work has already been conducted to deepen our understanding of how rhizobia and plants initiate symbiosis and how this process is regulated. However, it remains poorly understood how *e.g.* µ-proteins in NGR234 shape gene expression or plasmid copy number regulation as reported by others (Grote et al., 2016; Petersen, 2019) and why NGR234 may increase its symbiotic plasmid copy number when cultivated with spent medium of other bacteria. Studies on how these genes may be expressed and how the plasmid copy number develops during symbiosis and inside nodules can give further indications what their natural role in NGR234 is. This could be achieved by extracting bacterial RNA and DNA from root nodules, analyse expression levels of µ-proteins within nodules and measure the plasmid copy number inside nodules formed by NGR234. Combining the results of this study with previous and future results will deliver new insights into plant rhizobia interaction and open up new and exciting questions and possibly lead to new ideas how phenotypic heterogeneity shapes bacterial communities in nature.

6 References

Abda, E.M., Krysciak, D., Krohn-Molt, I., Mamat, U., Schmeisser, C., Förstner, K.U., Schaible, U.E., Kohl, T.A., Nieman, S., and Streit, W.R. (2015). Phenotypic heterogeneity affects *Stenotrophomonas maltophilia* K279a colony morphotypes and b-lactamase expression. Front. Microbiol. *6*, 1–16.

Ackermann, M. (2015). A functional perspective on phenotypic heterogeneity in microorganisms. Nat. Rev. Microbiol. *13*, 497–508.

Allen, E.K., and Allen, O.N. (1950). Biochemical and symbiotic properties of the rhizobia. Bacteriol. Rev. *14*, 273–330.

Alunni, B., and Gourion, B. (2016). Terminal bacteroid differentiation in the legume-rhizobium symbiosis: nodule-specific cysteine-rich peptides and beyond. New Phytol. *211*, 411–417.

Anetzberger, C., Pirch, T., and Jung, K. (2009). Heterogeneity in quorum sensing-regulated bioluminescence of *Vibrio harveyi*. Mol. Microbiol. *73*, 267–277.

Bassam, B.J., Djordjevic, M.A., Redmond, J.W., Batley, M., and Rolfe, B.G. (1988). Identification of a nodD-Dependent Locus in the *Rhizobium* strain NGR234 Activated by Phenolic Factors Secreted by Soybeans and Other Legumes. Mol. Plant-Microbe Interact. *1*, 161–168.

Baumgardt, K., Charoenpanich, P., McIntosh, M., Schikora, A., Stein, E., Thalmann, S., Kogel, K.H., Klug, G., Becker, A., and Evguenieva-Hackenberg, E. (2014). RNase E affects the expression of the acyl-homoserine lactone synthase gene *sinI* in *Sinorhizobium meliloti*. J. Bacteriol. *196*, 1435–1447.

Baumgardt, K., Šmìdovà, K., Rahn, H., Lochnit, G., Robledo, M., and Evguenieva-Hackenberg, E. (2016). The stress-related, rhizobial small RNA RcsR1 destabilizes the autoinducer synthase encoding mRNA sinI in Sinorhizobium meliloti. RNA Biol. *13*, 486–499.

Beijerinck, M.W. (1888). Die Bacterien der Papilionaceenknöllchen. Bot. Zeitung *46*, 726–735.

Beijerinck, M.W. (1901). Über oligonitrophile Mikroben. Cent. Für Bakteriol. Parasitenkunde, Infekt. Und Hygine, Abteilung II *7*, 561–582.

Bertani, G. (1951). Studies on lysogenesis. I. The mode of phage liberation by lysogenic *Escherichia coli*. J. Bacteriol. *62*, 293–300.

Bettenworth, V., Steinfeld, B., Duin, H., Petersen, K., Streit, W.R., Bischofs, I., and Becker, A. (2019). Phenotypic Heterogeneity in Bacterial Quorum Sensing Systems. J. Mol. Biol. *Volume 431*, 4530–4546.

Broughton, W.J., and Dilworth, M.J. (1971). Control of leghaemoglobin synthesis in snake beans. Biochem. J. *125*, 1075–1080.

Broughton, W.J., Heycke, N., Z.A., H.M., and Pankhurst, C.E. (1984). Plasmid-linked nif and “nod” genes in fast-growing rhizobia that nodulate *Glycine max, Psophocarpus tetragonolobus*, and *Vigna unguiculata*. Proc. Natl. Acad. Sci. *81*, 3093–3097.

Calatrava-Morales, N., McIntosh, M., and Soto, M.J. (2018). Regulation Mediated by N-acyl Homoserine Lactone Quorum Sensing Signals in the *Rhizobium*-Legume Symbiosis. Genes (Basel). *9*.

Carpenter, A.E., Jones, T.R., Lamprecht, M.R., Clarke, C., Kang, I.H., Friman, O., Guertin, D.A., Chang, J.H., Lindquist, R.A., Moffat, J., et al. (2006). CellProfiler: Image analysis software for identifying and quantifying cell phenotypes. Genome Biol. *7*.

Cervantes-Rivera, R., Pedraza-Lopez, F., Perez-Segura, G., and Cevallos, M.A. (2011). The replication origin of a repABC plasmid. BMC Microbiol. *11*, 158.

Cevallos, M.A., Cervantes-Rivera, R., and Gutiérrez-Ríos, R.M. (2008). The repABC plasmid family. Plasmid *60*, 19–37.

Cha, C., Gao, P., Chen, Y., Shaw, P.D., and Farrand, S.K. (1998). Production of acyl-homoserine lactone quorum-sensing signals by Gram-negative plant-associated bacteria. Mol. Plant-Microbe Interact. *11*, 1119–1129.

Chai, Y., and Winans, S.C. (2005). A small antisense RNA downregulates expression of an essential replicase protein of an *Agrobacterium tumefaciens* Ti plasmid. Mol. Microbiol. *56*, 1574–1585.

Chen, G., Jeffrey, P.D., Fuqua, C., Shi, Y., and Chen, L. (2007). Structural basis for antiactivation in bacterial quorum sensing. Proc. Natl. Acad. Sci. U. S. A. *104*, 16474–16479.

Cooper, J.E. (2007). Early interactions between legumes and rhizobia: disclosing

complexity in a molecular dialogue. J. Appl. Microbiol. *103*, 1355–1365.

Deakin, W.J., and Broughton, W.J. (2009). Symbiotic use of pathogenic strategies: Rhizobial protein secretion systems. Nat. Rev. Microbiol. *7*, 312–320.

Denarie, J., Debellé, F., and Promé, J.-C. (1996). Rhizobium Lipo-Chitooligosaccharide Nodulation Factors: Signaling Molecules Mediating Recognition and Morphogenesis. Annu. Rev. Biochem. *65*, 503–535.

Djordjevic, S.P., Chen, H., Batley, M., Redmond, J.W., and Rolfe, B.G. (1987). Nitrogen fixation ability of exopolysaccharide synthesis mutants of Rhizobium sp. strain NGR234 and Rhizobium trifolii is restored by the addition of homologous exopolysaccharides. J. Bacteriol. *169*, 53–60.

Ebersbach, G., and Gerdes, K. (2005). Plasmid segregation mechanisms. Annu. Rev. Genet. *39*, 453–479.

Ebersbach, G., Sherratt, D.J., and Gerdes, K. (2005). Partition-associated incompatibility caused by random assortment of pure plasmid clusters. Mol. Microbiol. *56*, 1430–1440.

Ehrhardt, D.W., Wais, R., and Long, S.R. (1996). Calcium spiking in plant root hairs responding to rhizobium nodulation signals. Cell *85*, 673–681.

Escobar, M.A., and Dandekar, A.M. (2003). *Agrobacterium tumefaciens* as an agent of disease. Trends Plant Sci. *8*, 380–386.

Esseling, J.J., Lhuissier, F.G.P., and Emons, A.M.C. (2003). Nod factor-induced root hair curling: Continuous polar growth towards the point of nod factor application. Plant Physiol. *132*, 1982–1988.

Feng, J., Li, Q., Hu, H.L., Chen, X.C., and Hong, G.F. (2003). Inactivation of the nod box distal half-site allows tetrameric NodD to activate *nodA* transcription in an inducer-independent manner. Nucleic Acids Res. *31*, 3143–3156.

Fetzner, S. (2014). Quorum quenching enzymes. J. Biotechnol. *201*, 2–14.

Flores, M., Mavingui, P., Girard, L., Perret, X., Broughton, W.J., Martinez-Romero, E., Davila, G., and Palacios, R. (1998). Three replicons of *Rhizobium* sp. Strain NGR234 harbor symbiotic gene sequences. J. Bacteriol. *180*, 6052–6053.

Fournier, J., Timmers, A.C.J., Sieberer, B.J., Jauneau, A., Chabaud, M., and Barker,

D.G. (2008). Mechanism of infection thread elongation in root hairs of *Medicago truncatula* and dynamic interplay with associated rhizobial colonization. Plant Physiol. *148*, 1985–1995.

Frank, B. (1889). Über die Pilzsymbiose der Leguminosen. Ber Detusche Botniasche Gesellschaft *Vol 7*, 332–346.

Fraysse, N., Jabbouri, S., Treilhou, M., Couderc, F., and Poinsot, V. (2002). Symbiotic conditions induce structural modifications of *Sinorhizobium* sp. NGR234 surface polysaccharides. Glycobiology *12*, 741–748.

Freiberg, C., Perret, X., Broughton, W.J., and Rosenthal, A. (1996). Sequencing the 500-kb GC-rich symbiotic replicon of *Rhizobium* sp. NGR234 using dye terminators and a thermostable “sequenase”: a beginning. Genome Res. *6*, 590–600.

Freiberg, C., Fellay, R., Bairoch, A., Broughton, W.J., Rosenthal, A., and Perret, X. (1997). Molecular basis of symbiosis between *Rhizobium* and legumes. Nature *387*, 394–401.

Frenken, L.G.J., Egmond, M.R., Batenburg, A.M., Bos, J.W., Visser, C., and Verrips, C.T. (1992). Cloning of the *Pseudomonas glumae* lipase gene and determination of the active site residues. Appl. Environ. Microbiol. *58*, 3787–3791.

Fuqua, C., and Winans, S.C. (1996). Conserved cis-acting promoter elements are required for density-dependent transcription of *Agrobacterium tumefaciens* conjugal transfer genes. J. Bacteriol. *178*, 435–440.

Fuqua, C., Burbea, M., and Winans, S.C. (1995). Activity of the *Agrobacterium* Ti plasmid conjugal transfer regulator TraR is inhibited by the product of the *traM* gene. J. Bacteriol. *177*, 1367–1373.

Fuqua, W.C., Winans, S.C., and Greenberg, E.P. (1994). Quorum sensing in bacteria: The LuxR-LuxI family of cell density- responsive transcriptional regulators. J. Bacteriol. *176*, 269–275.

Gao, M., Tang, M., Guerich, L., Salas-Gonzalez, I., and Teplitski, M. (2015a). Modulation of *Sinorhizobium meliloti* quorum sensing by Hfq-mediated post-transcriptional regulation of ExpR. Environ. Microbiol. Rep. *7*, 148–154.

Gao, R., Krysciak, D., Utpatel, C., Knapp, A., Schmeisser, C., Daniel, R., Voget, S., Jaeger, K.-E., and Streit, W.R. (2015b). Genome-wide RNA sequencing analysis of

quorum sensing-controlled regulons in the plant-associated *Burkholderia glumae* strain PG1. Appl. Environ. Microbiol. *81*, Submitted.

García-Betancur, J.-C., Goñi-Moreno, Á., Horger, T., Schott, M., Sharan, M., Eikmeier, J., Wohlmuth, B., Zernecke, A., Ohlsen, K., Kuttler, C., et al. (2017). Cell differentiation defines acute and chronic infection cell types in *Staphylococcus aureus*. Elife *6*, e28023-39.

Gehring, C.A., Irving, H.R., Kabbara, A.A., Parish, R.W., Boukli, N.M., and Broughton, W.J. (1997). Rapid, plateau-like increases in intracellular free calcium are associated with Nod-factor-induced root-hair deformation. Mol. Plant-Microbe Interact. *10*, 791–802.

Goedhart, J., Hink, M.A., Visser, A.J.W.G., Bisseling, T., and Gadella, T.W.J. (2000). *In vivo* fluorescence correlation microscopy (FCM) reveals accumulation and immobilization of nod factors in root hair cell walls. Plant J. *21*, 109–119.

Grandclément, C., Tannières, M., Moréra, S., Dessaux, Y., and Faure, D. (2015). Quorum quenching: Role in nature and applied developments. FEMS Microbiol. Rev. *40*, 86–116.

Green, M.R., and Sambrook, J. (2012). Molecular Cloning: A Laboratory Manual (Set of 3) (Cold Spring Harbor, NY: Cold Spring Harbor Laboratory Press).

Grote, J., Krysciak, D., Schorn, A., Dahlke, R.I., Soonvald, L., Müller, J., Hense, B.A., Schwarzfischer, M., Sauter, M., Schmeisser, C., et al. (2014). Evidence of Autoinducer-Dependent and -Independent Heterogeneous Gene Expression in *Sinorhizobium fredii*. Appl. Environ. Microbiol. *80*, 5572–5582.

Grote, J., Krysciak, D., Petersen, K., Güllert, S., Schmeisser, C., Förstner, K.U., Krishnan, H.B., Schwalbe, H., Kubatova, N., and Streit, W.R. (2016). The Absence of the N-acyl-homoserine-lactone Autoinducer Synthase Genes *traI* and *ngrI* Increases the Copy Number of the Symbiotic Plasmid in *Sinorhizobium fredii* NGR234. Front. Microbiol. *7*, 1858.

He, X., Chang, W., Pierce, D.L., Seib, L.O., Wagner, J., Fuqua, C., and Ort, L. (2003). Quorum Sensing in *Rhizobium* sp . Strain NGR234 Regulates Conjugal Transfer (*tra*) Gene Expression and Influences Growth Rate. J. Bacteriol. *185*, 809–822.

Hernandez-Valdes, J.A., van Gestel, J., and Kuipers, O.P. (2020). A riboswitch gives

rise to multi-generational phenotypic heterogeneity in an auxotrophic bacterium. Nat. Commun. *11*, 1–13.

Heyse, J., Buysschaert, B., Props, R., Rubbens, P., Skirtach, A.G., Waegeman, W., and Boon, N. (2019). Coculturing bacteria leads to reduced phenotypic heterogeneities. Appl. Environ. Microbiol. *85*, 1–13.

Hinsinger, P., Plassard, C., Tang, C., and Jaillard, B. (2016). Origins of root-mediated pH changes in the rhizosphere and their responses to environmental constraints : A review. Plant Soil *248*, 43–59.

Hoagland, D.R., and Arnon, D.I. (1950). The water-culture method for growing plants without soil. Calif. Agric. Exp. Stn. Circ. *347*, 1–32.

Horikoshi, T., Danenberg, K.D., Stadlbauer, T.H.W., Volkenandt, M., Shea, L.C.C., Aigner, K., Gustavsson, B., Leichman, L., Frosing, R., Ray, M., et al. (1992). Quantitation of Thymidylate Synthase, Dihydrofolate Reductase, and DT-Diaphorase Gene Expression in Human Tumors Using the Polymerase Chain Reaction. Cancer Res. *52*, 108–116.

Irmer, S., Podzun, N., Langel, D., Heidemann, F., Kaltenegger, E., Schemmerling, B., Geilfus, C.-M., Zörb, C., and Ober, D. (2015). New aspect of plant–rhizobia interaction: Alkaloid biosynthesis in *Crotalaria* depends on nodulation. Proc. Natl. Acad. Sci. U. S. A. *112*, 4164–4169.

Izquierdo, J., Venkova-Canova, T., Ramírez-Romero, M.A., Téllez-Sosa, J., Hernández-Lucas, I., Sanjuan, J., and Cevallos, M.A. (2005). An antisense RNA plays a central role in the replication control of a repC plasmid. Plasmid *54*, 259–277.

Jones, K.M., Kobayashi, H., Davies, B.W., Taga, M.E., and Walker, G.C. (2007). How rhizobial symbionts invade plants: the *Sinorhizobium-Medicago* model. Nat Rev Microbilogy *5*, 619–633.

Kang, Y., Kim, J., Kim, S., Kim, H., Jae, Y.L., Kim, M., Kwak, J., Jae, S.M., and Hwang, I. (2008). Proteomic analysis of the proteins regulated by HrpB from the plant pathogenic bacterium *Burkholderia glumae*. Proteomics *8*, 106–121.

Keyser, H.H., Bohlool, B.B., Hu, T.S., and Weber, D.F. (1982). Fast-Growing Rhizobia Isolated from Root Nodules of Soybean. Science (80-.). *215*, 1631–1632.

Khan, S.R., and Farrand, S.K. (2009). The BlcC (AttM) lactonase of *Agrobacterium*

tumefaciens does not quench the quorum-sensing system that regulates Ti plasmid conjugative transfer. J. Bacteriol. *191*, 1320–1329.

Kim, J., Kang, Y., Choi, O., Jeong, Y., Jeong, J.E., Lim, J.Y., Kim, M., Moon, J.S., Suga, H., and Hwang, I. (2007). Regulation of polar flagellum genes is mediated by quorum sensing and FlhDC in *Burkholderia glumae*. Mol. Microbiol. *64*, 165–179.

Kobayashi, H., Naciri-Graven, Y., Broughton, W.J., and Perret, X. (2004). Flavonoids induce temporal shifts in gene-expression of nod-box controlled loci in *Rhizobium* sp. NGR234. Mol. Microbiol. *51*, 335–347.

Kovach, M.E., Elzer, P.H., Hill, D.S., Robertson, G.T., Farris, M. a, Roop, R.M., and Peterson, K.M. (1995). Four new derivatives of the broad-host-range cloning vector pBBR1MCS, carrying different antibiotic-resistance cassettes. Gene *166*, 175–176.

Krol, E., and Becker, A. (2011). ppGpp in *Sinorhizobium meliloti*: Biosynthesis in response to sudden nutritional downshifts and modulation of the transcriptome. Mol. Microbiol. *81*, 1233–1254.

Krysciak, D., Schmeisser, C., Preuss, S., Riethausen, J., Quitschau, M., Grond, S., and Streit, W.R. (2011). Involvement of Multiple Loci in Quorum Quenching of Autoinducer I Molecules in the Nitrogen-Fixing Symbiont *Rhizobium (Sinorhizobium)* sp. Strain NGR234. Appl. Environ. Microbiol. *77*, 5089–5099.

Krysciak, D., Grote, J., Rodriguez Orbegoso, M., Utpatel, C., Forstner, K.U., Li, L., Schmeisser, C., Krishnan, H.B., and Streit, W.R. (2014). RNA Sequencing Analysis of the Broad-Host-Range Strain *Sinorhizobium fredii* NGR234 Identifies a Large Set of Genes Linked to Quorum Sensing-Dependent Regulation in the Background of a *traI* and *ngrI* Deletion Mutant. Appl. Environ. Microbiol. *80*, 5655–5671.

Krysciak, D., Orbegoso, M.R., Schmeisser, C., and Streit, W.R. (2015). Molecular Keys to Broad Host Range in *Sinorhizobium fredii* NGR234 , USDA257, and HH103. In Biological Nitrogen Fixation, F.J. de Bruijn, ed. (John Wiley and Sons, Inc.), pp. 325–336.

Lang, J., and Faure, D. (2014). Functions and regulation of quorum-sensing in *Agrobacterium tumefaciens*. Front. Plant Sci. *5*, 14.

Li, Y., Tian, C.F., Chen, W.F., Wang, L., Sui, X.H., and Chen, W.X. (2013). High-Resolution Transcriptomic Analyses of *Sinorhizobium* sp. NGR234 Bacteroids in

Determinate Nodules of *Vigna unguiculata* and Indeterminate Nodules of *Leucaena leucocephala*. PLoS One *8*.

Lithgow, J.K., Wilkinson, A., Hardman, A., Rodelas, B., Wisniewski-Dyé, F., Williams, P., and Downie, J.A. (2000). The regulatory locus *cinRI* in *Rhizobium leguminosarum* controls a network of quorum-sensing loci. Mol. Microbiol. *37*, 81–97.

Livak, K.J., and Schmittgen, T.D. (2001). Analysis of Relative Gene Expression Data Using Real-Time Quantitative PCR and the 2−ΔΔCT Method. Methods *25*, 402–408.

MacLellan, S.R., Smallbone, L.A., Sibley, C.D., and Finan, T.M. (2005). The expression of a novel antisense gene mediates incompatibility within the large *repABC* family of a-proteobacterial plasmids. Mol. Microbiol. *55*, 611–623.

Masson-Boivin, C., and Sachs, J.L. (2018). Symbiotic nitrogen fixation by rhizobia — the roots of a success story. Curr. Opin. Plant Biol. *44*, 7–15.

McAnulla, C., Edwards, A., Sanchez-Contreras, M., Sawers, R.G., and Downie, J.A. (2007). Quorum-sensing-regulated transcriptional initiation of plasmid transfer and replication genes in *Rhizobium leguminosarum* biovar *viciae*. Microbiology *153*, 2074–2082.

McIntosh, M., Meyer, S., and Becker, A. (2009). Novel *Sinorhizobium meliloti* quorum sensing positive and negative regulatory feedback mechanisms respond to phosphate availability. Mol. Microbiol. *74*, 1238–1256.

Mergaert, P., Uchiumi, T., Alunni, B., Evanno, G., Cheron, A., Catrice, O., Mausset, A.E., Barloy-Hubler, F., Galibert, F., Kondorosi, A., et al. (2006). Eukaryotic control on bacterial cell cycle and differentiation in the *Rhizobium*-legume symbiosis. Proc. Natl. Acad. Sci. U. S. A. *103*, 5230–5235.

Miller, M.B., and Bassler, B.L. (2001). Quorum Sensing in Bacteria. Annu. Rev. Microbiol. *55*, 165–199.

Miwa, H., Sun, J., Oldroyd, G.E.D., and Downie, J.A. (2006). Analysis of Nod-factor-induced calcium signaling in root hairs of symbiotically defective mutants of *Lotus japonicus*. Mol. Plant-Microbe Interact. *19*, 914–923.

Morrison, N.A., Hau, C.Y., Trinick, M.J., Shine, J., and Rolfe, B.G. (1983). Heat Curing of a Sym Plasmid in a Fast-Growing *Rhizobium* sp. that is able to nodulate legumes and the nonlegume *Parasponia* sp. J. Bacteriol. *153*, 527–531.

Murphy, L.D., Herzog, C.E., Rudick, J.B., Fojo, A.T., and Bates, S.E. (1990). Use of the Polymerase Chain Reaction in the Quantitation of *mdr-1* Gene Expression. Biochemistry *29*, 10351–10356.

Murray, J.D. (2011). Invasion by invitation: Rhizobial infection in legumes. Mol. Plant-Microbe Interact. *24*, 631–639.

Mus, F., Crook, M.B., Garcia, K., Garcia Costas, A., Geddes, B.A., Kouri, E.D., Paramasivan, P., Ryu, M., Oldroyd, G.E.D., Poole, P.S., et al. (2016). Symbiotic Nitrogen Fixation and the Challenges to Its Extension to Nonlegumes. Appl. Environ. Microbiol. *82*, 3698–3710.

Nealson, K.H., and Hastings, J.W. (1979). Bacterial bioluminescence: Its control and ecological significance. Microbiol. Rev. *43*, 496–518.

Nelson, M.S., and Sadowsky, M.J. (2015). Secretion systems and signal exchange between nitrogen-fixing rhizobia and legumes. Front. Plant Sci. *6*, 1–11.

Noonan, K.E., Beck, C., Holzmayer, T.A., Chin, J.E., Wunder, J.S., Andrulis, I.L., Gazdar, A.F., Willman, C.L., Griffith, B., Von Hoff, D.D., et al. (1990). Quantitative analysis of MDR1 (multidrug resistance) gene expression in human tumors by polymerase chain reaction. Proc. Natl. Acad. Sci. U. S. A. *87*, 7160–7164.

Novick, R.P., Clowes, R.C., Cohen, S.N., Iii, R.O.Y.C., and Falkow, S. (1976). Uniform nomenclature for bacterial plasmids: a proposal. Bacteriol. Rev. *40*, 525.

Oldroyd, G.E.D., and Downie, J.A. (2008). Coordinating Nodule Morphogenesis with Rhizobial Infection in Legumes. Annu. Rev. Plant Biol. *59*, 519–546.

Palmer, A.G., Senechal, A.C., Mukherjee, A., Ané, J.M., and Blackwell, H.E. (2014). Plant responses to bacterial N-acyl L-homoserine lactones are dependent on enzymatic degradation to L-homoserine. ACS Chem. Biol. *9*, 1834–1845.

Papenfort, K., and Bassler, B.L. (2016). Quorum sensing signal-response systems in Gram-negative bacteria. Nat. Rev. Microbiol. *14*, 576–588.

Pappas, K.M., and Winans, S.C. (2003a). The RepA and RepB autorepressors and TraR play opposing roles in the regulation of a Ti plasmid *repABC* operon. Mol. Microbiol. *49*, 441–455.

Pappas, K.M., and Winans, S.C. (2003b). A LuxR-type regulator from *Agrobacterium*

tumefaciens elevates Ti plasmid copy number by activating transcription of plasmid replication genes. Mol. Microbiol. *48*, 1059–1073.

Pérez-Oseguera, Á., and Cevallos, M.A. (2013). RepA and RepB exert plasmid incompatibility repressing the transcription of the *repABC* operon. Plasmid *70*, 362–376.

Perret, X., Staehelin, C., and Broughton, W.J. (2000). Molecular basis of symbiotic promiscuity. Microbiol. Mol. Biol. Rev. *64*, 180–201.

Perret, X., Kobayashi, H., and Collado-Vides, J. (2003). Regulation of expression of symbiotic genes in *Rhizobium* sp. NGR234. Indian J. Exp. Biol. *41*, 1101–1113.

Petersen, K. (2019). Quorum sensing - dependent expression of small proteins and structural analysis of new class of quorum quenching enzymes.

Pinto, U.M., Pappas, K.M., and Winans, S.C. (2012). The ABCs of plasmid replication and segregation. Nat. Rev. Microbiol. *10*, 755–765.

Poole, P., Ramachandran, V., and Terpolilli, J. (2018). Rhizobia: From saprophytes to endosymbionts. Nat. Rev. Microbiol. *16*, 291–303.

Pradhan, B.B., and Chatterjee, S. (2014). Reversible non-genetic phenotypic heterogeneity in bacterial quorum sensing. Mol. Microbiol. *92*, 557–569.

Price, N.P.J., Talmont, F., Wieruszeski, J.M., Promé, D., and Promé, J.C. (1996). Structural determination of symbiotic nodulation factors from the broad host-range *Rhizobium* species NGR234. Carbohydr. Res. *289*, 115–136.

Pueppke, S.G., and Broughton, W.J. (1999). *Rhizobium* sp. Strain NGR234 and *R. fredii* USDA257 Share Exceptionally Broad, Nested Host Ranges. Mol. Plant-Microbe Interact. *12*, 293–318.

Reinhold-Hurek, B., Hurek, T., Gillis, M., Hoste, B., Vancanneyt, M., Kersters, K., and De Ley, J. (1993). *Azoarcus* gen. nov., nitrogen-fixing Proteobacteria associated with roots of Kallar grass (*Leptochloa fusca* (L.) Kunth), and description of two species, *Azoarcus indigens* sp. nov. and *Azoarcus communis* sp. nov. Int. J. Syst. Bacteriol. *43*, 574–584.

Robledo, M., Jiménez-Zurdo, J.I., Velázquez, E., Trujillo, M.E., Zurdo-Pineiro, J.L., Ramírez-Bahena, M.H., Ramos, B., Díaz-Mínguez, J.M., Dazzo, F., Martínez-Molina,

E., et al. (2008). *Rhizobium* cellulase CelC2 is essential for primary. Proc. Natl. Acad. Sci. U. S. A. *105*, 7064–7069.

Rodelas, B., Lithgow, J.K., Wisniewski-Dye, F., Hardman, A., Wilkinson, A., Economou, A., Williams, P., and Downie, J.A. (1999). Analysis of quorum-sensing-dependent control of rhizosphere-expressed (*rhi*) genes in *Rhizobium leguminosarum* bv. viciae. J. Bacteriol. *181*, 3816–3823.

Rolfe, B.G., and Gresshoff, P.M. (1988). Genetic Analysis of Legume Nodule Initiation. Gene Expr. *39*, 297–319.

Roth, L.E., and Stacey, G. (1989). Bacterium release into host cells of nitrogen-fixing soybean nodules: the symbiosome membrane comes from three sources. Eur. J. Cell Biol. *49*, 13—23.

Schäper, S., Krol, E., Skotnicka, D., Kaever, V., Hilker, R., Søgaard-Andersen, L., and Becker, A. (2016). Cyclic di-GMP regulates multiple cellular functions in the symbiotic alphaproteobacterium *Sinorhizobium meliloti*. J. Bacteriol. *198*, 521–535.

Schauser, L., Roussis, A., Stiller, J., and Stougaard, J. (1999). A plant regulator controlling development of symbiotic root nodules. Nature *402*, 191–195.

Schlaman, H.R.M., Okker, R.J.H., and Lugtenberg, B.J.J. (1992). Regulation of nodulation gene expression by NodD in rhizobia. J. Bacteriol. *174*, 5177–5182.

Schmeisser, C., Liesegang, H., Krysciak, D., Bakkou, N., Le Quere, A., Wollherr, A., Heinemeyer, I., Morgenstern, B., Pommerening-Röser, A., Flores, M., et al. (2009). *Rhizobium* sp. Strain NGR234 Possesses a Remarkable Number of Secretion Systems. Appl. Environ. Microbiol. *75*, 4035–4045.

Schreiber, F., Littmann, S., Lavik, G., Escrig, S., Meibom, A., Kuypers, M.M.M., and Ackermann, M. (2016). Phenotypic heterogeneity driven by nutrient limitation promotes growth in fluctuating environments. Nat. Microbiol. *in press*, 1–7.

Schuldes, J., Orbegoso, M.R., Schmeisser, C., Krishnan, H.B., Daniel, R., and Streit, W.R. (2012). Complete genome sequence of the broad-host-range strain *Sinorhizobium fredii* USDA257. J. Bacteriol. *194*, 4483–4483.

Schultze, M., and Kondorosi, A. (1998). Regulation of Symbiotic Root Nodule Development. Annu. Rev. Genet. *32*, 33–57.

Shaw, P.D., Ping, G., Daly, S.L., Cha, C., Cronan, J.E., Rinehart, K.L., and Farrand, S.K. (1997). Detecting and characterizing N-acyl-homoserine lactone signal molecules by thin-layer chromatography. Proc. Natl. Acad. Sci. U. S. A. *94*, 6036–6041.

Smits, W.K., Kuipers, O.P., and Veening, J.-W. (2006). Phenotypic variation in bacteria: the role of feedback regulation. Nat. Rev. Microbiol. *4*, 259–271.

del Solar, G., Giraldo, R., Ruiz-Echevarría, M.J., Espinosa, M., and Díaz-Orejas, R. (1998). Replication and control of circular bacterial plasmids. Microbiol. Rev. *62*, 434–464.

Somasegaran, P., and Hoben, H.J. (1985). Methods in Legume-Rhizobium Technology.

Song, S., Jia, Z., Xu, J., Zhang, Z., and Bian, Z. (2011). N-butyryl-homoserine lactone, a bacterial quorum-sensing signaling molecule, induces intracellular calcium elevation in *Arabidopsis* root cells. Biochem. Biophys. Res. Commun. *414*, 355–360.

Spaink, H.P. (2000). Root nodulation and infection factors produced by rhizobial bacteria. Annu. Rev. Microbiol. *54*, 257–288.

Staehelin, C., Forsberg, L.S., D'Haeze, W., Gao, M.Y., Carlson, R.W., Xie, Z.P., Pellock, B.J., Jones, K.M., Walker, G.C., Streit, W.R., et al. (2006). Exo-oligosaccharides of *Rhizobium* sp. strain NGR234 are required for symbiosis with various legumes. J. Bacteriol. *188*, 6168–6178.

Stanley, J., and Cervantes, E. (1991). Biology and genetics of the broad host range *Rhizobium* sp. NGR234. J. Appl. Bacteriol. *70*, 9–19.

Storz, G., Wolf, Y.I., and Ramamurthi, K.S. (2014). Small Proteins Can No Longer Be Ignored. Annu. Rev. Biochem. *83*, 753–777.

Stougaard, J. (2000). Regulators and regulation of legume root nodule development. Plant Physiol. *124*, 531–540.

Streit, W.R., and Schmitz, R.A. (2004). Metagenomics - The key to the uncultured microbes. Curr. Opin. Microbiol. *7*, 492–498.

Trinick, M.J. (1980). Relationships Amongst the Fast-growing Rhizobia of Lablab purpureus, Leucaena leucocephala, Mimosa spp., Acacia farnesiana and Sesbania grandiflora and their Affinities with Other Rhizobial Groups. J. Appl. Bacteriol. *49*, 39–

53.

Tuteja, N., and Mahajan, S. (2007). Calcium signaling network in plants: An overview. Plant Signal. Behav. *2*, 79–85.

Unay, J., and Perret, X. (2020). A minimal genetic passkey to unlock many legume doors to root nodulation by rhizobia. Genes (Basel). *11*.

Vaghchhipawala, Z., Radke, S., Nagy, E., Russell, M.L., Johnson, S., Gelvin, S.B., Gilbertson, L.A., and Ye, X. (2018). RepB C-terminus mutation of a pRi-*repABC* binary vector affects plasmid copy number in *Agrobacterium* and transgene copy number in plants. PLoS One *13*, 1–12.

Vannini, A., Volpari, C., Gargioli, C., Muraglia, E., Cortese, R., De Francesco, R., Neddermann, P., and Di Marco, S. (2002). The crystal structure of the quorum sensing protein TraR bound to its autoinducer and target DNA. EMBO J. *21*, 4393–4401.

Veliz-Vallejos, D.F., Kawasaki, A., and Mathesius, U. (2020). The presence of plant-associated bacteria alters responses to N-acyl homoserine lactone quorum sensing signals that modulate nodulation in *Medicago truncatula*. Plants *9*, 1–22.

Venkova-Canova, T., Soberón, N.E., Ramírez-Romero, M.A., and Cevallos, M.A. (2004). Two discrete elements are required for the replication of a *repABC* plasmid: An antisense RNA and a stem-loop structure. Mol. Microbiol. *54*, 1431–1444.

Viprey, V., Rosenthal, A., Broughton, W.J., and Perret, X. (2000). Genetic snapshots of the *Rhizobium* species NGR234 genome. Genome Biol. *1*, RESEARCH0014.

Wais, R.J., Galera, C., Oldroyd, G., Catoira, R., Penmetsa, R. V, Cook, D., Gough, C., Denarié, J., and Long, S.R. (2000). Genetic analysis of calcium spiking responses in nodulation mutants of *Medicago truncatula*. Proc. Natl. Acad. Sci. U. S. A. *97*, 13407–13412.

Wais, R.J., Keating, D.H., and Long, S.R. (2002). Structure-function analysis of nod factor-induced root hair calcium spiking in Rhizobium-legume symbiosis. Plant Physiol. *129*, 211–224.

White, C.E., and Winans, S.C. (2007). Cell-cell communication in the plant pathogen *Agrobacterium tumefaciens*. Philos. Trans. R. Soc. B Biol. Sci. *362*, 1135–1148.

Whitehead, N.A., Barnard, A.M.L., Slater, H., Simpson, N.J.L., and Salmond, G.P.C.

(2001). Quorum-sensing in Gram-negative bacteria. FEMS Microbiol. Rev. *25*, 365–404.

Williams, P., Winzer, K., Chan, W.C., and Camara, M. (2007). Look who's talking: communication and quorum sensing in the bacterial world. Philos. Trans. R. Soc. B Biol. Sci. *362*, 1119–1134.

Wisniewski-Dyé, F., and Downie, J.A. (2002). Quorum-sensing in *Rhizobium*. Antonie van Leeuwenhoek, Int. J. Gen. Mol. Microbiol. *81*, 397–407.

Yates, E.A., Philipp, B., Buckley, C., Atkinson, S., Chhabra, S.R., Sockett, R.E., Goldner, M., Dessaux, Y., Cámara, M., Smith, H., et al. (2002). N-acylhomoserine lactones undergo lactonolysis in a pH-, temperature-, and acyl chain length-dependent manner during growth of *Yersinia pseudotuberculosis* and *Pseudomonas aeruginosa*. Infect. Immun. *70*, 5635–5646.

Żebracki, K., Koper, P., Marczak, M., Skorupska, A., and Mazur, A. (2015). Plasmid-Encoded RepA Proteins Specifically Autorepress Individual *repABC* Operons in the Multipartite *Rhizobium leguminosarum* bv. trifolii Genome. PLoS One *10*, e0131907.

Zhou-qi, C., Bo, Z., Guan-lin, X., Bin, L., and Shi-wen, H. (2016). Research Status and Prospect of *Burkholderia glumae*, the Pathogen Causing Bacterial Panicle Blight. Rice Sci. *23*, 111–118.

Zhu, J., and Winans, S.C. (2001). The quorum-sensing transcriptional regulator TraR requires its cognate signaling ligand for protein folding, protease resistance, and dimerization. Proc. Natl. Acad. Sci. U. S. A. *98*, 1507–1512.

7 Appendix

7.1 Single cell counting and fluorescence analysis

7.1.1 CellProfiler 3.1.8. pipeline

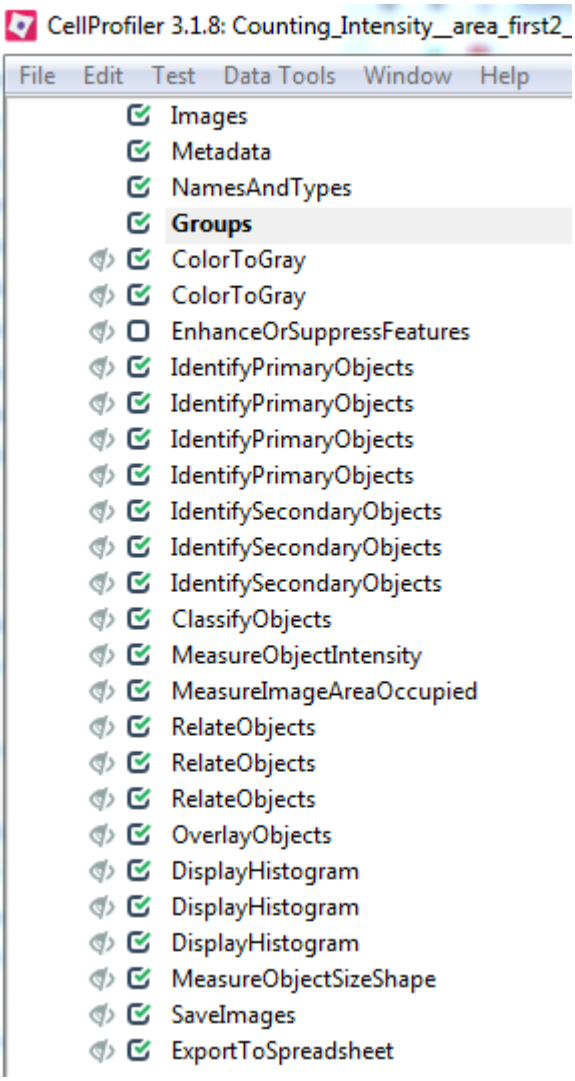

Figure A. 1: CellProfiler 3.1.8. pipeline overview. All pipeline modules implemented in the single cell counting and analysis pipeline designed with the CellProfiler 3.1.8 software.

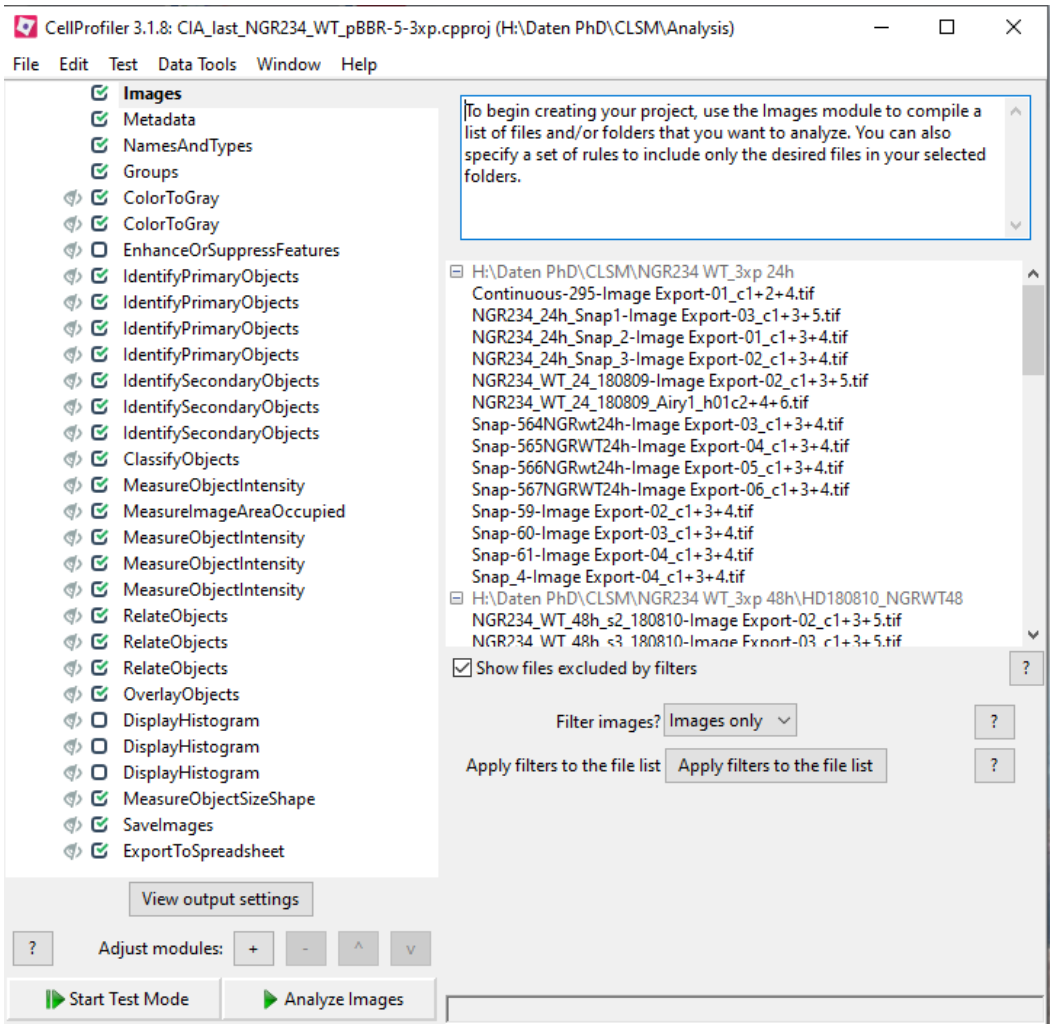

Figure A. 2: Importing images for analysis in CellProfiler 3.1.8. The images that were to be analysed were loaded in the CellProfiler 3.1.8 program.

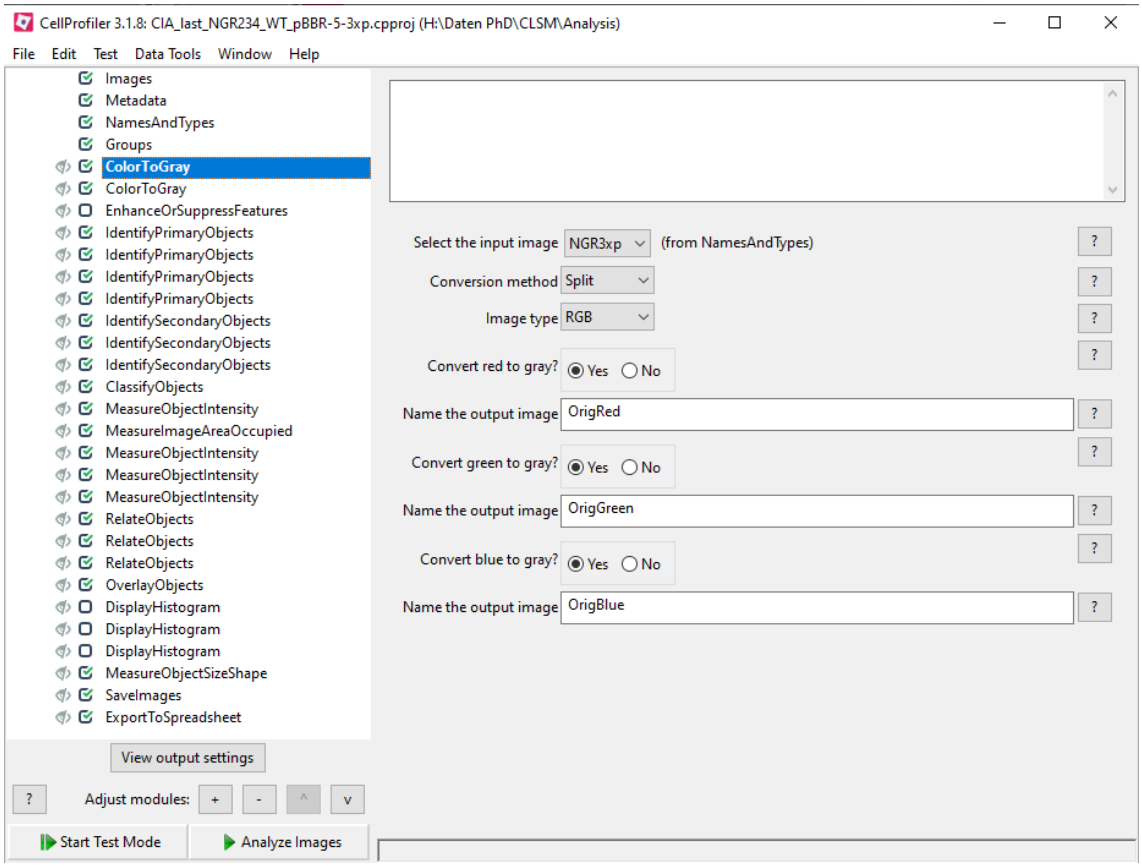

Figure A. 3: Assigning names to bacteria of each fluorescence channel. To analyse each fluorescence channel individually, three single channel images were created of each image.

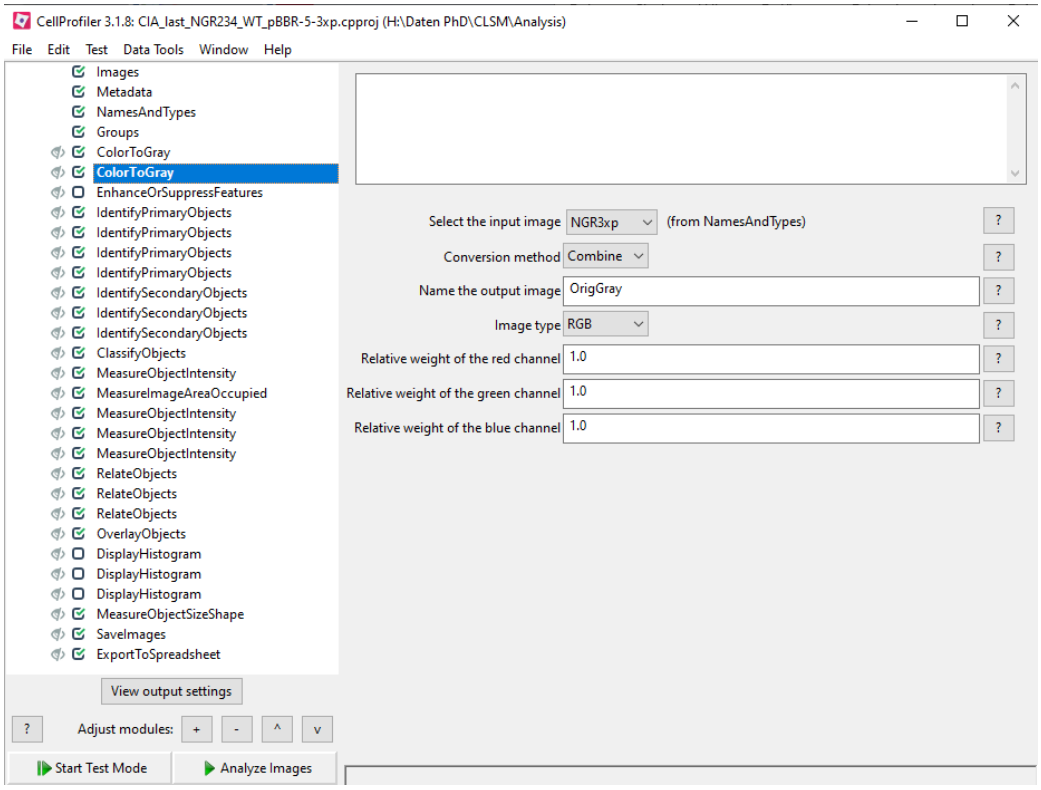

Figure A. 4: Assigning a merged fluorescence channel image. To analyse and count all the cells observed regardless of their expression patterns, a merged channel image was created. All fluorescence channels were weight equally for creating the image.

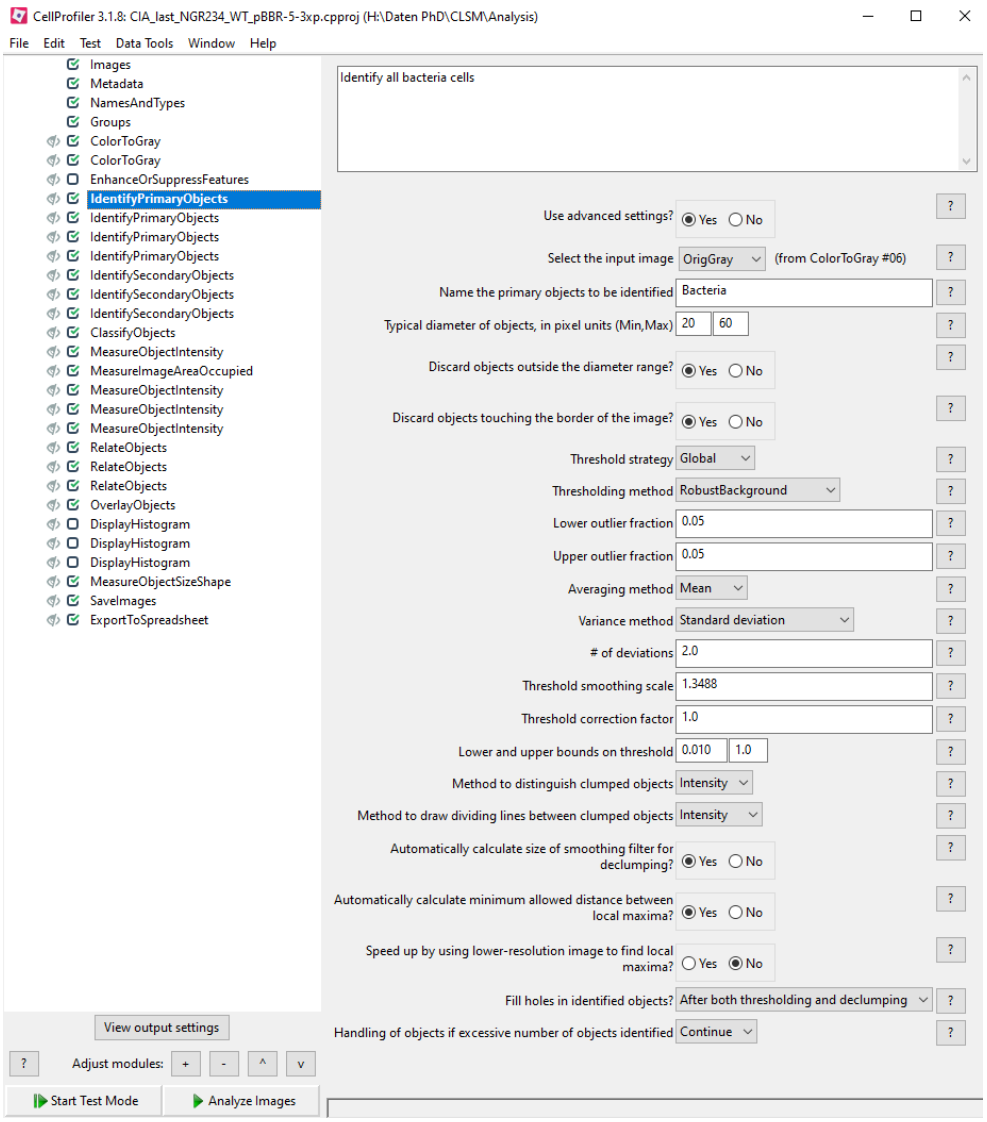

Figure A. 5: Identification of all bacteria as primary objects. To count all bacteria observed in CLMS analysis, the merged channel image was used for identification of all the fluorescing bacteria.

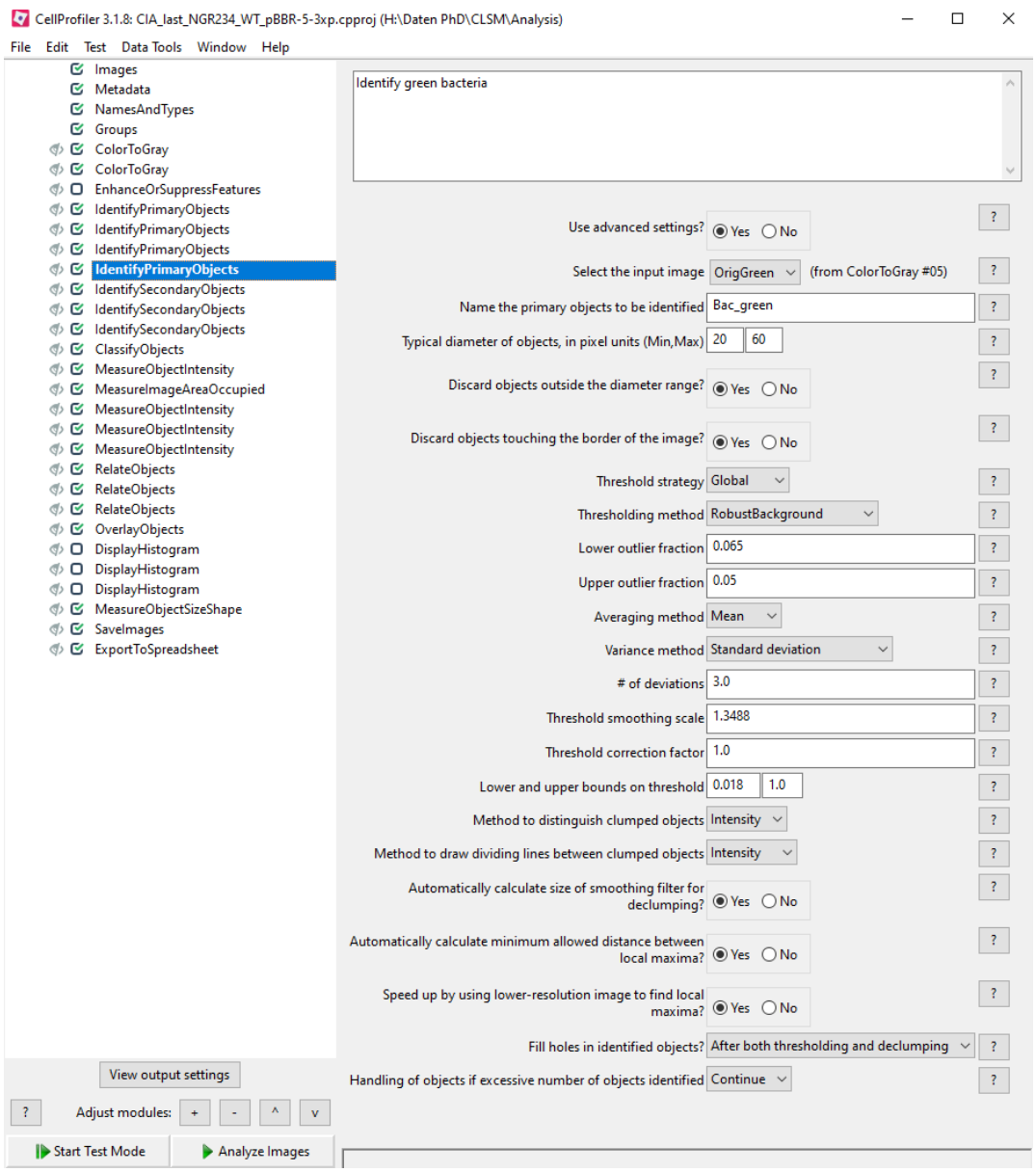

Figure A. 6: Individual identification of bacteria for each fluorescence channel. Identification of the bacteria for each fluorescence channel seperatly. Settings for all three channels were the same.

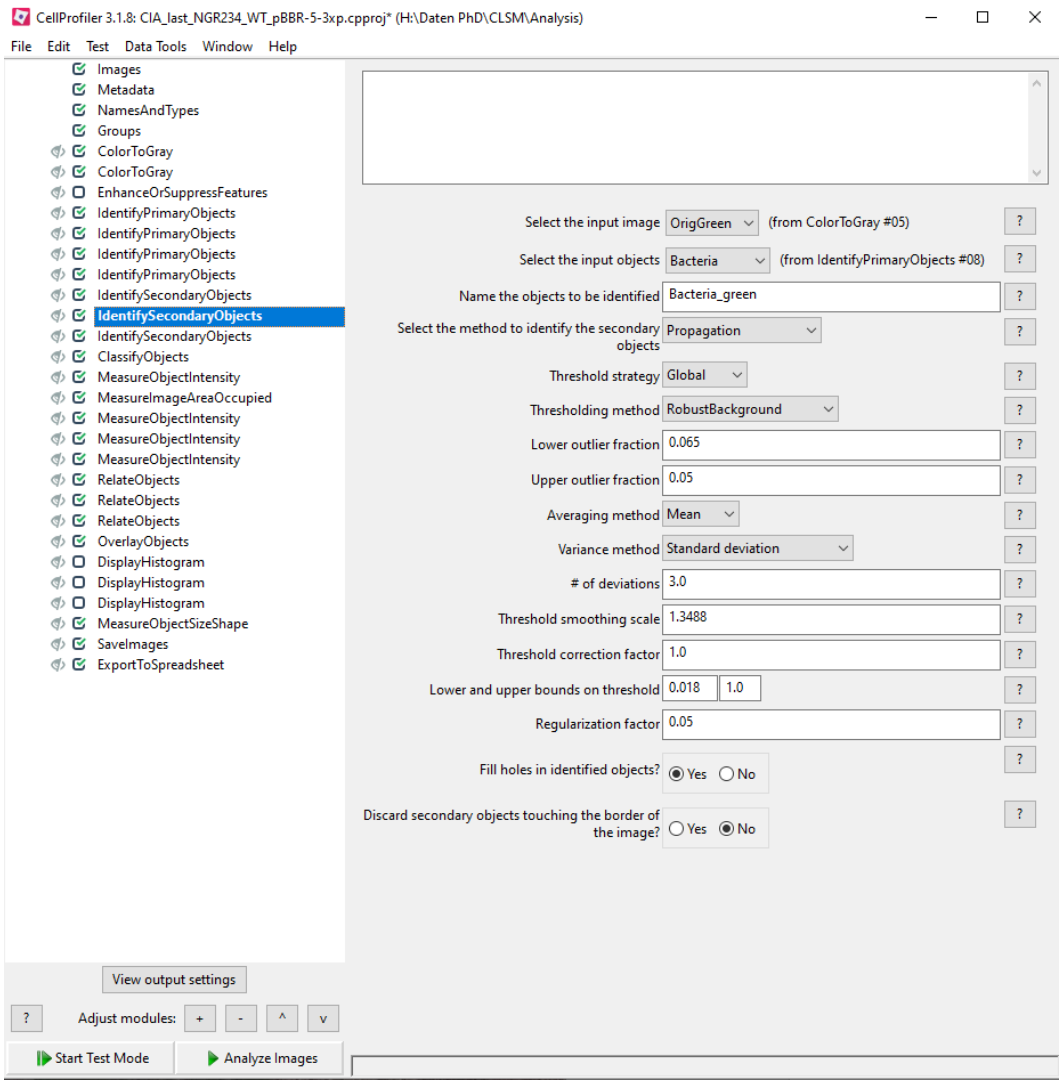

Figure A. 7: Connection of individual fluorescence channels and bacteria as primary objects. Connecting the identified bacteria for each channel to the overall identified bacteria on the merged fluorescence image.

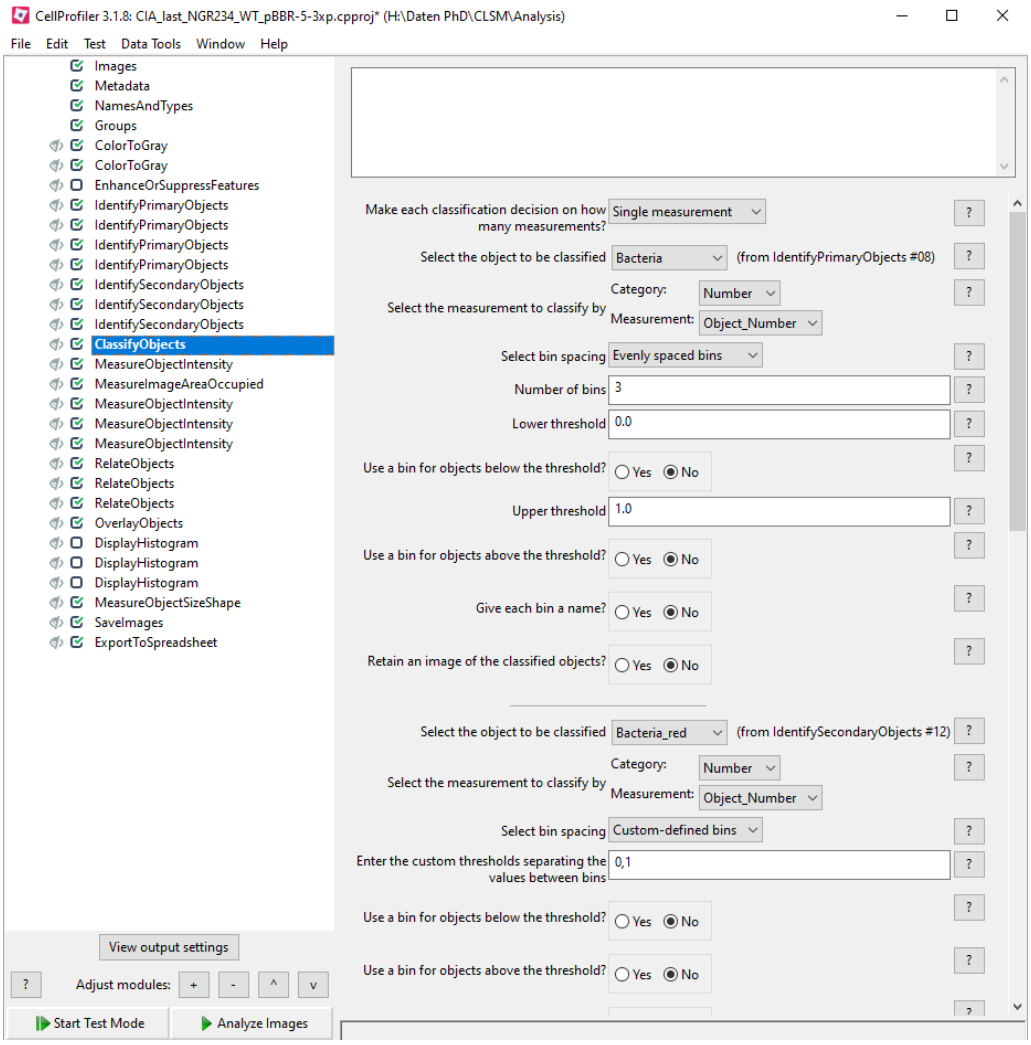

Figure A. 8: Classifying prior identified objects. Counting of all the identified bacteria using the primary object *bacteria* and the objects identified in each fluorescence channel (*e.g. Bacteria_red*).

7.2 Nodulation assay

7.2.1 Comparison of plant growth media

Table A. 1: Comparison of plant growth media used in this study. Indicated are final concentrations of each component utilised for each of the three plant growth media. (Hoagland and Arnon, 1950; Irmer et al., 2015)

Component	Hoagland	Hoagland 0.25 strength	NOD	Stock solution NOD
	Final concentration [mM]	Final concentration [mM]	Final concentration [mM]	
$MgSO_4$ x $7H_2O$	2	0.5	0.25	Stock E
$Ca(NO_3)_2$ x $4H_2O$	5	1.25	0	
KNO_3	5	1.25	5	Stock N
NH_4NO_3	1	0.25	0	
KH_2PO_4	1	0.25	0.5	Stock B1
K_2HPO_4	0	0	0.333	Stock B2
$CaCl_2$ x $2H_2O$	0	0	1	Stock A
Fe-EDTA-Lsg			0	
$FeCl_3$ x $6H_2O$	0.0597	0.01492	0	
EDTA	0.1026	0.02565	0	
Na/Fe III EDTA	0	0	0.02065	Stock D
$C_6H_5FeO_7$	0	0	0	
Trace element				Stock

Component	Hoagland	Hoagland 0.25 strength	NOD	Stock solution NOD
	Final concentration [mM]	Final concentration [mM]	Final concentration [mM]	
				MOD1B5b
H_3BO_3	0.0463	0.011565	0.0243	
$MnCl_2 \times 4H_2O$	0.0091	0.0022864	0	
$ZnSO_4 \times 7H_2O$	0.0008	0.00019125	0.0052	
$CuSO_4 \times 5H_2O$	0.0002	5.10625E-05	0.0005	
$H_2MoO_4 \times H_2O$	0.0005	0.000125025	0	
$Na_2MoO_4 \times 2H_2O$	0	0	0.0005	
$MnSO_4 \times H_2O$	0	0	0.0296	
KI	0	0	0.0023	
$CoCl_2 \times 6H_2O$	0	0	0.0005	
K_2SO_4	0	0	0	
$CoSO_4$	0	0	0	

8 Acknowledgment

First, I would like to thank Prof. Dr. Wolfgang Streit, for introducing me to *Sinorhizobium fredii* NGR234, its fascinating regulatory networks, for giving me the opportunity to work on this intriguing topic and joining his wonderful group. Furthermore, I appreciate that you were always welcoming scientific discussions, encouraged me to expand my knowledge and gave me the opportunity to work independently. Secondly, I would like to thank PD Dr. Eva Spieck, for taking over my co-supervision and for correction of my dissertation. Thank you both very much.

My special and deep thanks to my amazing colleagues, that made every minute spent at the institute, in the lab and working in this group one of the most interesting, stimulating, and fun times. Thank you for countless discussions, helpful input, support, and after-work sessions.

I would like to thank my family, supporting me, abetting me, and always having the trust in me taking the right path and encouraging me to follow it. My parents and especially my father who always has been a guardian and a counsellor for me, helping me through all stages of my life. Thank you, Heike and Imke for being role models to me. Seeing you stepping forward on your paths, encouraged me to look for my own and follow it with the same endurance.

The person supporting me the most during this time and to whom I owe the deepest gratitude is my best friend and husband Tobias. Without you I would not have had the strength to finish this work. Thank you for listening to my presentation and for enduring all these days I came home late, was frustrated from work, and could not stop talking about an experiment. Thank you for your advice and I am sorry for all those times when I did not follow it although I should have known better. Thank you for everything.

9 English Language Declaration

I hereby declare as a native English speaker that I have checked the thesis "Symbiotic plasmid (pNGR234*a*) copy number in the broad host range bacterium *Sinorhizobium fredii* NGR234 depends on quorum sensing and phenotypic heterogeneity" by Hilke J. Duin for grammatically correct English and the scientific accuracy of the language. I also confirm that I am a native English speaker.

Sincerely,

_____

Robert C. Armstrong